DROUGHT IN THE INSULAR CARIBBEAN: HISTORICAL AND FUTURE CLIMATE IMPACTS ON WATER RESOURCES AND AGRICULTURE

by

Flávia Dias de Souza Moraes

(Under direction of Thomas L. Mote)

ABSTRACT

The insular Caribbean experiences numerous climate and environmental hazards, including but not limited to hurricanes, floods, earthquakes, volcanic eruption, and drought. While some hazards are well known, such as hurricanes, drought is considered one of the neglected hazards. This dissertation contributes to the understanding of three aspects of drought events in the region: the spatial and temporal effects of low-frequency atmospheric variability on drought, the role of topography and climate on Puerto Rico water resources, and a comparative study of the impact of climate change on crop water needs in an island in the Greater Antilles (Puerto Rico) and a Lesser Antilles (St. Croix). The results indicated that the Atlantic Meridional Mode (AMM) was most strongly related with drought events in the insular Caribbean, followed by the North Atlantic Oscillation (NAO), and Central Pacific El Nino Southern Oscillation (CP ENSO). However, CP ENSO was only related to drought in the Lesser Antilles (LA), while the relationship between the two types of ENSO and the Greater Antilles (GA) was not statistically significant. The LA was also the region with more intense, widespread, and frequent drought events during 1950–2017. Projections of water stress indicated that St. Croix, representative of smaller islands in the insular Caribbean, will suffer from water deficit and decline in agriculture suitability of sweet pepper, banana, and plantain for at least half of the year starting in the mid-21st Century. In Puerto Rico, representative of larger islands, it is the southern region that will have crop suitability most affected by climate change. Conversely, the reduction in net infiltration in south, north, and east Puerto Rico may affect both the tropical forest in the Luquillo Mountains as well as the recharge of the two most important aquifers in the island: North Coast and South Coast Aquifers. These findings should assist the islands to better prepare for the potential effects of climate variability and change on water management and food security.

INDEX WORDS: Insular Caribbean, Drought, Climate Change, Water Budget, Teleconnection, Agriculture Suitability, scPDSI

DROUGHT IN THE INSULAR CARIBBEAN: HISTORICAL AND FUTURE CLIMATE IMPACTS ON WATER RESOURCES AND AGRICULTURE

by

FLÁVIA DIAS DE SOUZA MORAES

B.S., Universidade Federal do Rio Grande do Sul, Brazil, 2014

M.S., Universidade Federal do Rio Grande do Sul, Brazil, 2016

A Dissertation Submitted to the Graduate Faculty of The University of Georgia in Partial Fulfillment of the Requirements for the Degree

DOCTOR OF PHILOSOPHY

ATHENS, GEORGIA

2021

DROUGHT IN THE INSULAR CARIBBEAN: HISTORICAL AND FUTURE CLIMATE IMPACTS ON WATER RESOURCES AND AGRICULTURE

by

FLÁVIA DIAS DE SOUZA MORAES

Major Professor:	Thomas L. Mote
Committee:	Marguerite Madden
	J. Marshall Shepherd
	Todd Rasmussen
	Douglas Gamble

Electronic Version Approved:

Ron Walcott
Vice Provost for Graduate Education and Dean of the Graduate School
The University of Georgia
August 2021

DEDICATION

I dedicate this dissertation to all women in science, especially to the Latin American women. I know we face many challenges in academia to be accepted and respected in a predominantly male world. However, I hope by seeing me here you can be inspired to follow your dreams and believe that you can do everything you want.

ACKNOWLEDGEMENTS

First, I would like to thank my advisor, Dr. Thomas Mote, for the great opportunity to work with and learn from him, and for all the support he gave me during these academic years. He is not only a great and dedicated advisor who made me grow so much in academia, but also a kind person who became a good friend. I also thank my committee members, Dr. Marguerite Madden, Dr. Marshall Shepherd, Dr. Todd Rasmussen, and Dr. Douglas Gamble, for their many valuable contributions to improve this work and for the opportunity to learn from each one of them. Many thanks to the Department of Geography at UGA for the warm welcome provided to this international student, for the teaching assistantship that made my "study abroad dream" possible and made me fell in love with teaching, and for the great friends I made along the way. Thanks to all the current and former Climate Lab members with whom I exchange valuable academic experiences, especially Lori Wachowicz, Kyle Mattingly, Haylie Mikulak, Paul Miller, and Craig Ramseyer. I also thank my former advisors from the Universidade Federal do Rio Grande do Sul, Brazil, Dr. Francisco Aquino and Dr. Jefferson Simões, for all the encouragement to pursue my doctoral degree abroad and the support provided to help this dream come true. Dr. Aquino was a great advisor and friend, who was responsible for introducing me to Dr. Mote and making me believe that I could pursue an academic career abroad, so I have no words to thank him for that. Additionally, thanks to the NSF Luquillo Long-Term Ecological Research Program (DEB1239764) and NOAA Modeling, Analysis, Predictions and Projections (MAPP) grant (NA20OAR4310415) for the funding provided for research.

Finally, I want to thank my family for always believing in me and being an example of incredible and strong women. Especially, thanks to my mother, Ana Maria Dias, for valuing education over everything else, for understating my absence during the last five years and for always sending me lots of love in our online calls. I miss you every day! Thanks to my father, Flavio Moraes, for being my big fan and for providing support that allowed me to study for so many years. Most importantly, I thank my husband, Lucas Favero, for being the best partner I could have asked to go through this journey abroad with, for always being full of love and encouraging me to go further. You are an inspiration for me! A special thanks also to my husband's family who adopted me as their own child and supported our decision to live abroad even though this means their son would be very far away from home. Finally, thanks to my good friends who were by my side, even living thousands of miles away, and for the great Brazilian friends I made in Athens, GA, who helped me to feel at home in a foreign land.

TABLE OF CONTENTS

LIST OF TABLES

LIST OF FIGURES

Page

LIST OF ABBREVIATIONS

AET: Actual Evapotranspiration

AMM: Atlantic Meridional Mode

AWC: Available Water Capacity

CDO: Climate Data Operators

CLLJ: Caribbean Low-Level Jet

CMIP6: Coupled Model Intercomparison Project Phase 6

CP ENSO: Central Pacific El Niño Southern Oscillation

CPC: Climate Prediction Center

CROPRISK: Crop Risk Model

DS: Dry Season (December–March)

ENSO: El Nino Southern Oscillation

EOF: Empirical Orthogonal Function

EP ENSO: Eastern Pacific El Niño Southern Oscillation

ERS: Early Rainfall Season (April–July)

GA: Greater Antilles and The Bahamas

GIS: Geographic Information System

IPCC: Intergovernmental Panel on Climate Change

ITCZ: Intertropical Convergence Zone

Kc: Crop Coefficient

Ky: Yield Response Factor

LA: Lesser Antilles

LRS: Late Rainfall Season (August–November)

LUQ-LTER: Luquillo-Long-Term Ecological Research

LULC: Land Use and Land Cover

MSD: Mid-summer Dry Spell (July–August)

NAHP: North Atlantic Subtropical High

NAO: North Atlantic Oscillation

NOAA: National Oceanic and Atmospheric Administration

NSE: Nash-Sutcliffe efficiency

ONI: Oceanic Niño Index

PBIAS: Percent Bias

PET: Potential Evapotranspiration

PDSI: Palmer Drought Severity Index

PW: Precipitable Water

RSR: RMSE-Observations Standard Deviation Ratio

SAL: Saharan Air Layer

scPDSI: “self-calibration” Palmer Drought Severity Index

SIDS: Small Island Developing States

SLP: Sea Level Pressure

SPI: Standardized Precipitation Index

SSP-RCP: Socioeconomic Pathway-Representative Concentration Pathway

SST: Sea Surface Temperature

SWB2: Soil-Water-Balance Model Version 2.0

TNA: Tropical North Atlantic

TSA: Tropical South Atlantic

USDA: United States Department of Agriculture

USGS: United States Geological Survey

1 INTRODUCTION

1.1 Problem Statement and Significance

The insular Caribbean is located in the western Tropical North Atlantic Basin (TNA), between approximately 10ºN and 25ºN, and 90ºW and 60ºW. They form an archipelago extending southeastward in an arc between Florida and eastern Venezuela. The region is divided into three groups of islands consisting of The Bahamas; the Greater Antilles (Cuba, Dominican Republic, Haiti, Jamaica, and Puerto Rico); and the Lesser Antilles, composed of the smaller islands from the U.S. Virgin Islands to Trinidad and Tobago (Figure 1.1). Some studies also include the smaller isolated islands as part of the insular Caribbean (Aruba, Bonaire, Curacao (ABC), and the Cayman Islands), but this dissertation does not include them in the analysis. Despite the great cultural diversity among the Caribbean islands, the region shares similarities in regard to its rich biodiversity, including but not limited to rain forests, endemic species, volcanic features, coral reefs, and areas of marine mammals sanctuary (Geoghegan and Renard 2002).

However, this rich environment is susceptible to stress on water resources due to its physical geography. The geological composition is one of the most important characteristics affecting water availability because geology plays a role in physiographic control of rainfall patterns and the availability of surface and subsurface water (Hendry 1996). In the insular Caribbean, there are volcanic and carbonate islands. The inner arc of the Lesser Antilles (from St. Kitts to Grenada) are volcanic islands, while The Bahamas, the outer arc of the Lesser Antilles (from Anguilla to Barbados) and the Greater Antilles (mostly young volcanic islands in which carbonate sedimentation occurred during Eocene) are considered carbonate islands (Heileman

2007; Hendry 1996; Khudoley and Meyerhoff 1971). In the carbonate islands, most of the water resources are located at the subsurface, while in the volcanic islands the water supply is from the surface due to limited percolation, steep terrain and high runoff (Hendry 1996).

Additionally, the location of the insular Caribbean also affects its hydroclimatology. In the TNA, where evaporation normally exceeds precipitation, some of the small islands are already in a state of water stress, while most of them have few potable surface water resources with their population mostly depending on precipitation and groundwater for water supply (Gamble 2004; Karnauskas et al. 2018). Moreover, rainfall is not uniform within the Caribbean, with spatial and temporal variability resulting in semi-arid areas and areas with abundant rainfall (the windward side of the mountainous islands), while groundwater is limited in volcanic islands (Granger 1985).

Among the characteristics that affect the spatial and temporal variability of rainfall are changes in atmospheric pressure patterns. Teleconnections are large-scale spatial and temporal anomalies that appear as preferred modes of low-frequency (inter-annual, decadal, multidecadal) natural variability in the atmospheric circulation. Each teleconnection pattern has geographically fixed centers of action or "poles" (Hatzaki et al. 2007). Most importantly, teleconnections influence the variability of atmospheric pressure and wind (i.e., circulation), resulting in different impacts on precipitation across the region.

In the insular Caribbean, several studies have demonstrated the relationship between precipitation and teleconnections. Among the teleconnections examined are El Niño Southern Oscillation (ENSO), defined as anomalies in sea surface temperature (SST) in the equatorial Pacific Ocean (Trenberth 1997), and the North Atlantic Oscillation (NAO), which is described as a large-scale seesaw of atmospheric mass between North Atlantic regions of the subtropical high and the subpolar low (Charlery et al. 2006; Lamb and Peppler 1987). Ropelewski and Halpert

(1987) affirmed that during years of ENSO warm phase the Caribbean has a tendency to be slightly drier than normal. Giannini et al. (2000) and Giannini et al. (2001c) found that the negative correlation between positive NAO and negative precipitation anomaly is strongest around 15°N, 60°W (Lesser Antilles area). Mote et al. (2017) also indicated that a positive NAO was one of the atmospheric mechanisms related to severe drought events in the eastern Caribbean during 1994 and 2015.

Although the physical geography of the insular Caribbean and the effects of atmospheric circulation on precipitation point to the potential for drought to affect the region, few studies have focused on drought hazards. Drought is considered as one of the neglected climate hazard in the insular Caribbean (Gamble 2014), although regional models predict that a warmer planet (~2 °C) will increase freshwater stress by 25% at 2030 as a consequence of longer-lasting and more severe drought events in the Caribbean (Cashman et al. 2010; Karnauskas et al. 2018). A gradual drying trend has been already registered since 1950 (Herrera et al. 2018).

Considering the social and economic imperative to mitigate the impacts of drought, which necessarily calls for us to better understand how drought is related to physical geography and climate variability, this dissertation includes several goals. First, it determines periods when and where the insular Caribbean had drought events occurring from 1950–2017, and the spatial and temporal effects that the atmospheric low-frequency variability patterns that affect the TNA have over the islands. This work also analyzes the role of physical geography (rainfall, geographical and geological features) on a Greater Antilles (Puerto Rico) water resources, by estimating its water budget and assessing potential groundwater recharge. Finally, this study examines the potential impact of climate change on crop water need in a Greater Antilles (Puerto Rico) and a Lesser Antilles (St. Croix) based on climate projections.

1.2 Literature Review

1.2.1 Insular Caribbean precipitation climatology

Because the annual range of temperature is not large in the tropical islands (from 1.9° C in Trinidad to 5.5° C in Cuba), rainfall is the characteristic which determines seasonality and the bio-productive systems in the insular Caribbean (Granger 1996). Regardless of the various climate regimes governing the insular Caribbean, there are common seasonal precipitation patterns that present themselves in the region. Figure 1.2 shows the winter (December–March) as the period when the absolute minimum amount of precipitation occurs, referred to as the dry season (DS), and a relative minimum occurs annually during the summer (around July–August) and is known as mid-summer dry spell (MSD) (Gamble and Curtis 2008; Giannini et al. 2001a; Jury et al. 2007). This short, dry period separates the rainy seasons in the Caribbean into an early rainfall season (ERS, April–July) and a late rainfall season (LRS, August–November) (Angeles et al. 2010; Gamble and Curtis 2008; Gamble et al. 2008; Magaña et al. 1999; Taylor et al. 2002).

The seasonality evident in Caribbean precipitation climatology is a consequence of the location and the atmospheric dynamics of the region. The insular Caribbean is centered between the North Atlantic subtropical high (NAHP) and the Intertropical Convergence Zone (ITCZ). The presence of the NAHP helps to maintain easterly winds, and the Caribbean lies in the main current of the trade winds, while the movement of the ITCZ also govern the precipitation distribution (Granger 1985). When the TNA sea surface temperature (SST) presents an extensive warm pool, it also affects the precipitation pattern of the two rainy seasons (ERS and LRS) in the insular Caribbean (Taylor et al. 2002). On the other hand, in some regions of the Caribbean there is a period during the summer when the Bermuda High strengthens and dramatically decreases rainfall (Granger 1985).

This bi-modal structure of Caribbean precipitation is still not well understood (Gamble and Curtis 2008). The two maxima occur in May–June and September–October and are separated by what has been termed MSD (Magaña et al. 1999). However, MSD does not necessarily refer to drought conditions, but simply a period of decreased precipitation. The most accepted theory as to why this period of minimum precipitation occurs is that the NAHP strengthens and expands, leading to enhanced sinking motion in the Caribbean (Giannini et al. 2000; Granger 1985). Strengthening of the NAHP is accompanied by an intensification of the Caribbean Low-Level Jet (CLLJ), an increase of vertical wind shear, sinking motion, surface divergence, lower SST, and diminished Caribbean rainfall (Gamble 2014; Gamble and Curtis 2008; Giannini et al. 2000). Individual factors are not responsible for the decrease in precipitation; rather, these factors interact with each other, and combined they decrease the chance of precipitation occurring in the Caribbean and lead to the MSD (Angeles et al. 2010; Gamble and Curtis 2008).

However, there are differences in the rainfall seasonality depending on the location. The MSD, for example, is more pronounced in the Greater Antilles (or the western Caribbean) extending southward to northwestern South America. Moreover, the LRS peak is enhanced in the western Caribbean near Honduras, as well as along the northeast-facing coasts of the both Antilles (Giannini et al. 2001b).

1.2.2 Teleconnections and their effects on insular Caribbean rainfall patterns

Teleconnections are variability in atmospheric circulation that result in different impacts in different regions of the world. In this work, we focused on teleconnections patterns previously related with Caribbean rainfall, such as ENSO, NAO, and the Atlantic Meridional Mode (AMM) (George and Saunders 2001; Giannini et al. 2001b; Malmgren et al. 1998; Ropelewski and Halpert 1987; Smirnov and Vimont 2011). By understanding the relationship between these teleconnections and precipitation in the insular Caribbean, we can better comprehend the analysis of those atmospheric patterns with drought events in the region.

1.2.2.1 El Niño Southern Oscillation (ENSO)

Historically, there have been many definitions of ENSO in terms of location of SST anomalies, duration of the anomalies, seasonality of the anomalies, etc. One definition is that ENSO is a coupled atmosphere-ocean pattern identified by anomalies in SST in the equatorial Pacific Ocean and in sea-level pressure between Darwin and Tahiti, which starts around December (Trenberth 1997). Initial research found that most often SST anomalies were the strongest in the Eastern Pacific Ocean close to the South American coast (Cane 1983), and in time this region (the Niño 3 region as it came to be known) became the one used by many scientists when discussing ENSO (Giannini et al. 2001b). As more research regarding ENSO emerged, more studies found periods when the SST anomalies occurred closer to the Central Pacific. This led to the use of the Niño 3.4 region to represent ENSO, which encompasses regions closer to the Central Pacific (Jury et al. 2007).

Scientists studying ENSO recognized that the reason for these conflicting SST anomaly regions and the different timing and intensity of ENSO events may be due to more than one type of ENSO. There was a discussion about the different types, and it was dependent on the location of the SST anomalies (Ashok et al. 2007; Capotondi et al. 2015). Ashok et al. (2007) conducted an Empirical Orthogonal Function (EOF) analysis of the SSTs in the Pacific Ocean and found an SST anomaly pattern during El Niño events that had a different appearance than that of the typical El Niño (EOF1). Their second EOF identified a zonal tripole in the Pacific tropics, in which the east and west Pacific had negative anomalies, but the central Pacific Ocean had positive anomalies. This shift in location of the maximum positive SST anomalies, but similar appearance in response of the temperature field, led Ashok et al. (2007) to refer to this pattern as “El Niño Modoki”. “Modoki” is a Japanese word that means “a similar but different thing”. Over time, this pattern came to be associated with a different type of ENSO event.

A consensus on two different types of ENSO has emerged (Capotondi et al. 2015; Kao and Yu 2009; Mo 2010). An Eastern Pacific (EP) type has its main SST anomaly development in the eastern Pacific, and mainly covers the Niño 1+2 and Niño 3 regions (Kao and Yu 2009). The positive phase of EP ENSO, known commonly as El Niño or warm phase, is the “canonical” type, or the pattern that many authors associate with the term “El Niño” (Cane 1983; Giannini et al. 2000). The Central Pacific (CP) type has an SST anomaly centered over the central Pacific Ocean, near the date line, and covers the Niño 3.4 and Niño 4 regions (Kao and Yu 2009). Meteorologists are beginning to recognize the difference between the atmospheric circulations and features associated with each type of ENSO. This shift in SST anomaly location has been identified as the key feature used to separate ENSO types (Kao and Yu 2009). In addition to the different location of SST anomalies, some studies suggested that the seasonal evolution also differs. During EP events, SST anomalies usually appear in the eastern Pacific during boreal spring and expand to the west during the summer and fall. With CP events, the anomalies expand west during boreal spring and summer (Capotondi et al. 2015).

Most of the work analyzing EP and CP ENSO has focused on their impacts in the United States only, while the effects of ENSO from regions Nino 3 and/or 3.4 on Caribbean precipitation have been examined in few studies. Overall, the response of Caribbean precipitation occurs in three different phases, corresponding to the atmospheric, and then the oceanic responses to mature El Niño events. Giannini et al. (2001b) found that during the latter half of the boreal fall season that precedes the mature ENSO phase (i.e., when the SST anomaly is building), a divergent surface circulation dominates the region leading to drier than average conditions across the Caribbean. Then, during the boreal winter season, when the effect of El Niño is most highly correlated to climate in most regions around the world, only the northern areas of the Caribbean are affected by anomalous storm activity. As the El Niño event begins to weaken, the Caribbean begins to experience warm TNA SSTs and more convection and rainfall occur in the region. Essentially, the time period before and after mature El Niño events are the periods when the Caribbean is most affected (Giannini et al. 2001b).

However, a more recent review by Gamble (2014), suggested that more variability of the spatial and temporal impacts of ENSO in the insular Caribbean has emerged. While some studies indicated that, regardless of ENSO type, El Niño events are related to a decrease in LRS rainfall due to the strong vertical wind shear and lower frequency of hurricanes in TNA (Patricola et al. 2014; Patricola et al. 2016; Taylor et al. 2002), other research found no relationship between ENSO and rainfall in islands such as Puerto Rico (Torres-Valcárcel 2018).

1.2.2.2 Atlantic Meridional Mode (AMM)

The AMM is defined as the meridional gradient in SST near the ITCZ (Vimont and Kossin 2007). In a negative AMM event, cold SST anomalies and anomalously high northeasterly surface wind speeds occur in the TNA, warm SST anomalies occur in the Tropical South Atlantic (TSA), and the ITCZ shifts to south of the Equator. When the AMM is positive, the SST anomalies shift, there are southwesterly wind anomalies in the TNA, and the ITCZ is displaced north of the Equator (Rugg et al. 2016). In boreal spring, the AMM tends to peak (i.e. SST gradients are strongest in the North Atlantic), and the ITCZ is most sensitive to shifts due to these strong anomalies (Foltz et al. 2012).

Relatively little is known about the AMM connection to precipitation in the Caribbean, outside of the effect on hurricane activity (Patricola et al. 2014; Smirnov and Vimont 2011; Vimont and Kossin 2007), and no research has been identified regarding AMM and Caribbean drought. Vimont and Kossin (2007) discussed how the positive phase of the AMM is related to a reduction in wind shear, an increase in SST anomalies, and decreased pressure over the main development region over the North Atlantic, which is defined as the region between 20°–60°E and 10°–20°N off the coast of west Africa. This wind shear reduction favors tropical cyclone activity, but not all of these storms make landfall in Caribbean islands. Smirnov and Vimont (2011) examined how the AMM affects boreal summer and fall, and said that as the ITCZ shifts north, higher rainfall anomalies can be found in the western portion of the same main development region discussed in Vimont and Kossin (2007). Patricola et al. (2014) studied the composites of accumulated cyclone energy of tropical systems that have passed through the Caribbean region. Based on their findings, they concluded that analysis of the AMM by itself is not enough to explain seasonal Atlantic tropical cyclone variability. Rather, a positive AMM in addition to a La Niña is desirable for tropical cyclone activity.

1.2.2.3 North Atlantic Oscillation (NAO)

The NAO can be defined and calculated by the difference between the normalized sea level pressures (SLP) over Azores (subtropical high) and Iceland (polar low) (Charlery et al. 2006; Jury et al. 2007). Because the NAO is related to the surface pressure anomalies, each phase determines the strength and orientation of the pressure gradient over the North Atlantic. The pressure difference can be greater than 15 hPa, and it influences the speed and direction of both the westerly and trade winds over the North Atlantic Ocean (George and Saunders 2001; Hurrell 1995; Lamb and Peppler 1987). The NAO's amplitude and areal coverage are more pronounced during boreal winter (December–March), but it is evident in all seasons (Marshall et al. 2001).

The positive NAO phase, also known as high NAO, occurs when there is anomalously high pressure over Gibraltar and an anomalous low pressure over Iceland. With a stronger pressure gradient in the North Atlantic, the westerly winds are stronger (Hurrell 1995). Consequently, the trade winds originating in the subtropical high region, which is experiencing anomalous high pressure, are also stronger than normal, while they flow equatorward over the TNA. Therefore, a positive NAO enhances the wind-induced latent heat flux (pushing it far away from the TNA), resulting in lower SSTs and lower availability of atmospheric moisture content (George and Saunders 2001). The negative NAO has the opposite effect. These characteristics make the NAO the dominant mode of wintertime climate variability in the North Atlantic region, North America, Europe, and parts of Northern Asia. It is also one of the main drivers of precipitation over the Northern Hemisphere, and its effects extend as far south as southeastern Africa (Giannini et al. 2000; Jury et al. 2007).

Changes in North Atlantic SLP due to the NAO can affect Caribbean precipitation patterns both directly, by changing the patterns of wind flow over the region and creating anomalous subsidence, and indirectly, by changing the SST anomalies (Giannini et al. 2000; Giannini et al. 2001a). The displacement and strength of the high-pressure center and its associated winds during the winter affect the boreal spring and early summer SST anomalies in the tropical and mid-latitude North Atlantic (George and Saunders 2001; Malmgren et al. 1998). The indirect influences of the NAO on North Atlantic SST anomalies are important because they affect the amount of moisture available for evaporation, convection, and precipitation.

As the insular Caribbean is along a relatively land-free tropical ocean, changes in SST directly affects its source of moisture and seasonal rainfall patterns (Taylor et al. 2002). Therefore, the insular Caribbean is one of the areas of the globe most strongly affected by the NAO phases (George and Saunders 2001; Giannini et al. 2000; Jury et al. 2007; Malmgren et al. 1998). A link between the large-scale circulation and the extremely dry or wet periods in the Caribbean has been observed since the 1970s (Giannini et al. 2000), but analysis regarding the effect of NAO on insular Caribbean drought events is still needed.

The effects of the positive NAO on Caribbean precipitation patterns are most pronounced during boreal spring, at the start of the ERS (Giannini et al. 2001a). This is because the cooling of the TNA reaches maximum spatial coherence during spring, which is related to weaker convection and less precipitation in the Caribbean. The effect of the negative correlation between positive NAO and SST cooling persists from winter to the beginning of the ERS, which means that the impact on precipitation is strongest from May to June. The maximum values of negative correlation (on the order of 0.4 or greater) were found around 15°N, 60°W, east of Martinique (Giannini et al. 2000; Giannini et al. 2001c).

1.2.3 Physical geography and insular Caribbean water resources

The physical geography of the Caribbean islands – including the interaction of topography and climate on precipitation, runoff and storage – plays a large role in the availability of water resources. The second chapter in this dissertation focuses on low-frequency climate variability in the insular Caribbean. The third chapter turns the focus on the geomorphic and geologic characteristics that affect the water supply in the region.

The insular Caribbean is a mix of carbonate and volcanic islands. Some of the low-lying limestone islands, like the Bahamas, have had problems with availability and distribution of freshwater resources, because of the rapid infiltration of rainfall in the bedrock (i.e., no surface rivers draining the island), and the exaggerate usage and pollution of the groundwater (Cant 1996). Another water resource issue with carbonate islands is that the limited amount of freshwater at the surface, which is only exposed in lower altitude areas due to water table lying at or above sea level, are frequently hypersaline because evaporation exceeds precipitation. Therefore, these islands are particularly vulnerable to drought as rain water catchments and freshwater lenses in groundwater are the only options of water supply, and both are dependent on the rainfall recharge (Cant 1996; Falkland 1999).

Volcanic islands, on the other hand, normally have more surface water available than groundwater. However, the impacts of their watersheds by agriculture sedimentation and growing population have revealed the importance of the potential development of groundwater sources (Hendry 1996). In Grenada, as in most of the volcanic islands, the primary source of water supply comes from surface water, but groundwater sources have helped to augment surface sources during the dry season (UNDESA 2012). Volcanic islands' steep watercourses and abundant rainfall can allow them to have even some small-scale hydroelectric plants, such as in Dominica, which has a hydropower system that contributes to approximately 31% of effective capacity (Hendry 1996).

In Puerto Rico, which is the focus of Chapter 3, a mix of mountainous topography in the central and east and karst landscape toward the coastal area forms an island with both surface and groundwater water availability. Groundwater represents more than 20% of the water used in Puerto Rico (Dieter et al. 2018), and it becomes more important during drought events when surface water is unavailable (Mendez-Tejeda et al. 2016). The topography of the island also affects its rainfall pattern, allowing for orographic rainfall to occur on the windward side of the mountains while the leeward side is drier, with annual rainfall totals over the island ranging from 700 mm in the south to more than 4,000 mm in the east (Garcia-Martino et al. 1996; Hosannah et al. 2019). Moreover, the two major aquifers of Puerto Rico, the North Coast and the South Coast Aquifers, are mostly dependent on direct rainfall for recharge (Mendez-Tejeda et al. 2016), which make them vulnerable to drought events.

Therefore, the insular Caribbean geology and rainfall climatology led Cashman et al. (2010) to question how the seasonality of the rainfall and the physical environment are related to the ability of these islands to capture the water during rainy seasons and retain it available during dry seasons or drought events. Many of the islands in the Caribbean have already experienced problems in meeting water demand during some periods of the year, and the dry season can see reduction in available fresh water in excess of 40% (Cashman et al. 2010).

According to Farrell et al. (2010), the geology, topography, climate and the lack of economic diversity in the insular Caribbean make drought one of the most frequent climate hazards, resulting in economic losses and water shortages. Islands like Barbados and Antigua and Barbuda already rely on desalinization for their supply, while Grenada, St. Lucia, St. Vincent, Dominica, and the Grenadines have experienced water shortages and have had water shipped by the government (CEHI 2002; Durrant et al. 2007; USACE 2004). In addition, some studies indicated that future climate change is projecting a decrease in groundwater recharge in the insular Caribbean, which will affect groundwater supply and the ability to support current pumping regimes to meet water needs in the future (Holding et al. 2016).

1.2.4 Climate change impacts on the insular Caribbean

The Caribbean will be one of the regions to experience earliest and most severely impact of climate change during the 21st Century (Mimura et al. 2007; Pulwarty et al. 2010; Rhiney 2015). In addition to the current limitation of water resources in the insular Caribbean, many studies have indicated that climate change is making and will make the region warmer and drier. Studies have already shown that the percentage of days with very high temperature minima or maxima increased strongly since the 1950s, while the percentage of days with cold temperatures decreased (Bates et al. 2008; Peterson et al. 2002). Additionally, a negative trend in rainfall during the ERS and LRS started in the 1960s (Taylor et al. 2002).

According to the Intergovernmental Panel on Climate Change (IPCC) Fifth Assessment Report (AR5), projections for the Caribbean indicated both an increase in temperature of 1.2–2.3 °C by 2100, compared to a 1986–2005 baseline, and a decrease in precipitation of about 6%, which indicate potential problems for agriculture and water availability (Nurse et al. 2014). However, the projected changes in global climate by GCMs are not going to have a uniform impact across the Caribbean due to its difference in island size, topography, and population, as well as in its adaptative capacity and socio-economic conditions (Rhiney 2015).

Because the predictions of GCMs are coarse and generalized for the region, downscaled climate projections have been generated for Caribbean countries using the Hadley Centre PRECIS regional model. According to Rhiney (2015), the model projects a 1–5 °C increase in annual mean temperature for the Caribbean by 2080 (compared to a 1960–1990 baseline). The greater warming will occur in the northwest sub-region (Jamaica, Cuba, Hispaniola, and Belize) in comparison to the eastern Caribbean, and greater warming in the summer months than in the drier boreal winter months. A moderate decline in precipitation is expected across the northern Caribbean together with a greater variability (seasonal and inter-annual) and prolonged dry spells during the summer (Gamble and Curtis 2008; Rhiney 2015).

While the impacts of hurricanes receive more attention, drought is the focus of few studies in the Caribbean, despite the findings of drying trends from regional models (Bates et al. 2008).

However, predicted increases in temperature, decreased length of the rainy season, increased length of the dry season, more intense rainstorms, and increase in sea level could result in the reduction of the already scarce water availability in the Caribbean due to the increase of evapotranspiration rates, more flooding and aquifer depletion (reduced recharge), and salinity intrusion into groundwater and coastal aquifers (Ault 2016; Cashman et al. 2010; Farrell et al. 2010; Karnauskas et al. 2016; Pulwarty et al. 2010). The IPCC also highlighted that groundwater is slow-moving in most cases, which in drier conditions can result in reductions in groundwater reserves that could be irreversible due to their slow recovery capacity. Additionally, the projected drought and more frequent and intense hurricanes projected as part of climate change can cause loss of soil fertility and degradation, negatively impacting agriculture and food security in the Caribbean (Bates et al. 2008).

Studies have suggested that farming systems in the Caribbean are vulnerable to climate change, especially changes in temperature and precipitation, due to its relatively high dependence on rainfall (Bates et al. 2008; Cashman et al. 2010; Curtis et al. 2014). Impacts of a drier and warmer Caribbean climate can include, but are not limited to: reduction in plant-available moisture due to increased rates of evapotranspiration, increased spread of some pests and diseases, decrease in crop suitability, and increased stress on food productivity and sustainability (Cashman et al. 2010; Curtis et al. 2014; McGregor et al. 2009). For short rotation crops studied in Jamaica, drought and water deficits are major problems already affecting growth rate, fertilization, and yield (Rhiney et al. 2018). Other studies suggested that important crops such as coffee production would have an estimated reduction in up to 84% of highly suitable growing conditions in top producing municipalities in Puerto Rico by 2070 (Fain et al. 2018).

Finally, it is important to emphasize that agriculture was highlighted as one of the human systems most impacted by climate change at the community level (Robinson and Wren 2020). Results from the Fifth Assessment Report (AR5) of the Intergovernmental Panel on Climate Change (IPCC) confirmed that climate change will impact agriculture in the Caribbean mainly due to changes in surface temperatures and water availability, significantly impacting regional food security (Lincoln Lenderking et al. 2021).

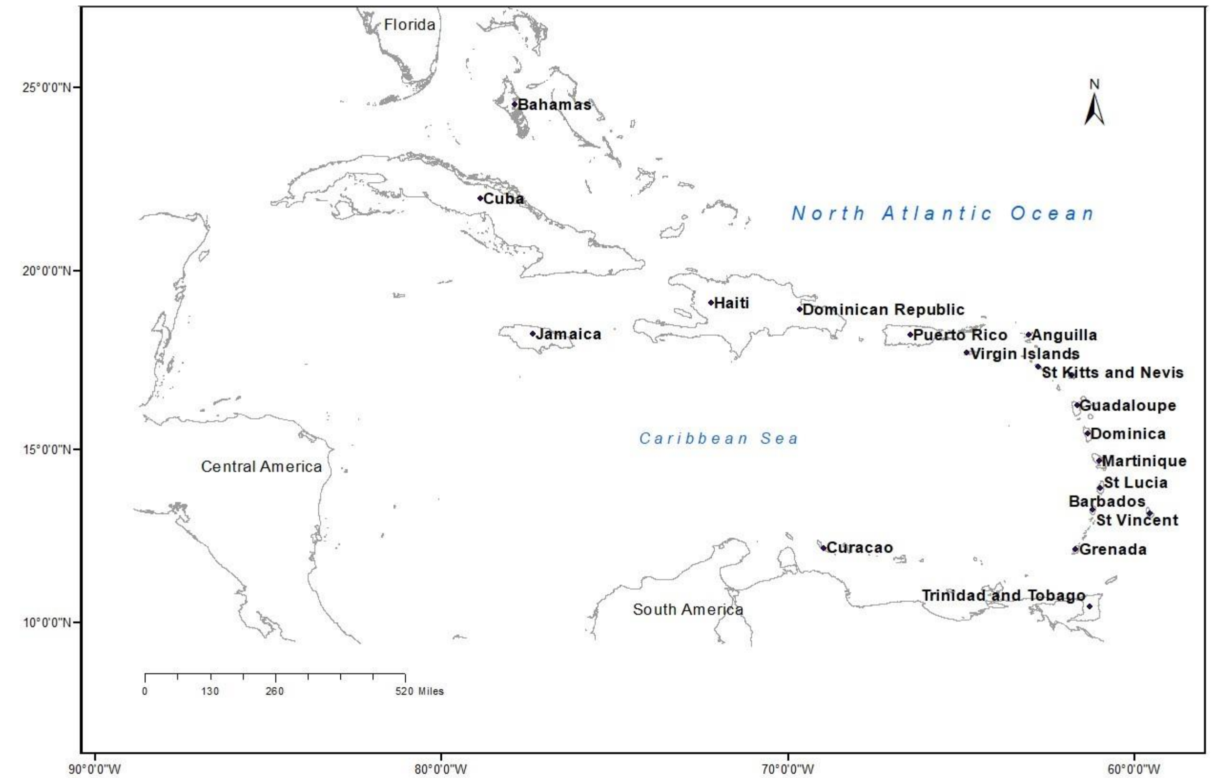

Figure 1.1 – The insular Caribbean location.

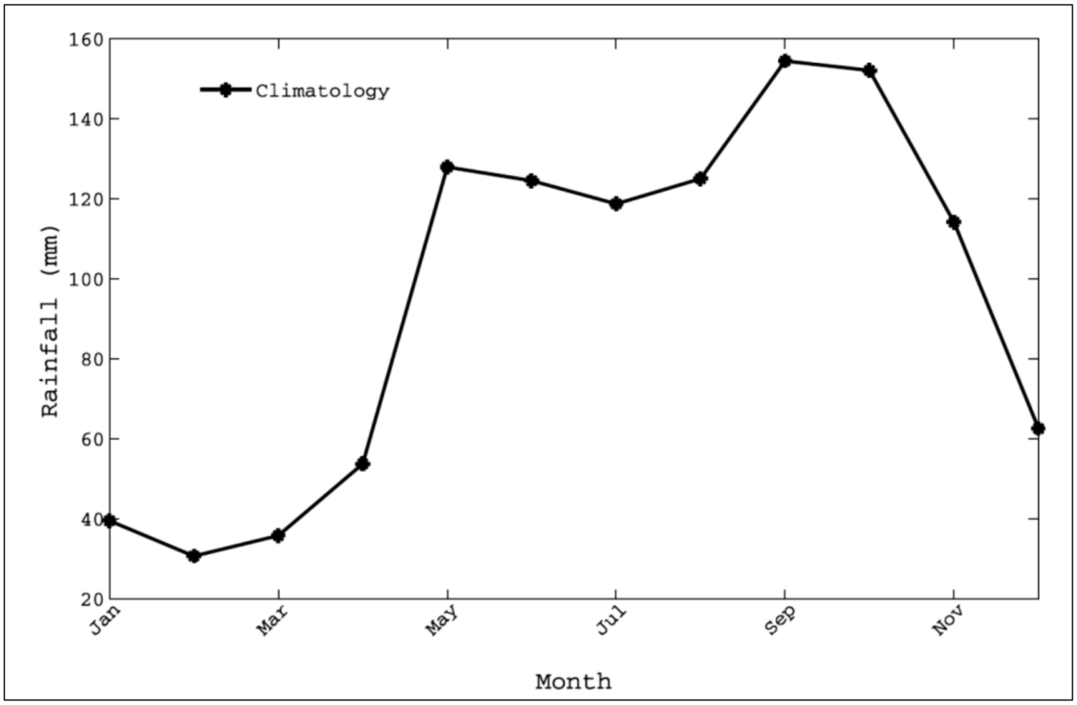

Figure 1.2 – Twenty-year monthly mean Caribbean precipitation climatology (1983–2004). Source: Angeles et al. (2010).

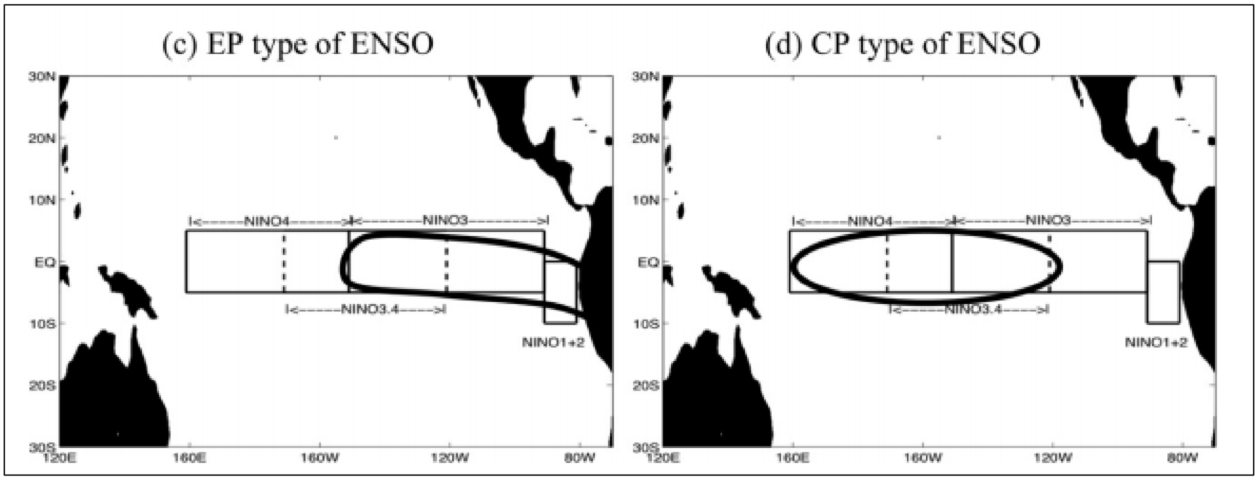

Figure 1.3 – A map of the equatorial Pacific Ocean and the different Niño regions (source: Kao and Yu (2009)**,** Figure 1 c) and d)). The authors reference the Niño 1+2 and 3 regions (left panel) as the location of anomalies associated with EP ENSO events. To describe the pattern of CP ENSO, the Niño 3.4 and 4 regions are used (right panel).

2 LOW-FREQUENCY OCEAN-ATMOSPHERE VARIABILITY AND DROUGHT IN THE INSULAR CARIBBEAN [1]

[1] Moraes, F.D.S, T. Mote, and L. Seymour. Low-Frequency Ocean-Atmosphere Variability and Drought in the Insular Caribbean. To be submitted to *International Journal of Climatology*.

Abstract

The insular Caribbean experiences numerous climate and environmental hazards, including but not limited to hurricanes, floods, earthquakes, volcanic eruption, and drought. While some hazards are well explored in scientific literature, such as hurricanes, drought is considered one of the neglected hazards because of the lack of studies focusing on its causes and effects. This study identifies the spatial distribution of seasonal drought in insular Caribbean from 1950–2017, and its relationship with Eastern Pacific (EP) and Central Pacific (CP) ENSO, North Atlantic Oscillation (NAO), and Atlantic Meridional Mode (AMM). It brings a new perspective over the region by dividing the Caribbean into Greater Antilles and Bahamas (GA), and the Lesser Antilles (LA) to compare the role of those three teleconnection patterns on drought events over larger versus smaller islands. We used an existing high-resolution drought atlas (4 km) based on monthly estimates of the self-calibrating Palmer Drought Severity Index (scPDSI). Results indicate that there is a drying trend in all seasonal-average scPDSI for both the GA and the LA, but more intense and frequent drought events occur in the LA. The LA is also the region with more widespread drought events, registering 12 years when the mid-summer dry spell (MSD, July–August) had drought ≥ 80% of the area, while the GA registered only two years of MSD that extensive. The peak season AMM had the strongest positive correlation with both GA and LA drought during April–November, while the NAO is slightly stronger correlated with GA than with LA from July–November. For ENSO, CP El Niño years related stronger with drought in the LA from December–July, while the relationship between the two types of ENSO and the GA is not statistically significant. This effort aims to improve drought regional forecasts to help the region to better prepare for the prediction of seasonal droughts.

2.1 Introduction

The insular Caribbean is located in the western Tropical North Atlantic (TNA), between approximately 10°N and 25°N, and 90°W and 60°W, forming an archipelago extending southeastward in an arc between Florida and eastern Venezuela. Because the annual range of temperature is not large in these tropical islands (from 1.9°C in Trinidad to 5.5°C in Cuba), rainfall is the characteristic which determines seasonality (Granger 1996). Four common seasonal precipitation patterns are evident in the region. The boreal winter (December–March) has the absolute minimum precipitation, referred to as the dry season (DS) (Giannini et al. 2001a; Jury et al. 2007). The two rainy seasons are called the early rainfall season (ERS, April–July) and late rainfall season (LRS, August–November) (Angeles et al. 2010; Gamble and Curtis 2008; Taylor et al. 2002). The end of the ERS and the beginning of the LRS is separated by a relative minimum in rainfall that occurs annually during the summer (July–August) and is known as midsummer dry spell (MSD) (Allen et al. 2010; Gamble et al. 2008; Magaña et al. 1999). However, MSD does not explicitly refer to drought conditions in the Caribbean but instead refers to a period of decreased precipitation.

The seasonality evident in Caribbean precipitation climatology is a consequence of the location of the Caribbean and the atmospheric dynamics of the region. The insular Caribbean is centered between the North Atlantic subtropical high (NAHP) and the Intertropical Convergence Zone (ITCZ). The presence of this subtropical high helps to maintain easterly winds, and the Caribbean lies in the main current of the trade winds, while the movement of the ITCZ also governs the precipitation distribution (Granger 1985). When the TNA sea surface temperature (SST) presents an extensive warm pool, it also affects the precipitation pattern of the two rainy seasons (ERS and LRS) in the insular Caribbean (Taylor et al. 2002). On the other hand, in some regions of the Caribbean there is a period during the summer when the Bermuda High strengthens and dramatically decreases rainfall (Granger 1985).

Among the characteristics that affect the spatial and temporal variability of rainfall are a small number of low-frequency modes of variability known as teleconnections, which explain much of the overall variability in atmospheric pressure. Teleconnections are large-scale spatial and temporal anomalies that appear as preferred modes of low-frequency (inter-annual, decadal, multidecadal) natural variability in the atmospheric circulation. Each teleconnection pattern has geographically fixed centers of action or “poles” (Hatzaki et al. 2007). Most importantly, teleconnections influence the variability of atmospheric pressure and wind (i.e., circulation).

In the insular Caribbean, previous studies have discussed the relationship between precipitation and well-known teleconnection patterns. Among the teleconnections most commonly examined are El Niño Southern Oscillation (ENSO), the North Atlantic Oscillation (NAO), and the Atlantic Meridional Mode (AMM) (George and Saunders 2001; Giannini et al. 2001b; Malmgren et al. 1998; Ropelewski and Halpert 1987; Smirnov and Vimont 2011). ENSO is a coupled atmosphere-ocean pattern identified by anomalies in SST in the equatorial Pacific Ocean and in sea-level pressure between west and east Pacific Ocean, which starts around December (Trenberth 1997). Early research found that most often SST anomalies were the strongest in the Eastern Pacific (EP) Ocean close to the South American coast (Cane 1983), and in time this region (the Niño 3 region as it came to be known) became the one used by many scientists when discussing ENSO (Giannini et al. 2001b). As more research regarding ENSO emerged, studies found that at times the SST anomalies occurred closer to the Central Pacific (CP). Therefore, a consensus on two different types of ENSO has emerged known as EP and CP ENSO (Capotondi et al. 2015; Kao and Yu 2009; Mo 2010).

The NAO is defined and calculated by the difference between the normalized sea level pressures (SLP) over Gibraltar (subtropical high) and Iceland (polar low) (Charlery et al. 2006; Jury et al. 2007). Because the NAO is related to the surface pressure anomalies, each phase determines the strength and orientation of the pressure gradient over the North Atlantic. The pressure difference can be greater than 15 hPa, and it influences the speed and direction of both the westerly and trade winds over the North Atlantic Ocean (George and Saunders 2001; Hurrell 1995; Lamb and Peppler 1987). The AMM, on the other hand, is defined as the meridional gradient in SST near the ITCZ (Vimont and Kossin 2007). In a negative AMM event, cold SST anomalies occur in the TNA, warm SST anomalies in the Tropical South Atlantic (TSA), anomalously high northeasterly surface wind speeds in the TNA, and the ITCZ shifts to south of the Equator (Rugg et al. 2016).

The effects of these teleconnection patterns in the insular Caribbean rainfall have a regional variation. Overall, there is tendency for the Caribbean to be drier than normal during years of EP El Niño (i.e., an ENSO warm event) during the LRS, while the ERS can register positive SST anomalies that could result in more convection and rainfall (Giannini et al. 2001b; Jury et al. 2007; Ropelewski and Halpert 1987). To the best of our knowledge, the effects of CP ENSO have not been explored in the insular Caribbean.

A positive NAO is also related to drought in the insular Caribbean, but this normally occurs during boreal spring, at the start of the ERS, with the strongest correlation registered around the eastern Caribbean (15°N, 60°W) (George and Saunders 2001; Giannini et al. 2000; Giannini et al. 2001c; Malmgren et al. 1998; Mote et al. 2017). Previous literature reveals that relatively little is known about the AMM connection to precipitation in the Caribbean, with most studies suggesting a relationship between positive AMM and tropical cyclone activity, but concluding that the AMM by itself is not enough to explain seasonal Atlantic tropical cyclone variability (Patricola et al. 2014; Smirnov and Vimont 2011; Vimont and Kossin 2007).

Although the effects of these atmospheric circulation patterns on precipitation point to the potential for drought to affect the insular Caribbean, few studies have focused on drought hazards. Drought is considered as one of the neglected climate hazard in the insular Caribbean (Gamble 2014), although regional models predict that a warmer planet (~2 °C) will increase freshwater stress by 25% at 2030 as a consequence of longer-lasting and more severe drought events in the Caribbean (Cashman et al. 2010; Karnauskas et al. 2018). A gradual drying trend has been already registered since 1950 (Herrera et al. 2018).

Therefore, there is a need to further investigate drought in the insular Caribbean and to understand how drought is related to climate variability. This study intends to indicate regions and periods when the insular Caribbean had drought events occurring from 1950–2017. After analyzing the distribution of drought, this work examines when and where EP and CP ENSO, NAO, and AMM are most related to drought events in the insular Caribbean. This work is unique because it analyzes the two ENSO types, NAO, and AMM together and against a drought metric, instead of precipitation data. The focus on drought metric and teleconnections should indicate the role of these low-frequency atmospheric circulation variability in affecting the balance between the variables used to estimate drought, such as precipitation, soil moisture and evapotranspiration. Because drought events are expected to be more severe and affect water availability in the Caribbean, understanding this relationship is important. Additionally, this study assesses the role of CP and EP ENSO in the insular Caribbean drought, as well as divides the region into western Caribbean (Greater Antilles and Bahamas) and eastern Caribbean (Lesser Antilles) to compare how drying trends are affecting larger versus smaller islands in the Caribbean.

2.2 Data and Methods

2.2.1 Defining drought in the insular Caribbean

Drought is considered a normal feature of climate and is linked to physical conditions of negative anomalies of moisture levels, which could be deficits of precipitation, streamflow or groundwater, or low soil moisture compared to their expected normal values (Gamble 2017; Pandey et al. 2010). Previous studies vary significantly regarding the methods they use to define drought, with some focusing more on meteorological drought, while others mixed one or two types of droughts (e.g. hydrologic, agricultural, and socioeconomic droughts) (Gamble 2017; Wilhite 2000).

One of the most prominent and extensively used indices of drought is the Palmer Drought Severity Index (PDSI), which was created to quantify the cumulative departure in atmospheric moisture supply and demand at the surface by using surface air temperature and precipitation as input (Dai et al. 2004). In this study, we use the high-resolution drought atlas (4 km), created by Herrera and Ault (2017), based on monthly estimates of the self-calibrating PDSI (scPDSI). scPDSI retains the essential components of PDSI, based on the amount of actual precipitation and the amount of precipitation required to result in a normal water-balance. However, the “self-calibrating” version proposed by Wells et al. (2004) and used by Herrera and Ault (2017) does not use empirically derived climatic characteristics and duration factors, but values automatically calculated based upon the historical data of a location. Additionally, the Penman-Monteith method used to estimate evapotranspiration in the scPDSI is an approach considered more physically realistic than the Thornthwaite equation normally used in the PDSI (Herrera and Ault 2017; Smerdon et al. 2015; Van der Schrier et al. 2013; Williams et al. 2015). At least eight different datasets were used to downscale all the products (precipitation, temperature, cloud cover, wind speed, elevation, and available water holding capacity) to 4 km resolution and find which the dry years were in the area of study (for more detailed methodology see Herrera and Ault, 2017).

Because the drought atlas contains information from Florida Peninsula, Central America, northern South America, and the insular Caribbean, we subset the area to focus on the insular Caribbean only. Within the insular Caribbean, we divided the region into two subregions: The Bahamas and Greater Antilles (Cuba, Dominican Republic, Haiti, Jamaica, and Puerto Rico) here called the GA, and the Lesser Antilles (smaller islands from the U.S. Virgin Islands to Trinidad and Tobago) here called the LA (see GA and LA location in figures 2.3 and 2.4, respectively). This allowed us to compare drought patterns between the western and larger islands versus the eastern and smaller islands in the insular Caribbean.

Within the subregions, we used the United States Drought Monitor categories to indicate the severity of drought of the scPDSI: abnormally dry (-1.0 to -1.9), moderate drought (-2.0 to -2.9), severe drought (-3.0 to -3.9), extreme drought (-4.0 to -4.9), and exceptional drought (-5.0 or less). The seasonal average percentage of grid cells with scPDSI $\leq$ -1 were calculated to visualize which drought events are local or region-wide spread considering each subregion. To help with the visualization of when and where drought was more severe and spatially distributed within each subregion, we created seasonal composites of scPDSI of the 5 years with greater percentage of grid cells with scPDSI $\leq$ -1. This threshold was established to consider only the top years when the subregions were having at least an abnormally dry event. Time series graphs showing seasonal average scPDSI also help to understand the temporal distribution of drought, while a linear regression model was employed to detect positive or negative trends of scPDSI in the GA and the LA. Finally, cross-correlation between the scPDSI in the GA and LA was performed to assess if there were cyclical patterns in drought events between the two subregions.

2.2.2 Assessing the relationship between drought and teleconnection patterns

After defining drought events in the insular Caribbean, we analyzed the relationship between the scPDSI and the NAO, the AMM, and the two types of ENSO (EP and CP). We used the Oceanic Niño Index (ONI) (Huang et al. 2017) to identify ENSO events on the basis of the Climate Prediction Center (CPC) definition: a threshold of ±0.5°C of the 3-month running mean of SST anomalies for five consecutive overlapping seasons. We defined as EP ENSO events when the SST anomalies occurred in the Niño 1+2 and Niño 3 regions, and as CP ENSO events when the anomalies occurred in the Niño 3.4 and Niño 4 regions as defined in previous studies (Capotondi et al. 2015; Kao and Yu 2009). The index used for NAO is also from CPC and is based on pressure, height, and temperature anomalies from 1981–2010 mean, between Greenland and the Azores. The combination of these factors produces an index of monthly numerical values from 1950–2020. Because the AMM is primarily based on SST, the index we used in this study are SST anomalies from the region 21°S–32°N, 74°W–15°E. These are monthly anomaly values from a 1950–2005 baseline, for a 1948–2020 period of record.

Empirical Orthogonal Functions (EOF) are used to understand the patterns of variability of the Pacific and Atlantic Ocean during the period of analysis of drought events in the insular Caribbean (1950–2017). EOF is the method used to represent the maximum variance of the data in a minimum number of new variables, which are the EOFs. For each EOF, a dimension of the relevance is indicated (Björnsson and Venegas 1997; Jury et al. 2007). This work used the "eofs" library available for Python (Dawson 2016), with monthly mean values of the Extended Reconstructed Sea Surface Temperature (SST) V5 from the National Oceanic and Atmospheric Administration (NOAA) averaged by seasons (December–February and March–May) and used as the SST input data. The EOF finds both time series and spatial patterns, being the patterns normally referred to as “EOFs” or “principal components loading patterns”, and the time series as “EOF time series” or “principal components” (Björnsson and Venegas 1997). In this work we will refer to the spatial patterns as the EOFs and the time series as EOF time series.

A Pearson’s correlation analysis investigated the relationship between each one of these teleconnection indices during their peak season, here defined based on previous studies as December–February for EP/CP ENSO (Capotondi et al. 2015), January–March for NAO (Marshall et al. 2001), and March–May for AMM (Foltz et al. 2012), and seasonal average scPDSI (DS, ERS, MSD, and LRS) for both the GA and the LA. In order to investigate the combined effects of those three teleconnections with seasonal scPDSI, we created a regression model for the LA and the GA and the appropriate lagged atmospheric oscillation index. The seasons analyzed in the model excluded the MSD because we would need to treat July and August as their own season so that the regression parameters for the seasons would be identifiable (Casella and Berger 2021). For trend analysis, a linear regression model was performed for each teleconnection index and the scPDSI to analyze if they have positive/negative signs that, when combined, could suggest a tendency for the occurrence of more or less drought events.

Finally, seasonal composites of sea level pressure (SLP), vector wind (700 hPa winds), and precipitable water (PW) anomalies were created for years when seasonal average scPDSI was ≤ -1 for the GA and the LA to understand the potential forcings those variables have on drought events. SLP composites anomalies are used to show the phase of NAO, while 700 hPa winds and PW anomalies are analyzed as proxies of the Saharan Air Layer (SAL), to understand if there is any influence on seasonal drought from earlier than normal dust intrusion into the insular Caribbean. SAL events reaching far west normally peak from late June to mid-August as an intrusion of hot, dry air in the low to middle troposphere (around 700 hPa), producing thermodynamically stable conditions and limited rainfall in the insular Caribbean (Dunion 2011; Miller and Ramseyer 2020; Mote et al. 2017).

2.3 Results and Discussion

The results and discussion will start with the analysis of the spatial and temporal distribution of drought (section 2.3.1), followed by the analysis relating drought events and the teleconnections patterns (section 2.3.2). The word "dry" is used here to describe more negative scPDSI values.

2.3.1 Drought in the insular Caribbean

When comparing the seasonal average scPDSI, from 1950 to 2017, a drying trend was evident (Figure 2.1). All seasons for both the GA and the LA presented a negative trend for average scPDSI, indicating a drier trend in the entire region. The 2015 drought event was the most intense drought year for all seasons in GA (Figure 2.1a,b,c,d), and 2015–2016 was the most intense drought years for all seasons in LA (Figure 2.1e,f,g,h). Among the seasons, the typical seasonal cycle in average negative scPDSI during the climatology period of 1981–2010 (Figure 2.2) indicated that negative scPDSI was more intense in the LA than in the GA over all the seasons. The ERS was the least dry season in which both regions registered the least negative average scPDSI values in April. On the other hand, the LRS was the driest in both regions with peak negative scPDSI values occurring in August for the LA and in October for the GA (Figure 2.2). The LRS also had more drought events (scPDSI $\leq$ -1.0) registered in both the LA (22 years) and the GA (16 years), as well as it is the season that had the more negative average scPDSI for the LA during the intense drought event of 2015 (-5.3, exceptional drought). For the GA, on the other hand, the 2015 drought registered the more negative average scPDSI during the MSD (-4.1, extreme drought). This suggests a temporal shift in peak drought conditions during the 2015 drought across the domain. Additionally, the seasonal mean scPDSI indicated that from 1950 to 2017 the LA registered on average 18.7 years of seasonal drought while the GA had an average of 11.5 years of seasonal drought. Therefore, the scPDSI data show that more *intense* and *frequent* drought events occurred in the LA.

The LA also had more *widespread* drought events. Figure 2.3 shows the seasonal percentage of grid cells with negative scPDSI (≤ -1.0) for each subregion. Overall, both subregions presented a positive linear trend in their percentage of grid cells with negative scPDSI during all seasons, indicating an increase in the spatial distribution of drought events over time. However, when comparing both the GA and the LA distribution of seasonal drought, the LA registered 12 years when its MSD has drought ≥ 80% of the area, while the GA registered only two years of its MSD meeting this criterion (Figure 2.3). Although both the GA and the LA registered their greatest number of years with the most widespread drought events (≥ 80% of the area) during the MSD, the LA had six times more years with widespread drought than the GA during this season. One of the reasons for this different drying could be related to the difference in physical geography of these subregions, since the lower relief environment of the LA are less able to modify prevailing winds and lift maritime moisture to the condensation level to develop local storms (Gamble 2004; Granger 1985). Another possible explanation for the difference in the extent of drought events could be the number of stations used as input for precipitation data within the scPDSI calculation. For many of the smaller islands, there are normally less observing stations, which result in less spatial heterogeneity drought index results when compared to larger islands such as Hispaniola and Cuba, which have more reporting stations. However, during the 2015–2016 drought, considered the most intense and widespread drought over the insular Caribbean (Herrera et al.

2018; Mote et al. 2017), the difference in area between the GA and the LA has not impacted the percentage of the area affected. The GA had 95% of its area with at least abnormally dry conditions during the ERS, MSD, and LRS (Figure 2.3c,e,g), while the LA had 100% of its area in the same conditions in the LRS, 97% in the MSD, and 91% in the ERS (Figure 2.3d,f,h).

Previous studies have already demonstrated a drying trend in the Caribbean since 1950, with a rate of -0.09 scPDSI units per decade, together with several multiyear droughts (Herrera and Ault 2017; Herrera et al. 2018). This work confirms that trend but also demonstrates a seasonal trend, as well as a trend toward more widespread drought. Here we show that all seasons presented a negative scPDSI trend both in the GA and the LA islands, and that the percentage of area with at least abnormally dry conditions is increasing over the region for all seasons since 1950.

The seasonal composites of the five years with the greatest percentage of negative scPDSI (≤ -1.0) for the GA (Figure 2.4) and for the LA (Figure 2.5) also indicated that the LA had the more widespread and more intense drought events. While the five years with most widespread drought range from 60%–95% of the area in the GA, the LA registered 83%–100% of the area with spatially distributed drought. Figure 2.4 shows that the most intense drought events in the GA occur during the LRS (Figure 2.4d) with moderate drought (-2.0 to -2.9) over eastern-central Puerto Rico and Cuba, northern Jamaica, and most of Hispaniola and Bahamas; severe drought (-3.0 to -3.9) in parts of Cuba, Bahamas and central Hispaniola; and extreme drought (-4.0 to -4.9) in the border between Haiti and Dominican Republic. Figure 2.5(d) also shows the LRS as the period with most intense drought for the LA. However, the drought events in the LA were more intense than in the GA, with the southern islands (from St Lucia to Grenada) registering an exceptional drought (-5.0 or less) ranging from -7.0 to -9.0 scPDSI.

Several studies have already highlighted the 2015–2016 drought event in the Caribbean as the most severe in the region, with record-low reservoir and river levels, millions of people facing food insecurity due to crop loss (Herrera et al. 2018; Mote et al. 2017; OCHA 2015). On top of the current drying trend in the Caribbean, studies have projected increases in temperature and decreases in precipitation over the region that can result in more drought events and may affect water availability (increased risk of water stress) as well as local agriculture and food supply (Hayhoe 2013; Karnauskas et al. 2018; Ramseyer and Mote 2018).

When analyzing the yearly average scPDSI for the GA and the LA together (Figure 2.6a) it is possible to see that the magnitude of the scPDSI was greater for the LA than the GA for almost all years, confirming the seasonal climatology pattern discussed before, while it seems that both dry and wet annual spells occurred first in the GA. This lagged relationship is confirmed in the cross-correlation analysis between GA and LA yearly average scPDSI (Figure 2.6b), which showed a negative one-year significant correlation between GA and LA, indicating that a wet or dry period occurred in the GA a year in advance and then it was likely to occur in the LA the next year with the same sign (Figure 2.6c). Although the reasons on why the GA presented dry or wet periods before they occurred in the LA should be further investigated, this could be aligned with the spatial differences between the seasonal cycle of rainfall in the region discussed by Martinez et al. (2019). The authors indicated that in the northwestern Caribbean a stronger ERS, weaker and early-peaking LRS occurred, while a weaker ERS, stronger and late-peaking LRS occurred in the southeastern Caribbean, reinforcing the lag in rainfall patterns among the regions.

2.3.2 Teleconnection patterns and drought in the insular Caribbean

In this section we analyze the relationship between EP and CP ENSO, NAO, and AMM with seasonal drought in the insular Caribbean, by examining the spatial variability of SST in the

Pacific and in the Atlantic through EOF analysis and its correlation with seasonal drought events in the LA and the GA. Finally, we focus on drought events only and analyze the spatial patterns of SST, SLP, 700 hPa winds, and PW composites during these events in the insular Caribbean.

2.3.2.1 EOF, correlation, and trend analysis

An EOF analysis using SST data as input was performed to understand the spatial variability of SST in the Pacific and in the Atlantic from 1950 to 2017. In order to depict ENSO-patterns and AMM-patterns in SST variability, we run the SST EOF for the Pacific basin during ENSO peak season (December–February), and for the Atlantic basin during AMM peak season (March–May).

The December–February SST EOF analysis for the Pacific resulted in three EOFs that together explained almost 60% of the variance in SST (Figure 2.7a,b,c). When analyzing the spatial patterns of SST from each EOF, we see that EOF1 presented an ENSO-like pattern that is spread over the equatorial Pacific and could be interpreted as a combination of EP and CP ENSO, but with a stronger pool in central Pacific. The EOF2 suggested a weak CP ENSO pattern, while EOF3 could be interpreted as EP ENSO pattern, but shifted to the south. However, when comparing the EOF time series and the EP and CP ENSO indices, only the EOF1 time series could represent ENSO events by aligning with December–February CP and EP ENSO indices (Figure 2.7d). The correlation between this wintertime SST EOF1 time series and seasonal scPDSI from the GA and the LA also confirmed the stronger relationship with regional drought index, mainly in the LA. There was a negative correlation between EOF1 time series and all seasonal mean scPDSI in the LA, with stronger correlations for DS (-0.5) and ERS (-0.4) at 95% level. This means that when the ENSO warm events peak in December–February, the LA is more likely to have drought events in the first half of the year, but it can be extended to the entire year. For the GA, on the other hand, the correlation with EOF1 time series was weak (ERS 0.2, and MSD 0.1) and it was not statistically significant (p-value ≥ 0.05). Because both EP and CP ENSO are highly correlated with each other and with the EOF1 time series, it is not clear which type of ENSO was more correlated with drought in the Caribbean. Therefore, a more detailed correlation isolating each ENSO index will be discussed below.

In the Atlantic basin, the March–May SST EOF analysis also presented three main EOFs that together could explain most of the variance (55%). Among the three EOFs, EOF2 resembled the AMM SST pattern (Figure 2.8a,b,c). The EOF2 time series was also the only one that aligns with the AMM index, but with the opposite sign. This means that a positive AMM index has a negative EOF2 time series normalized value (Figure 2.8d,e). The correlation between EOF2 time series and the LA and the GA scPDSI seasonal mean was also the strongest for all seasons at 95% level and has the same sign for both regions. In the GA, a negative correlation ranged from -0.4 in the ERS to -0.5 for MSD and LRS seasons, while in the LA the negative correlation ranged from -0.5 in the ERS to -0.7 in MSD and LRS. Considering the flipped sign between the EOF2 time series and the AMM index, a negative correlation means that a negative AMM in the peak season was strongly related to drought in the GA and the LA from April to November.

Because the EOF SST analysis did not include patterns that indicate NAO, which is primarily an atmospheric phenomenon, and could not isolate EP ENSO from CP ENSO, we ran the Pearson's Correlation between each teleconnection index three-monthly running mean with seasonal average scPDSI (DS, ERS, MSD, LRS) for the GA and the LA (Table 2.1) to analyze when they were strongly correlated. The peak seasons of AMM (March–May), NAO (January–March), and EP-CP ENSO (December–February) were better correlated with seasonal scPDSI in LA and GA, in general, as we will discuss next.

Considering the EP and CP ENSO peak season relationship with seasonal drought events, the LA showed stronger and significant negative correlation coefficient with peak season CP ENSO during the DS (-0.5) and ERS (-0.4), as well as with EP ENSO during DS (-0.4) and ERS (-0.3) (Table 2.1). On the other hand, the GA presented only a weak positive correlation with CP ENSO during ERS (0.2) and MSD (0.2), but they were not statistically significant (p-value $\geq$ 0.05). The only period when GA's correlation with ENSO was statistically significant was during September–November EP and CP ENSO phase and the LRS (-0.3), indicating that while ENSO warm phase is developing in the Pacific, the LRS had negative scPDSI in western Caribbean. Therefore, peak season ENSO warm events in EP and CP can be related to drought events in the LA during the first half of the year, but not with the GA drought events.

Considering that the correlation values between peak season CP ENSO and the LA and the GA seasonal scPDSI are similar to the values from the December–February EOF1 analysis, we can state that ENSO events occurring in the CP region were more closely related to drought events in the eastern Caribbean. Although some studies have indicated the possibility of an increase in precipitation in the Caribbean during the ERS of ENSO warm event years (Giannini et al. 2001b; Jury et al. 2007), others have found the stronger negative relationship between boreal wintertime ENSO and rainy season in the Caribbean, which could result in lower frequency of hurricanes (Herrera and Ault 2017; Patricola et al. 2014; Taylor et al. 2002). The results found here showing stronger negative correlation between ENSO and the first half of the year average scPDSI could reinforce the indication that strong ENSO warm event years, such as 2015, can be related to severe and widespread drought in the eastern Caribbean during the beginning of the rainy season (Herrera et al. 2018; Mote et al. 2017).

For the NAO index, the relationship with GA was stronger than with the LA. The negative correlation between the NAO and the seasonal average scPDSI in the GA was stronger during MSD (-0.4) and LRS (-0.5), meaning a positive NAO phase during the boreal winter can be related with drier than normal July–November (Table 2.1). Although the GA presented significant negative correlation coefficients over all seasons with NAO (p-value ≤ 0.05), they were weaker (-0.3) during DS and ERS. The LA also had significant negative correlation with NAO occurring in the second half of the year, during MSD (-0.3) and LRS (-0.4). However, the relationship between the LA and NAO was slightly weaker than with CP ENSO (Table 2.1). This weaker relationship between the NAO and LA drought is an interesting finding because previous studies have suggested the region as one of the areas with stronger relationship between NAO and precipitation (George and Saunders 2001; Giannini et al. 2000; Giannini et al. 2001c; Jury et al. 2007).

The highest correlation for both subregions was with the AMM index, when all seasons had statistically significant correlation (p-value ≤ 0.05), reinforcing what was found in the EOF analysis discussed above. The GA presents a similar positive correlation coefficient with AMM all over the seasons, from 0.4 in ERS to 0.6 in LRS. The LA, on the other hand, presented a larger positive correlation coefficient during the second half of the year (0.6 for both MSD and LRS), while the correlation for ERS was 0.3 (Table 2.1). A positive correlation between the seasonal average scPDSI and the peak season AMM indicates that a negative phase AMM is related to drying in the insular Caribbean.

The relationship between peak season negative AMM and April–November drought events in the insular Caribbean is also an important finding, because most of the studies have focused on relating the effects of AMM with hurricane development during the LRS (Patricola et al. 2014; Smirnov and Vimont 2011; Vimont and Kossin 2007). Although not focusing on drought in the

Caribbean, some studies have discussed the role of mixed layer dynamics and how strong AMM events are related with stronger NE trade winds and the strengthening of NAHP resulting in SST anomalies of 1°C colder than normal and the southward shift of the ITCZ (Foltz et al. 2012; Rugg et al. 2016). Therefore, they have highlighted important features that are already known for being related to dry periods in the Caribbean (Allen et al. 2010; Angeles et al. 2010; Gamble 2014; Gamble et al. 2008; Ramseyer and Mote 2016, 2018).

In Figure 2.9 we present the time series with linear trend for all the teleconnection indices peak season averages. For both EP and CP ENSO (Figure 2.9 a,b) the linear trends are positive, indicating a trend for El Niño/ENSO warm years. According to the correlation analysis, more ENSO warm events could indicate more drought events during DS and ERS in the LA (Table 2.1). For the GA, on the other hand, more ENSO warm events could mean less drought events in ERS and MSD. The NAO (Figure 2.9c) also presented a positive trend. Because positive NAO was related to drought in both the GA and the LA, this suggests we could have more drought events occurring in MSD and LRS in both subregions. The AMM is the only index that presented a negative trend (Figure 2.9d). Given that negative AMM was related to negative scPDSI, this trend also points to more drought events in both GA and LA, mainly during MSD and LRS.

2.3.2.2 The combined impacts of teleconnections on Caribbean scDPSI

In addition to the analysis of the individual relationship of each teleconnection peak season and the seasonal scPDSI, it is important to analyze the combined effects of ENSO, AMM, and NAO on insular Caribbean scPDSI. After performing cross-correlation tests to assess the significant lag correlation between each teleconnection and the seasonal scPDSI, we run the regression model with the appropriate lag. Because the overall CP ENSO correlations structure with both LA and the GA seasonal scPDSI was much weaker, it was not included in the model.

We found that the combination of all teleconnections with the GA seasonal scPDSI resulted in significant EP ENSO lag of 14 months with a positive trend of 0.080, NAO lag of 4 months with a negative trend of -0.014, and AMM lag of 2 months with a positive trend of 0.030. For the LA seasonal scPDSI, the model indicated a significant NAO lag of 10 months with a negative trend of -0.015, AMM lag of 3 months with a positive trend of 0.058, and EP ENSO lag of 4 months with e negative trend of -0.166. These results suggest that for both subregions the EP ENSO had the strongest relationship in the presence of everything else for both subregions, followed by the AMM, and then the NAO. Therefore, the significant relationship within the regression model for the GA started with a negative EP ENSO 14 months before the drought event, followed by a positive NAO 4 months before drought, and a negative AMM 2 months before drought. In the LA, a positive NAO started 10 months before the drought event and was followed by a positive EP ENSO 4 months before drought and a negative AMM 3 months before drought.

The combined effect of the lagged correlation between these three teleconnection patterns and drought in the insular Caribbean is a unique finding because it indicates the most significant timing in which each atmospheric variability pattern can affect the Caribbean drought index in case they occur together. We have not found other studies investigating ENSO, AMM, and NAO together with Caribbean drought, but only studies focusing on the impacts of the combination of two of these teleconnections in the Caribbean rainfall (Giannini et al. 2001a; Giannini et al. 2001b; Huang et al. 1998; Jury et al. 2007; Malmgren et al. 1998; Patricola et al. 2014).

2.3.2.3 SLP, 700 hPa winds, and PW composites

Besides the analysis of the relationship between the teleconnection patterns and the seasonal scPDSI, it is also important to investigate patterns of SLP, 700 hPa winds, and PW occurring during or previous to the GA and the LA drought events. Some studies have already indicated the relationship between some of these features and drought events in the Caribbean islands (e.g., (Mote et al. 2017), due to the intrusion of the SAL. In this study, we analyze the seasonal composites of SLP, 700 hPa winds, and PW when seasonal average scPDSI was ≤ -1, which means the Caribbean has registered at least an abnormally dry event.

Figure 2.10, Figure 2.11, and Figure 2.12, show seasonal composites of SLP, 700 hPa winds, and integrated PW for years when the LA and the GA registered seasonal scPDSI ≤ -1. For each seasonal drought period, we created composites correspondent to December–March and March–May periods, in case these periods precede and/or are coincide with the season being analyzed. These windows were selected because December–March is important to detect NAO-like patterns in SLP, and March–May could detect SAL patterns in 700 hPa winds and/or PW. Because the climatology for SAL indicates its occurrence in the low to middle troposphere (around 700 hPa) with larger outbreaks reaching farther west from mid-June to late July (Dunion 2011), analyzing 700 hPa winds and integrated PW anomalies during March–May are also good proxies to indicate dust transport and atmospheric humidity that could be related to early SAL intrusion into the insular Caribbean. Here, we show only the composites that presented stronger spatial patterns of NAO and/or SAL for either LA or GA seasonal drought.

The comparison between the overall composite patterns of SLP (Figure 2.10) indicated that anomaly patterns were more intense for years when the GA (Figure 2.10b,d) experienced seasonal drought than for the LA (Figure 2.10a,c). The SLP anomaly composites from December–March indicated that both the LA and the GA had a positive NAO-like pattern preceding their seasonal drought events. The clear pattern of boreal winter NAO occurred mainly for drought during MSD and LRS (Figure 2.10), which were the seasons stronger correlated with the NAO in both subregions. The relationship between positive NAO and negative rainfall anomalies in the insular

Caribbean is well documented and can be one of the reasons leading to drought in the region (George and Saunders 2001; Jury et al. 2007; Malmgren et al. 1998; Rodriguez-Vera et al. 2019). Additionally, MSD and LRS drought in the GA and the LA also presented enhanced high-pressure anomalies over western Atlantic during positive NAO (Figure 2.10). This could be a consequence of the stronger trade winds and lower SST related to NAO, which enhances the NAHP earlier than normal and results in moisture advection away from the Caribbean and less humidity available in the region for rainfall formation (Giannini et al. 2000; Giannini et al. 2001c).

Finally, the 700 hPa winds anomaly composites indicated that both the GA and the LA had stronger winds anomalies over TNA region (from Africa west coast to the Caribbean) during March–May periods preceding their ERS and MSD drought years (Figure 2.11 and Figure 2.12). Similar patterns of wind anomalies were suggested by Ramseyer and Mote (2018) when analyzing the relationship between regional climate forcing and drying trend of precipitation in Puerto Rico. These winds anomalies were well aligned with PW anomalies over the TNA for all LA seasonal drought, but with a stronger pattern presented before ERS and MSD drought events (Figure 2.11), while they were not as clear to depict for GA seasonal drought (Figure 2.12). The patterns seen in Figure 2.11 suggest that an early SAL intrusion could be occurring during March–May when the LA ERS and MSD had drought events. A few studies have already discussed the relationship between ERS drought in the eastern Caribbean and earlier than normal SAL intrusions (Miller et al. 2021; Mote et al. 2017). SAL not only transports dust to the insular Caribbean, which can affect cloud microphysical processes, but it is also responsible for the intrusion of anomalously hot, dry air in the low to middle troposphere, producing thermodynamically stable conditions and inhibiting convection and rainfall (Kuciauskas et al. 2016; Kuciauskas et al. 2018; Prospero and Mayol-Bracero 2013). The climatology of the SAL indicates larger outbreaks reaching farther west from mid-June to late July, which results in fewer hurricanes during LRS season (Dunion 2011). However, when earlier than normal transport occurs in March–May, this can result in drier than normal ERS and MSD, as we saw in the LA PW composites. For the GA, the lack of a clear SAL pattern in negative PW anomalies suggests SAL may not play a significant role in drought for the western Caribbean.

2.4 Conclusions

The insular Caribbean is one of the areas of the globe where more hazard-related events occur, including but not limited to hurricanes, floods, earthquakes, volcanic eruption, and drought. While hurricane hazards are well explored in scientific literature, drought is considered one of the neglected hazards because of the lack of studies focusing on its causes and effects. However, climate models have predicted drought events to be more intense and frequent in the Caribbean due to a warming world, which creates a need for a better understanding of this hazard.

This study analyzed the spatial and temporal distribution of drought events in the insular Caribbean and the relationship of these events with low-frequency atmospheric circulation patterns such as EP and CP ENSO, AMM, and NAO. It brought a new perspective over the region by dividing the Caribbean into western (Greater Antilles and Bahamas, GA), and the eastern Caribbean (Lesser Antilles, LA) to compare the role of those three teleconnection patterns on drought events over larger versus smaller islands, as well as to investigate how intense and widespread drought events compare on those regions. It was also the first time that CP and EP ENSO are related to drought in the Caribbean.

By using the scPDSI drought atlas from 1950 to 2017, and comparing the two subregions, the LA had more intense, frequent, and widespread drought than the GA. While the five years with most widespread drought range from 60%–95% of the area in the GA, the LA registered 83%–100% of the area with spatially distributed drought. Most of the drought years (scPDSI $\leq$ -1) were registered during the LRS, both in the LA (22 years) and the GA (16 years), while 2015–2016 was considered the most intense drought year for all seasons in both subregions.

For the teleconnections, we can suggest that peak season AMM was the one most strongly related with drought events in the insular Caribbean during April–November. This finding brings new insight regarding the connection of the AMM with insular Caribbean drought because most of the AMM-focused studies investigated only the effects on hurricane development. Additionally, a positive NAO was significantly related to drought in the insular Caribbean during the second half of the year, mainly in the GA. On the other hand, CP warm event indicated more drought events in the LA from December–July, while the relationship between the two types of ENSO and the GA was not statistically significant (p-value $\geq$ 0.05). However, when all three teleconnections were combined and assumed to be occurring together, the effects of EP ENSO on seasonal scPDSI are stronger for both subregions, followed by AMM, then NAO.

Finally, the composites of spatial patterns anomalies such as SLP, 700hPa winds, and PW confirmed the relationship between NAO-like patterns occurring during boreal winter before the seasonal drought events start. However, the LA was the only region that present a clear pattern of wind and PW that suggests an early SAL intrusion occurring during March–May when the LA experienced drought during the ERS and MSD. Although further investigation is needed, this extra forcing could be one of the reasons why the most intense and widespread events have occurred in the LA compared to the GA. Therefore, future studies could investigate the main reasons why the LA was the region with more widespread, frequent, and intense drought in the insular Caribbean, as well as why the individual relationship of the two ENSO types did not present statistically significant correlation with drought in the GA but it did with drought in the LA. Moreover, it would be interesting to further investigate the combined effects of EP ENSO, NAO, and AMM on Caribbean scPDSI in order to better predict drought events when all those teleconnections are occurring together.

Acknowledgements

The authors thank Dr. Dimitris Herrera for sharing the scPDSI dataset developed for the Caribbean, Dr. Craig Ramseyer and Dr. Paul Miller for providing insightful comments and suggestions that improved this manuscript, as well as MSc. Lori Wachowicz and Dr. Kyle Mattingly for helping with some of the Python scripts. We also thank the NOAA Modeling, Analysis, Predictions and Projections (MAPP) grant (NA20OAR4310415) for the funding provided, the Climate Prediction Center (CPC) at the National Oceanic and Atmospheric Administration (NOAA) for the online availability of the sea surface temperature anomalies data for all Niño regions (Niño1+2, Niño3, Niño3.4, and Niño4 (http://www.cpc.ncep.noaa.gov/data/indices/ersst5.nino.mth.81-10.ascii), and the NAO index (http://www.cpc.ncep.noaa.gov/products/precip/CWlink/pna/norm.nao.monthly.b5001.current.ascii.table), as well as NOAA Earth System Research Laboratories (ESRL) for the AMM index (https://www.esrl.noaa.gov/psd/data/timeseries/monthly/AMM/).

2.5 References

Allen, T. L., S. Curtis, and D. W. Gamble, 2010: The midsummer dry spell's impact on vegetation in Jamaica. *Journal of Applied Meteorology and Climatology*, **49,** 1590-1595.

Angeles, M. E., J. E. Gonzalez, N. D. Ramírez-Beltrán, C. A. Tepley, and D. E. Comarazamy, 2010: Origins of the Caribbean rainfall bimodal behavior. *Journal of Geophysical Research: Atmospheres*, **115**.

Björnsson, H., and S. Venegas, 1997: A manual for EOF and SVD analyses of climatic data. *CCGCR Report*, **97,** 112-134.

Cane, M. A., 1983: Oceanographic events during el nino. *Science*, **222,** 1189-1195.

Capotondi, A., and Coauthors, 2015: Understanding ENSO diversity. *Bulletin of the American Meteorological Society*, **96,** 921-938.

Casella, G., and R. L. Berger, 2021: *Statistical inference.* Cengage Learning.

Cashman, A., L. Nurse, and C. John, 2010: Climate change in the Caribbean: the water management implications. *The Journal of Environment & Development*, **19,** 42-67.

Charlery, J., L. Nurse, and K. Whitehall, 2006: Exploring the relationship between the North Atlantic oscillation and rainfall patterns in Barbados. *International Journal of Climatology: A Journal of the Royal Meteorological Society*, **26,** 819-827.

Dai, A., K. E. Trenberth, and T. Qian, 2004: A global dataset of Palmer Drought Severity Index for 1870–2002: relationship with soil moisture and effects of surface warming. *Journal of Hydrometeorology*, **5,** 1117-1130.

Dawson, A., 2016: eofs: A library for EOF analysis of meteorological, oceanographic, and climate data. *Journal of Open Research Software*, **4**.

Dunion, J. P., 2011: Rewriting the climatology of the Tropical North Atlantic and Caribbean Sea atmosphere. *Journal of Climate*, **24,** 893-908.

Foltz, G. R., M. J. McPhaden, and R. Lumpkin, 2012: A strong Atlantic meridional mode event in 2009: the role of mixed layer dynamics. *Journal of Climate*, **25,** 363-380.

Gamble, D., 2014: The neglected climatic hazards of the Caribbean: overview and prospects in a warmer climate. *Geography Compass*, **8,** 221-234.

Gamble, D. W., 2004: Water resource development on small carbonate islands: solutions offered by the Hydrologic Landscape concept. *WorldMinds: Geographical Perspectives on 100 Problems: Commemorating the 100th Anniversary of the Association of American Geographers 1904–2004*, D. G. Janelle, B. Warf, and K. Hansen, Eds., Springer Netherlands, 503-507.

Gamble, D. W., 2017: Droughts and water shortages. *The International Encyclopedia of Geography*.

Gamble, D. W., and S. Curtis, 2008: Caribbean precipitation: review, model and prospect. *Progress in Physical Geography,* **32,** 265-276.

Gamble, D. W., D. B. Parnell, and S. Curtis, 2008: Spatial variability of the Caribbean mid-summer drought and relation to north Atlantic high circulation. *International Journal of Climatology*, **28,** 343-350.

George, S. E., and M. A. Saunders, 2001: North Atlantic Oscillation impact on tropical north Atlantic winter atmospheric variability. *Geophysical Research Letters*, **28,** 1015-1018.

Giannini, A., Y. Kushnir, and M. A. Cane, 2000: Interannual variability of Caribbean rainfall, ENSO, and the Atlantic Ocean. *Journal of Climate*, **13,** 297-311.

Giannini, A., M. A. Cane, and Y. Kushnir, 2001a: Interdecadal changes in the ENSO teleconnection to the Caribbean region and the North Atlantic Oscillation. *Journal of Climate*, **14,** 2867-2879.

Giannini, A., Y. Kushnir, and M. Cane, 2001b: Seasonality in the impact of ENSO and the North Atlantic high on Caribbean rainfall. *Physics and Chemistry of the Earth, Part B: Hydrology, Oceans and Atmosphere,* **26,** 143-147.

Giannini, A., J. C. Chiang, M. A. Cane, Y. Kushnir, and R. Seager, 2001c: The ENSO teleconnection to the tropical Atlantic Ocean: contributions of the remote and local SSTs to rainfall variability in the tropical Americas. *Journal of Climate*, **14,** 4530-4544.

Granger, O. E., 1985: Caribbean climates. *Progress in Physical Geography,* **9,** 16-43.

——, 1996: Geography of small tropical islands: implications for sustainable development in a changing world. *Coastal and Estuarine Studies***,** 157-204.

Hatzaki, M., H. Flocas, D. Asimakopoulos, and P. Maheras, 2007: The eastern Mediterranean teleconnection pattern: identification and definition. *International Journal of Climatology*, **27,** 727-737.

Hayhoe, K., 2013: Quantifying key drivers of climate variability and change for Puerto Rico and the Caribbean. *Raleigh, North Carolina: Caribbean Landscape Conservation Cooperative*.

Herrera, D., and T. Ault, 2017: Insights from a new high-resolution drought atlas for the Caribbean spanning 1950–2016. *Journal of Climate*, **30,** 7801-7825.

Herrera, D. A., T. R. Ault, J. T. Fasullo, S. J. Coats, C. M. Carrillo, B. I. Cook, and A. P. Williams, 2018: Exacerbation of the 2013–2016 pan-Caribbean drought by anthropogenic warming. *Geophysical Research Letters,* **45,** 10,619-610,626.

Huang, B., and Coauthors, 2017: Extended reconstructed sea surface temperature, version 5 (ERSSTv5): upgrades, validations, and intercomparisons. *Journal of Climate*, **30,** 8179-8205.

Huang, J., K. Higuchi, and A. Shabbar, 1998: The relationship between the North Atlantic Oscillation and El Niño-Southern Oscillation. *Geophysical Research Letters*, **25,** 2707-2710.

Hurrell, J. W., 1995: Decadal trends in the North Atlantic Oscillation: regional temperatures and precipitation. *Science,* **269,** 676-679.

Jury, M., B. A. Malmgren, and A. Winter, 2007: Subregional precipitation climate of the Caribbean and relationships with ENSO and NAO. *Journal of Geophysical Research: Atmospheres*, **112**.

Kao, H.-Y., and J.-Y. Yu, 2009: Contrasting eastern-Pacific and central-Pacific types of ENSO. *Journal of Climate*, **22,** 615-632.

Karnauskas, K. B., C.-F. Schleussner, J. P. Donnelly, and K. J. Anchukaitis, 2018: Freshwater stress on small island developing states: population projections and aridity changes at 1.5 and 2 °C. *Regional Environmental Change*, **18,** 2273-2282.

Kuciauskas, A. P., P. Xian, E. J. Hyer, M. I. Oyola, and J. R. Campbell, 2016: Providing the Caribbean community with VIIRS-derived weather satellite and dust model output in preparation for African dust impacts. IN31A-1750.

Kuciauskas, A. P., P. Xian, E. J. Hyer, M. I. Oyola, and J. R. Campbell, 2018: Supporting weather forecasters in predicting and monitoring Saharan Air Layer dust events as they impact the greater Caribbean. *Bulletin of the American Meteorological Society*, **99,** 259-268.

Lamb, P. J., and R. A. Peppler, 1987: North Atlantic Oscillation: concept and an application. *Bulletin of the American Meteorological Society*, **68,** 1218-1225.

Magaña, V., J. A. Amador, and S. Medina, 1999: The midsummer drought over Mexico and Central America. *Journal of Climate*, **12,** 1577-1588.

Malmgren, B. A., A. Winter, and D. Chen, 1998: El Nino–southern oscillation and North Atlantic oscillation control of climate in Puerto Rico. *Journal of Climate*, **11,** 2713-2717.

Marshall, J., and Coauthors, 2001: North Atlantic climate variability: phenomena, impacts and mechanisms. *International journal of climatology*, **21,** 1863-1898.

Martinez, C., L. Goddard, Y. Kushnir, and M. Ting, 2019: Seasonal climatology and dynamical mechanisms of rainfall in the Caribbean. *Climate Dynamics*.

Miller, P. W., and C. A. Ramseyer, 2020: Did the Climate Forecast System anticipate the 2015 Caribbean drought? *Journal of Hydrometeorology*, **21,** 1245-1258.

Miller, P. W., M. Williams, and T. Mote, 2021: Modeled atmospheric optical and thermodynamic responses to an exceptional trans-Atlantic dust outbreak. *Journal of Geophysical Research: Atmospheres*, **126,** e2020JD032909.

Mo, K. C., 2010: Interdecadal modulation of the impact of ENSO on precipitation and temperature over the United States. *Journal of climate*, **23,** 3639-3656.

Mote, T. L., C. A. Ramseyer, and P. W. Miller, 2017: The Saharan Air Layer as an early rainfall season suppressant in the Eastern Caribbean: The 2015 Puerto Rico drought. *Journal of Geophysical Research: Atmospheres*, **122**.

OCHA, U. N. O. f. t. C. o. H. A., 2015: Annual Report 2015.

Pandey, R. P., A. Pandey, R. V. Galkate, H.-R. Byun, and B. C. Mal, 2010: Integrating hydro-meteorological and physiographic factors for assessment of vulnerability to drought. *Water Resources Management*, **24,** 4199-4217.

Patricola, C. M., R. Saravanan, and P. Chang, 2014: The impact of the El Niño–Southern Oscillation and Atlantic Meridional Mode on seasonal Atlantic tropical cyclone activity. *Journal of Climate*, **27,** 5311-5328.

Prospero, J. M., and O. L. Mayol-Bracero, 2013: Understanding the Transport and Impact of African Dust on the Caribbean Basin. *Bulletin of the American Meteorological Society*, **94,** 1329-1337.

Ramseyer, C. A., and T. L. Mote, 2016: Atmospheric controls on Puerto Rico precipitation using artificial neural networks. *Climate Dynamics*, **47,** 2515-2526.

——, 2018: Analysing regional climate forcing on historical precipitation variability in Northeast Puerto Rico. *International Journal of Climatology*, **38,** e224-e236.

Rodriguez-Vera, G., R. Romero-Centeno, C. L. Castro, and V. M. Castro, 2019: Coupled interannual variability of wind and sea surface temperature in the Caribbean Sea and the Gulf of Mexico. *Journal of Climate*, **32,** 4263-4280.

Ropelewski, C. F., and M. S. Halpert, 1987: Global and regional scale precipitation patterns associated with the El Niño/Southern Oscillation. *Monthly weather review*, **115,** 1606-1626.

Rugg, A., G. R. Foltz, and R. C. Perez, 2016: Role of mixed layer dynamics in tropical North Atlantic interannual sea surface temperature variability. *Journal of Climate*, **29,** 8083-8101.

Smerdon, J. E., B. I. Cook, E. R. Cook, and R. Seager, 2015: Bridging past and future climate across paleoclimatic reconstructions, observations, and models: a hydroclimate case study. *Journal of Climate*, **28,** 3212-3231.

Smirnov, D., and D. J. Vimont, 2011: Variability of the Atlantic Meridional Mode during the Atlantic hurricane season. *Journal of Climate*, **24,** 1409-1424.

Taylor, M. A., D. B. Enfield, and A. A. Chen, 2002: Influence of the tropical Atlantic versus the tropical Pacific on Caribbean rainfall. *Journal of Geophysical Research: Oceans*, **107,** 10-11-10-14.

Trenberth, K. E., 1997: The definition of El Nino. *Bulletin of the American Meteorological Society*, **78,** 2771-2778.

Van der Schrier, G., J. Barichivich, K. R. Briffa, and P. D. Jones, 2013: A scPDSI-based global data set of dry and wet spells for 1901–2009, **118,** 4025-4048.

Vimont, D. J., and J. P. Kossin, 2007: The Atlantic Meridional Mode and hurricane activity. *Geophysical Research Letters*, **34**.

Wells, N., S. Goddard, and M. J. Hayes, 2004: A self-calibrating Palmer Drought Severity Index. *Journal of Climate*, **17,** 2335-2351.

Wilhite, D. A., 2000: Drought as a natural hazard: concepts and definitions.

Williams, A. P., R. Seager, J. T. Abatzoglou, B. I. Cook, J. E. Smerdon, and E. R. Cook, 2015: Contribution of anthropogenic warming to California drought during 2012–2014. *Geophysical Research Letters*, **42,** 6819-6828.

Table 2.1 – Correlation analysis between each teleconnection index during their peak season and the seasonal average scPDSI for the Greater Antilles (GA) and the Lesser Antilles (LA). In bold are the correlation coefficients with statistical significance at 95% confidence interval (p-value < 0.05).

Subregion	**Seasons**	**EP ENSO**	**CP ENSO**	**NAO**	**AMM**
GA	*DS*	0.0	0.0	**-0.3**	**0.5**
	ERS	0.1	0.2	**-0.3**	**0.4**
	MSD	0.1	0.2	**-0.4**	**0.5**
	LRS	0.1	0.1	**-0.5**	**0.6**
LA	*DS*	**-0.4**	**-0.5**	-0.1	**0.2**
	ERS	**-0.3**	**-0.4**	-0.1	**0.3**
	MSD	-0.1	-0.2	**-0.3**	**0.6**
	LRS	-0.1	-0.1	**-0.4**	**0.6**

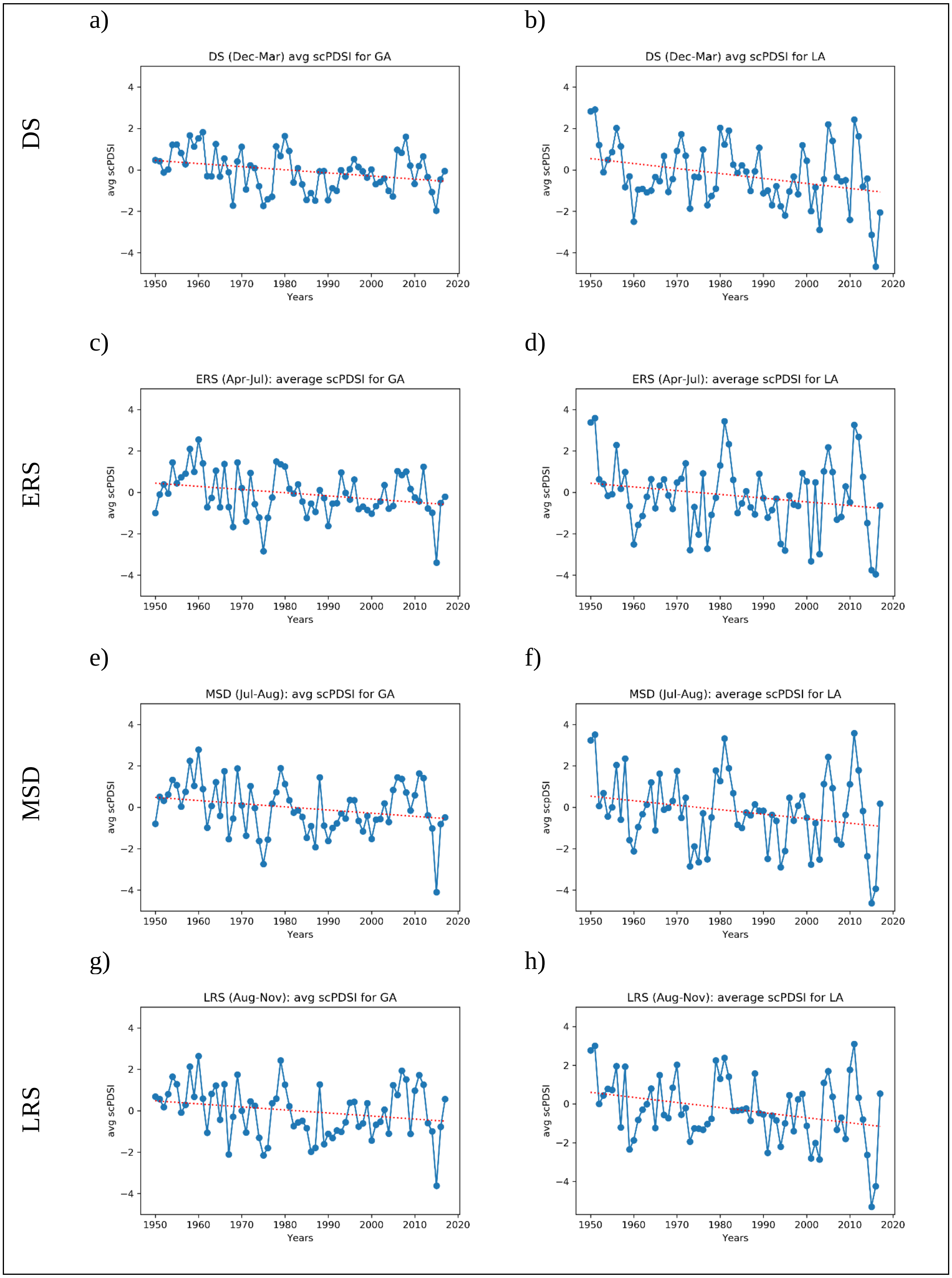

Figure 2.1 – Seasonal average scPDSI for GA (a, c, e, and g) and LA (b, d, f, and h).

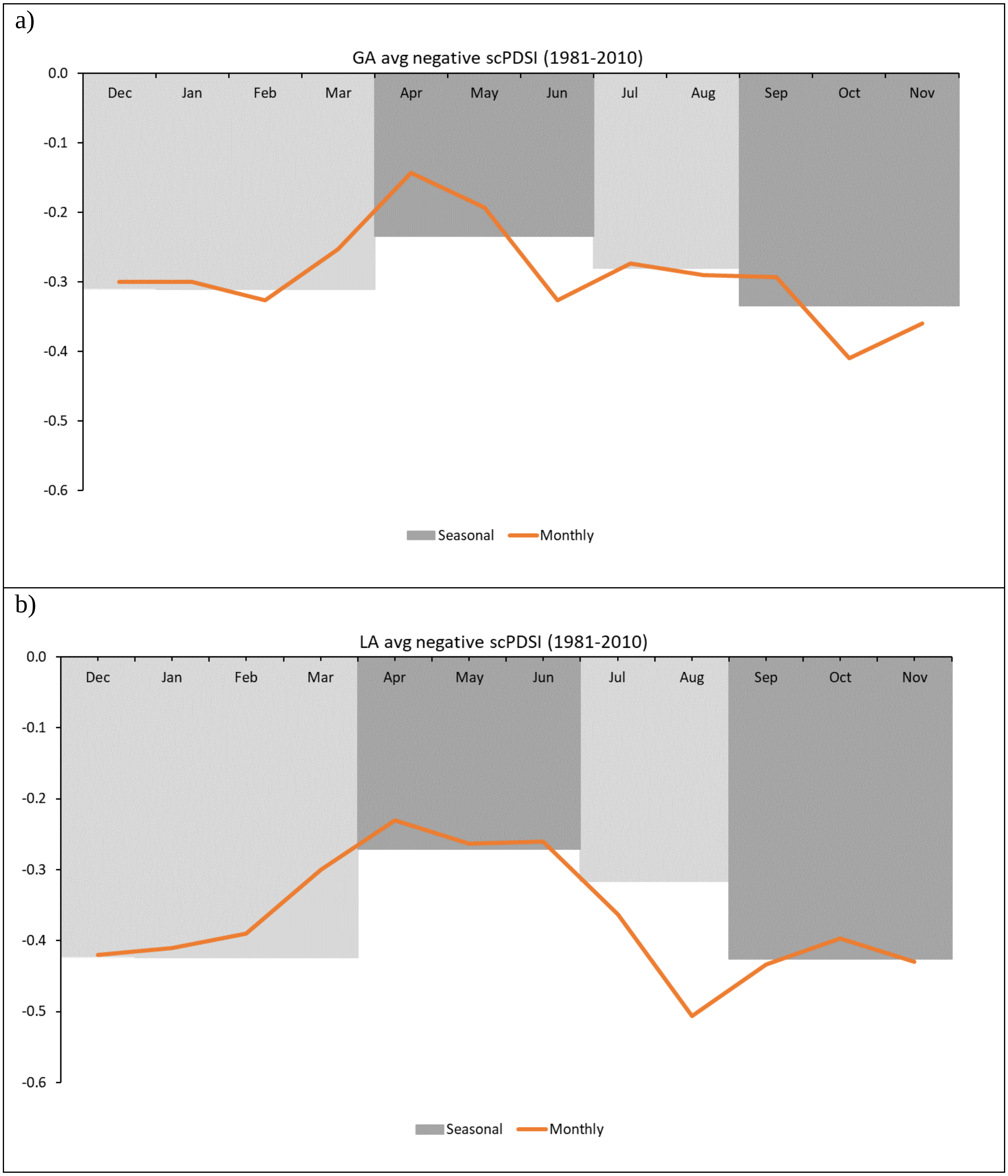

Figure 2.2 – Seasonal and monthly average negative scPDSI climatology (1981–2010) for (a) the GA, and (b) the LA. From the left to the right, the bars indicate the seasons as follow: DS, ERS, MSD, and LRS.

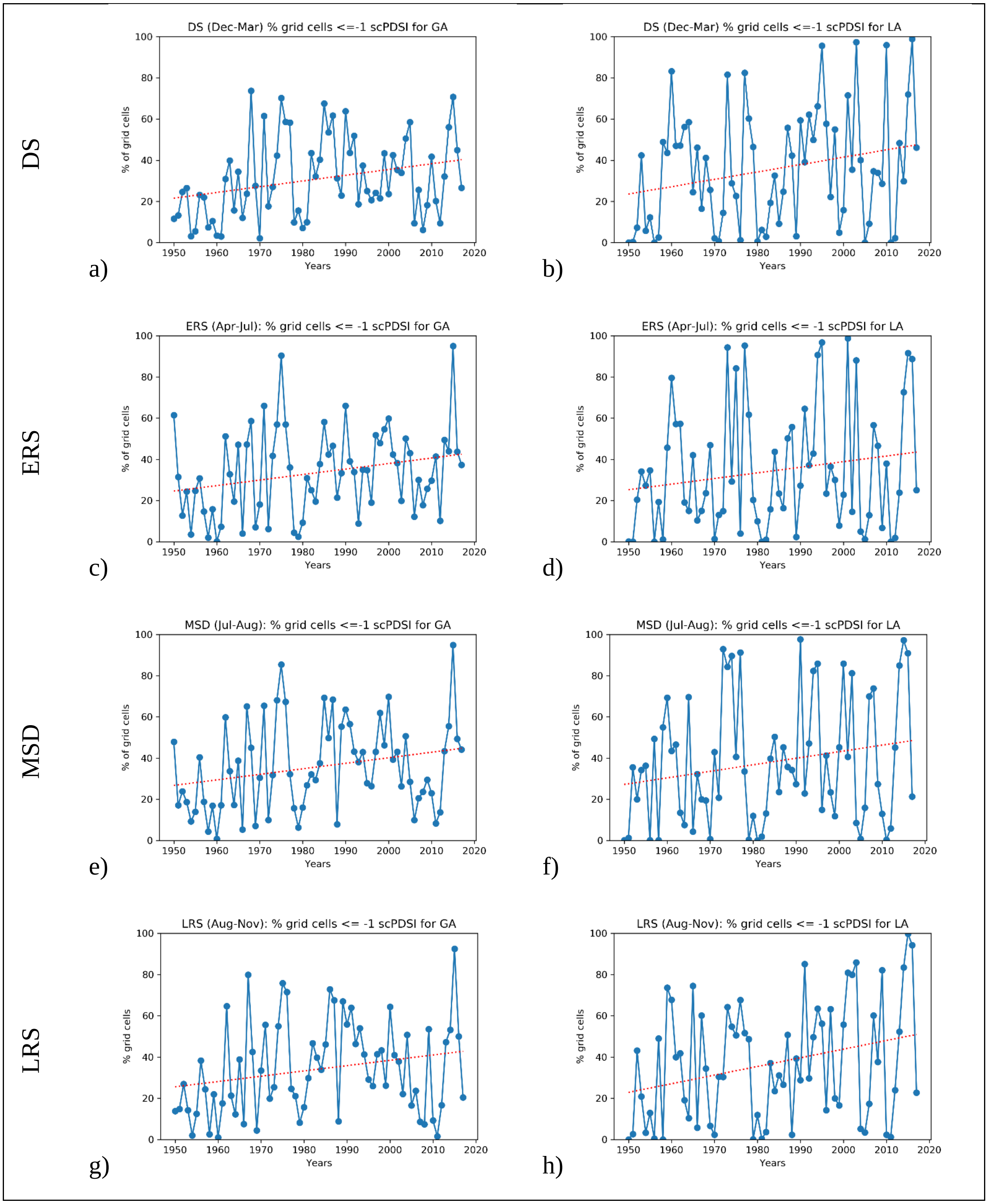

Figure 2.3 – Seasonal percentage of grid cells with negative scPDSI for GA (a, c, e, and g) and LA (b, d, f, and h).

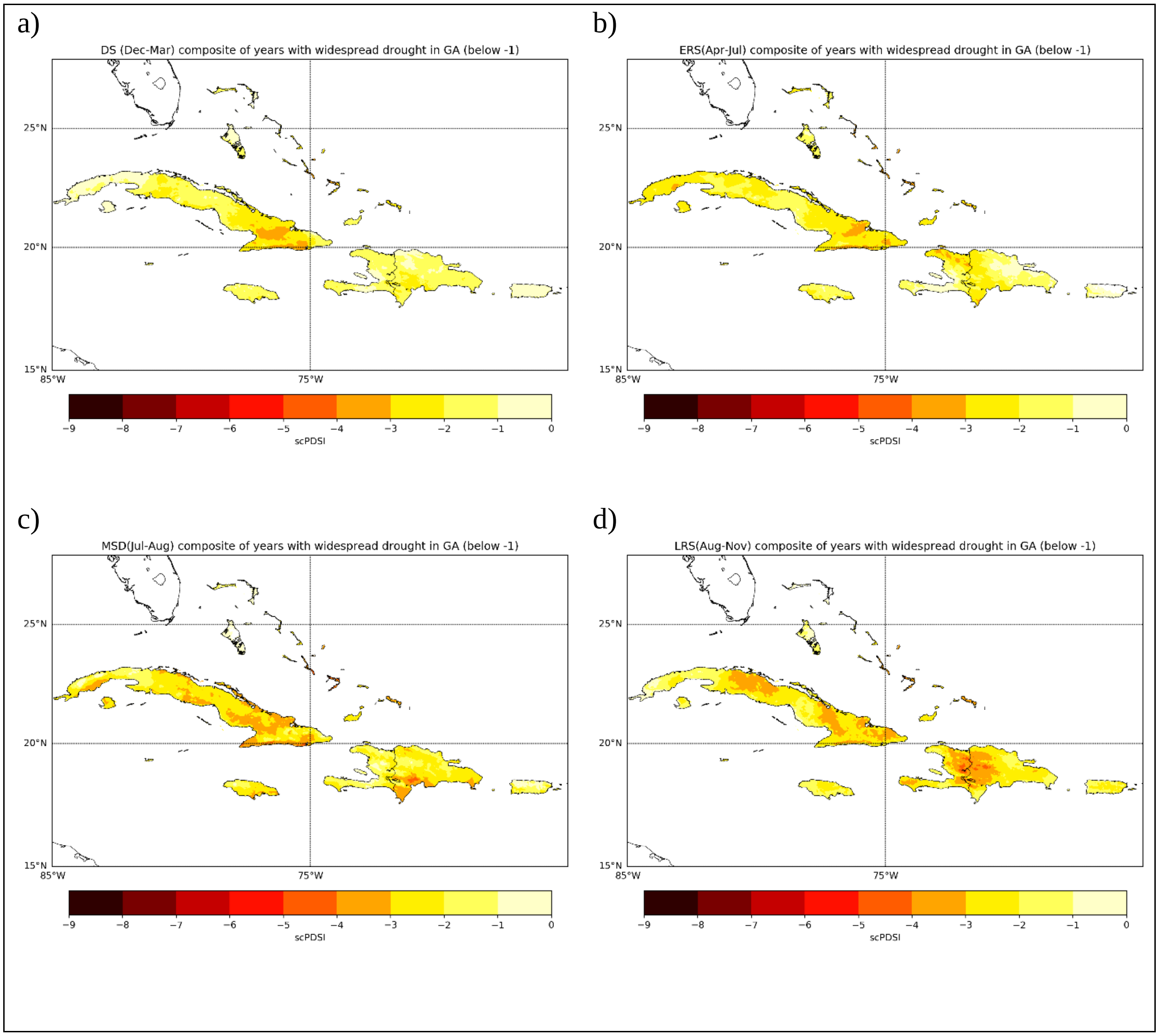

Figure 2.4 - Top five years with more widespread drought in the GA by season. (a) DS, (b) ERS, (c) MSD, and (d) LRS.

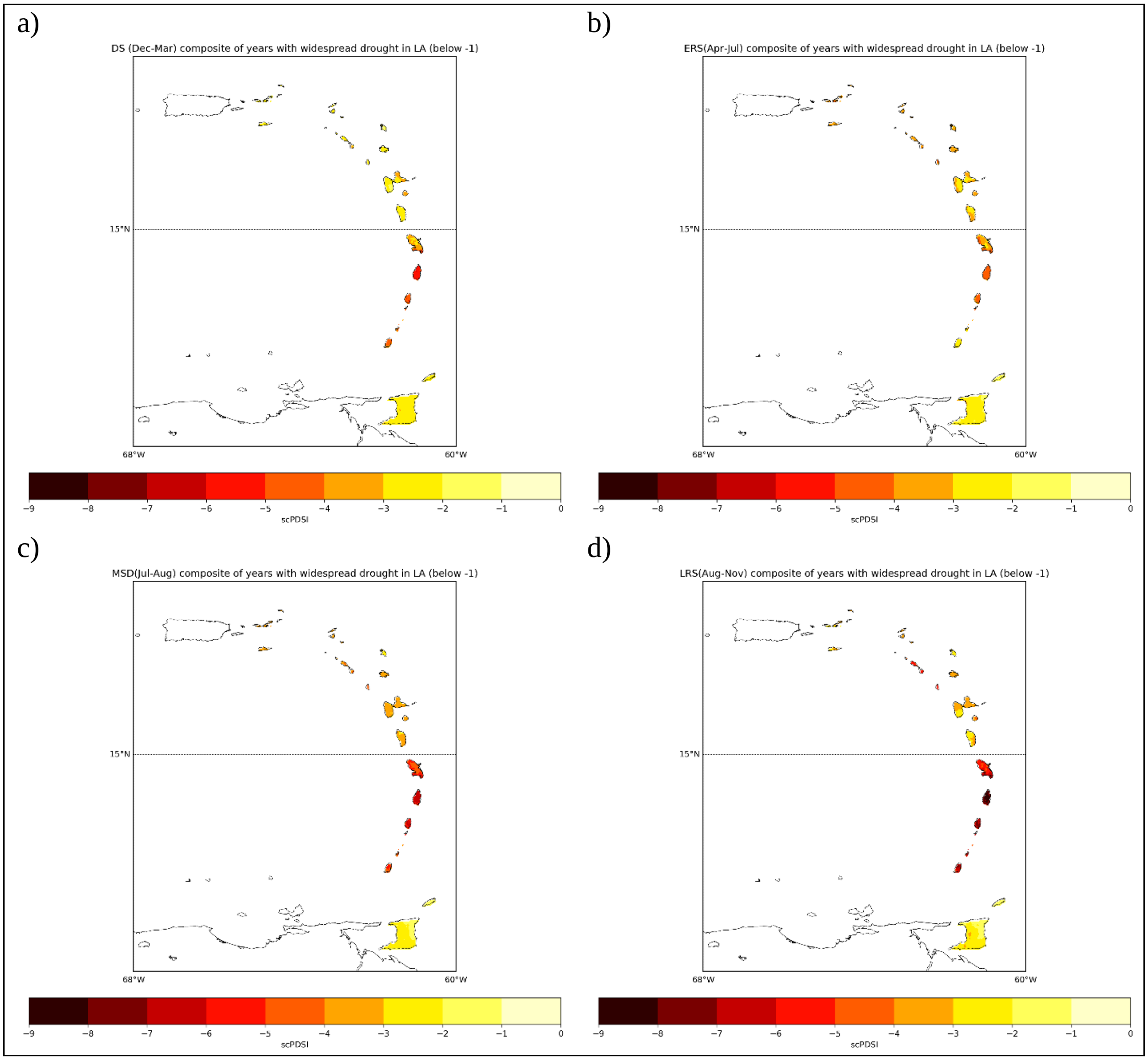

Figure 2.5 – Top five years with more widespread drought in the LA by season. (a) DS, (b) ERS, (c) MSD, and (d) LRS.

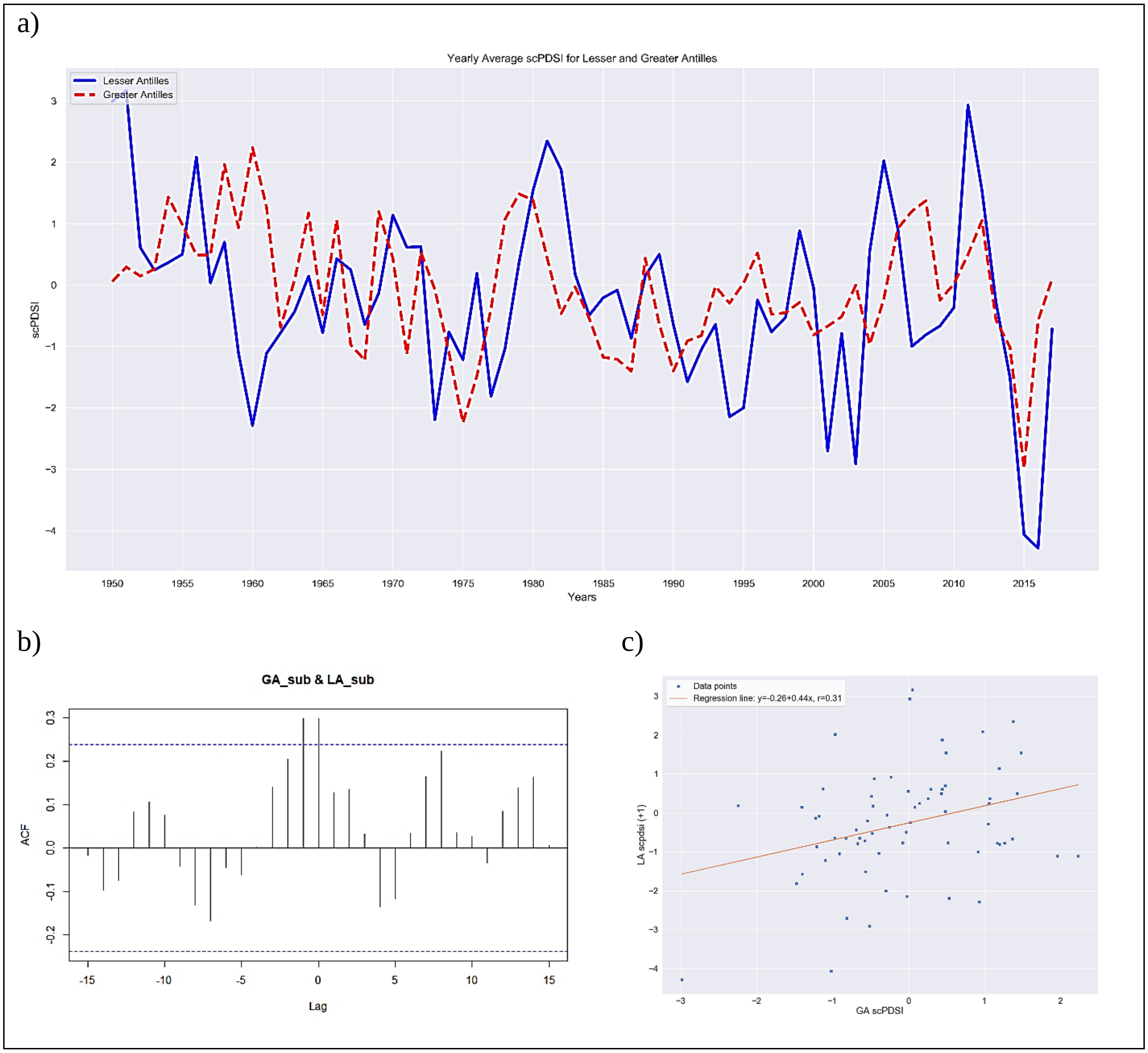

Figure 2.6 – (a) Yearly average scPDSI for LA (solid blue line) and GA (dashed red line), (b) their cross-correlation, and (c) correlation.

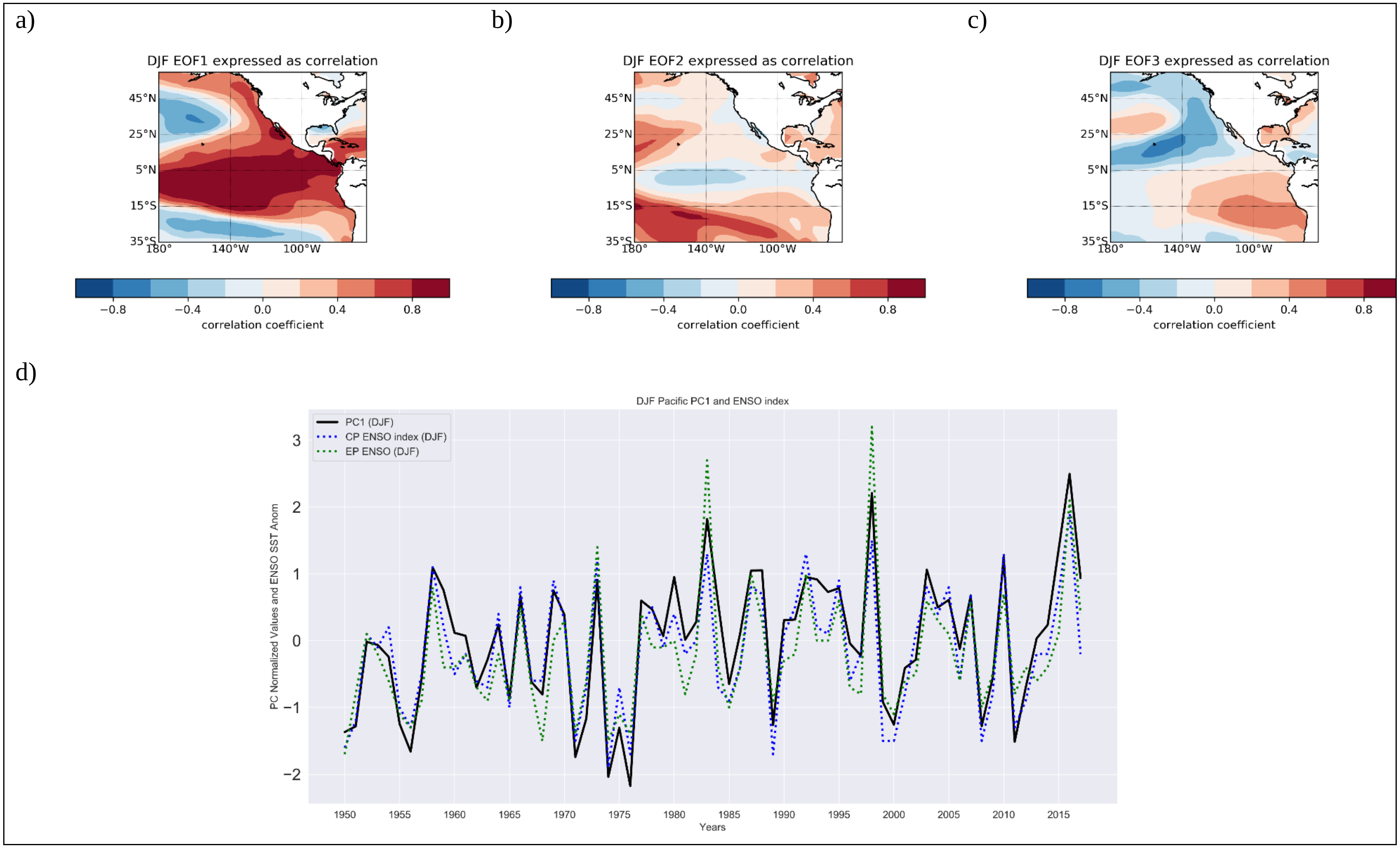

Figure 2.7 – December–February SST EOF analysis for the Pacific basin (a EOF1, b EOF2, c EOF3), and (d) EOF1 time series against CP and EP ENSO December–February indices.

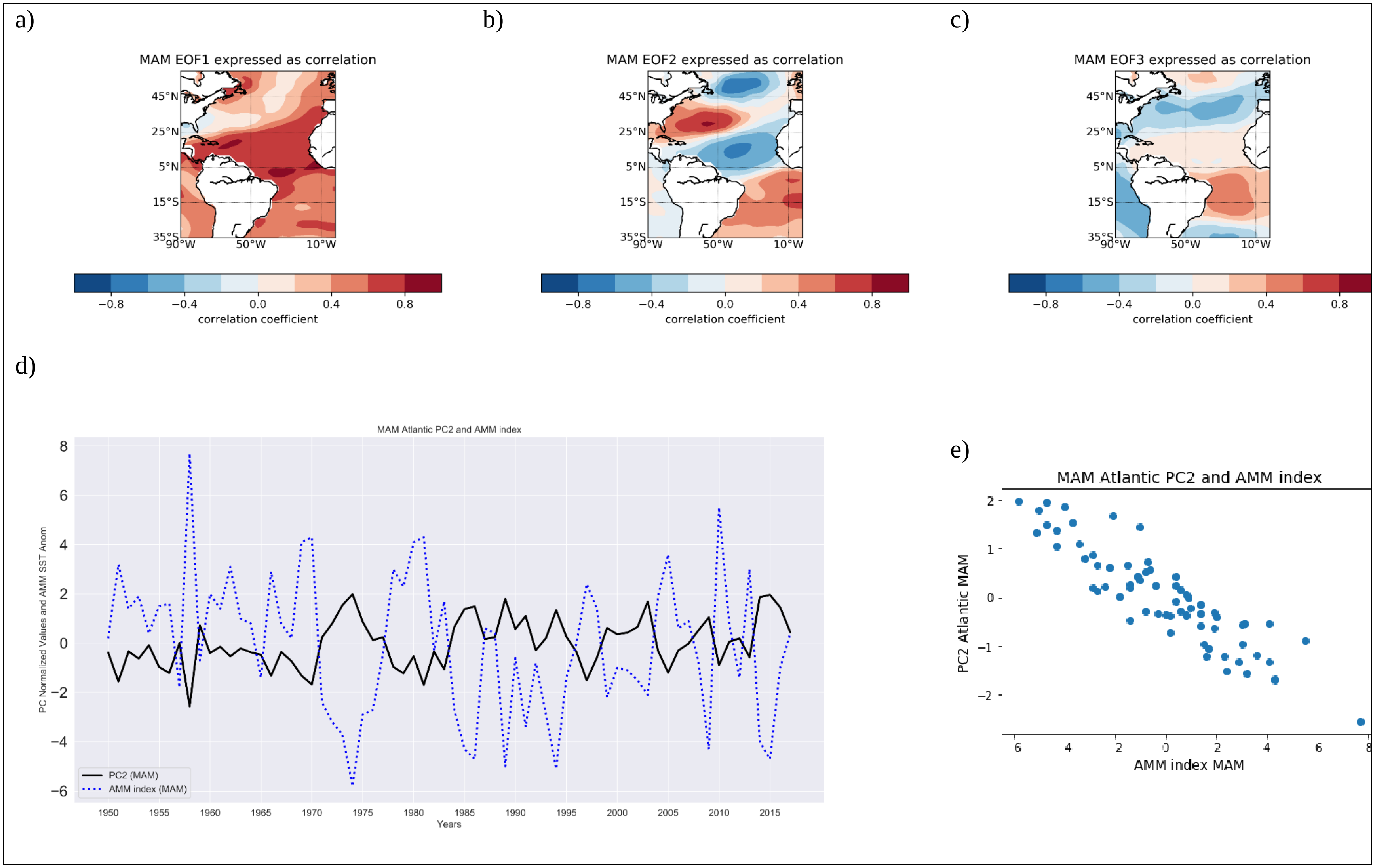

Figure 2.8 – March–May SST EOF analysis for the Atlantic basin (a EOF1, b EOF2, c EOF3), and (d and e) EOF2 time series against March–May AMM index.

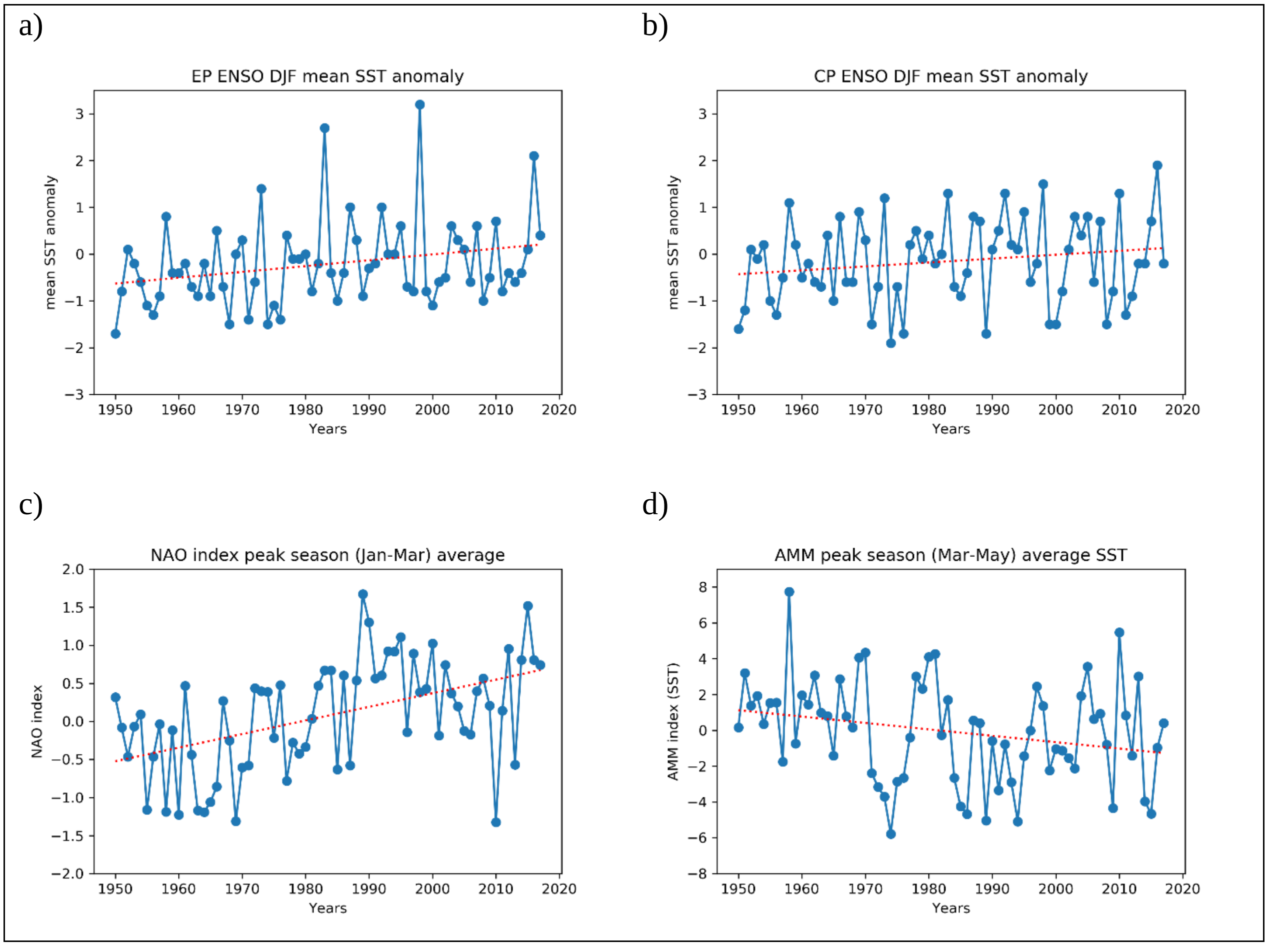

Figure 2.9 – Peak season mean teleconnection indices time series. (a) EP ENSO (December–February), (b) CP ENSO (December–February), (c) NAO (January–March), and (d) AMM (March–May).

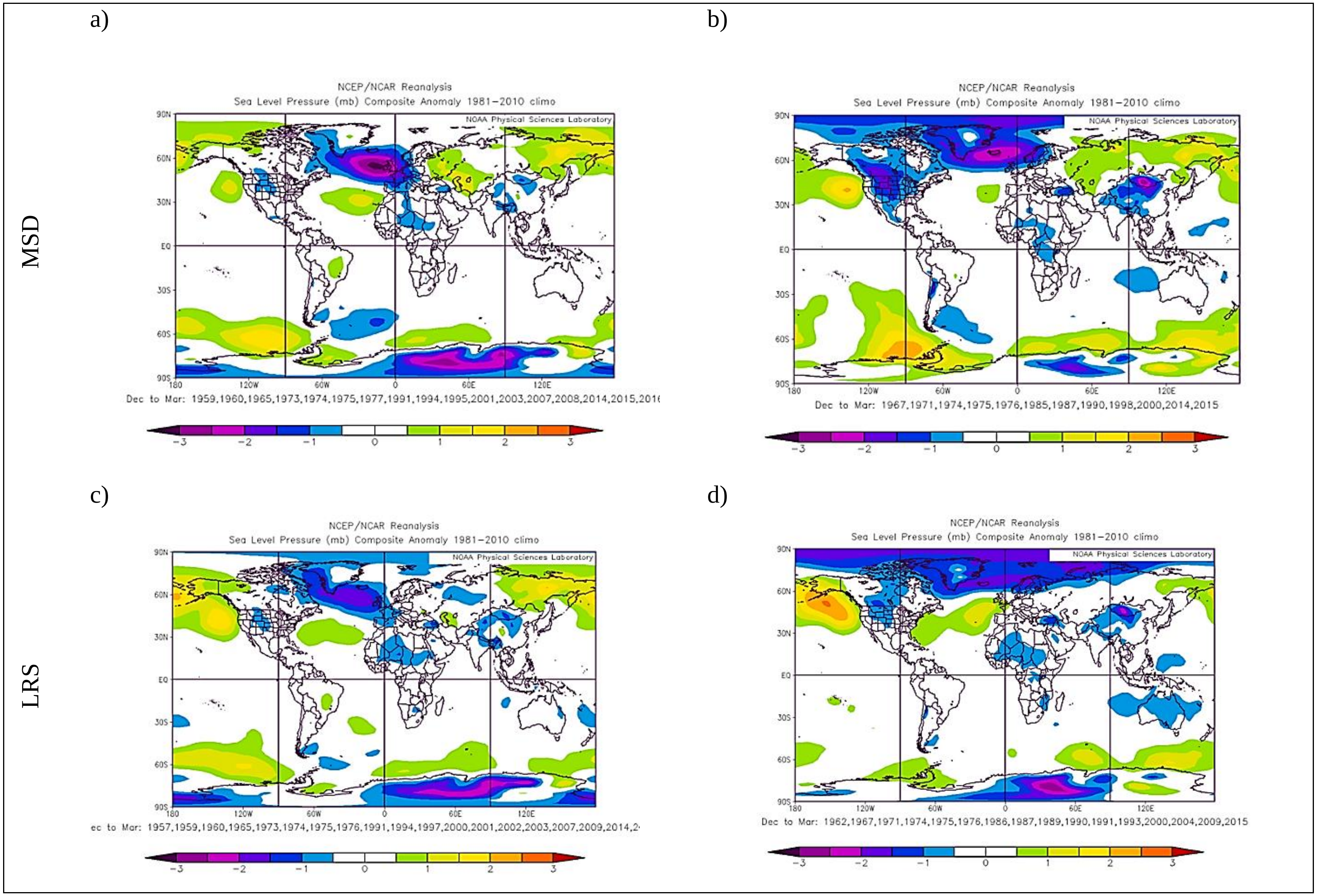

Figure 2.10 – Sea level pressure (SLP) seasonal composites anomaly (December–March) for years when the LA (a, c) and GA (b, d) have seasonal drought events during MSD and LRS.

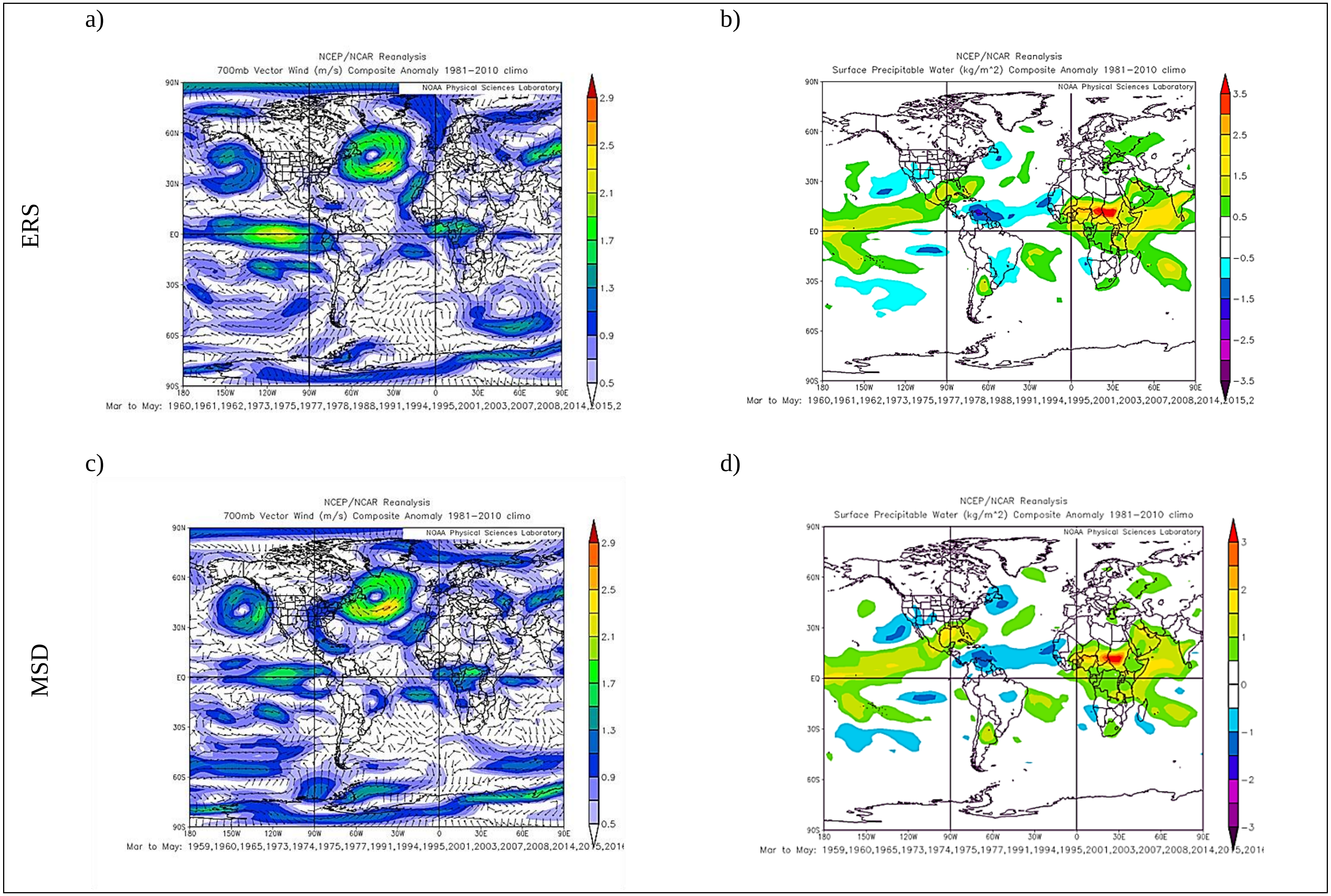

Figure 2.11 – Vector wind (700 hPa winds) (a, c) and Integrated Precipitable Water (PW) (b, d) seasonal composites anomaly for the LA seasonal drought events during ERS and MSD.

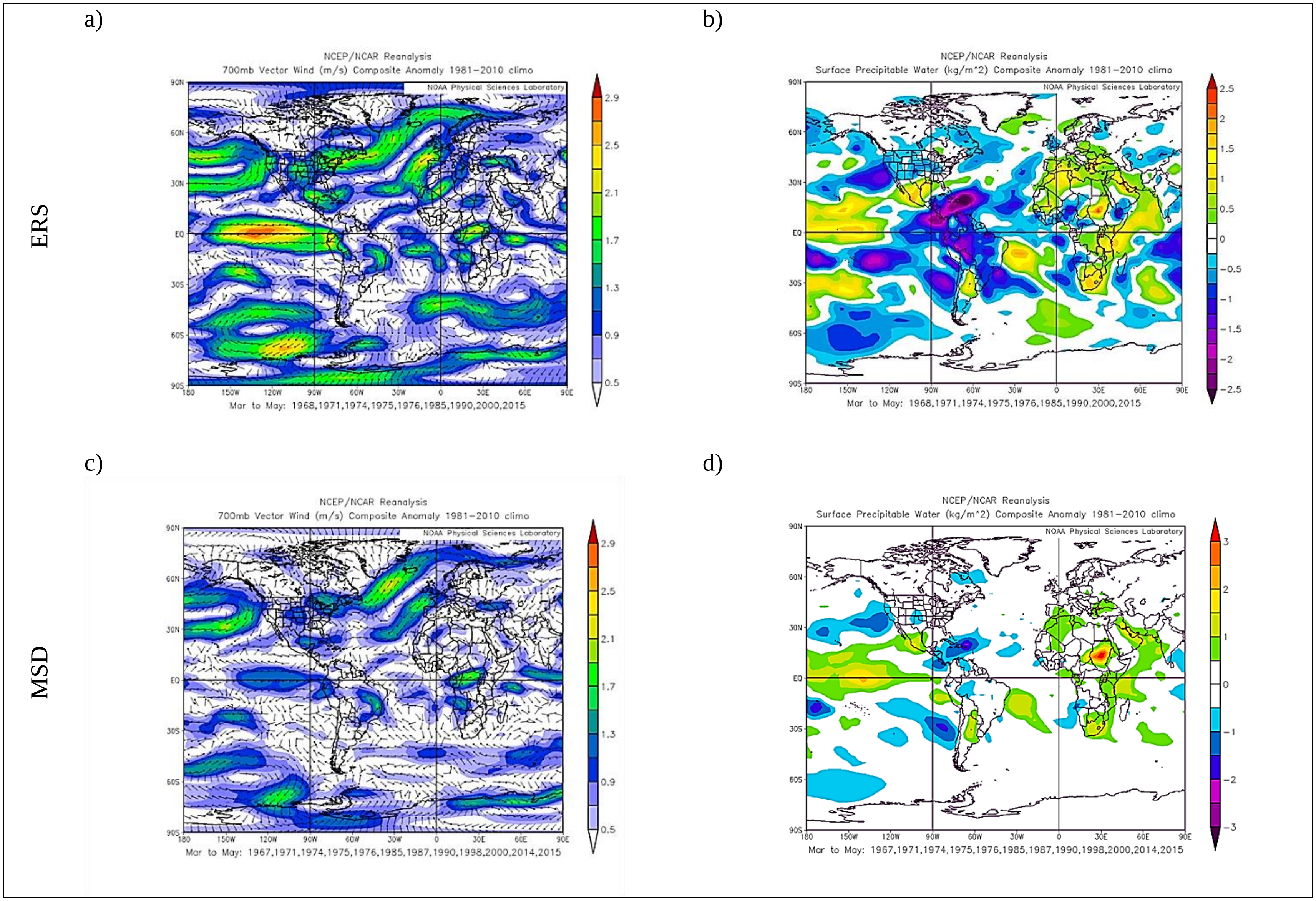

Figure 2.12 – Vector wind (700 hPa winds) (a, c) and Integrated Precipitable Water (PW) (b, d) seasonal composites anomaly for the GA seasonal drought events during ERS and MSD.

3 THE ROLE OF PHYSICAL GEOGRAPHY ON PUERTO RICO WATER BUDGET AND POTENTIAL GROUNDWATER RECHARGE[2]

[2] Moraes, F.D.S, T. Mote, and T. Rasmussen. The Role of Physical Geography on Puerto Rico Water Budget and Potential Groundwater Recharge. To be submitted to *Water Resources Research*.

Abstract

The insular Caribbean has limited water resources due to the sizes of the islands and their geomorphic characteristics. This study focused on Puerto Rico to evaluate the role of physical geography on the island's water budget and net infiltration during three different periods: a baseline climatology (1981–2010), a recent decade (2010–2019), and multiple drought years (1991, 1994, 1997, and 2015). We used the new Soil-Water-Balance (SWB2) model Version 2.0 from the U.S. Geological Survey (USGS) to estimate Puerto Rico's water budget. The findings here suggested that mountainous and vegetated areas of Cordillera Central and the Luquillo Mountains contributed to the greater net infiltration occurring in the central west, north, and eastern Puerto Rico both during the baseline climatology and the recent decade periods. On the other hand, the low-lying, less vegetated, and drier southern Puerto Rico located in the rain shadow area of Cordillera Central had less net infiltration occurred over time. During drought events, the decrease in net infiltration and rainfall was most dramatic over central and east Puerto Rico, which together with the reduction in net infiltration that occurred in northern and southern areas resulted in greater concern on water availability. The north and south regions are home to the North Coast and the South Coast Aquifers, the most important aquifers for drinking water, irrigation, and public supply in Puerto Rico. Those aquifers are both recharged by direct rainfall and by streamflow coming from the Cordillera Central. Therefore, the decreased in rainfall and net infiltration in those areas, may represent a challenge for the island to have water available to meet its demand during drought events, which may lead to the increase in the use of the high-energy demand desalinization and its consequent environmental impacts.

3.1 Introduction

The insular Caribbean has a great cultural diversity among the islands, but the region shares similarities in regards to its rich biodiversity, including but not limited to rain forests, endemic species, volcanic features, and coral reefs (Geoghegan and Renard 2002). However, this rich environment has limited water resources due to the sizes of the islands and their geomorphic characteristics.

The geological composition is one of the most important characteristics affecting water availability, because geology plays a role in physiographic control of rainfall patterns and the availability of surface and subsurface water (Hendry 1996). In the Caribbean carbonate islands, most of the water resources are located at the subsurface, while the limited amount of freshwater at the surface is frequently hypersaline because of high evaporation demand. Therefore, these islands are particularly vulnerable to drought as rainwater catchments and groundwater freshwater lenses are the main options of water supply, and both are dependent on the rainfall recharge (Cant 1996; Falkland 1999). In the volcanic islands, on the other hand, the water supply is from the surface due to limited percolation, steep terrain and high runoff, which normally result in more surface water available than groundwater (Hendry 1996). Additionally, the topography of the islands can also affect the magnitude and the location of rainfall, with orographic uplifting from the mountains resulting in more rainfall occurring on the windward side of Caribbean islands (Jury 2020; Martinez et al. 2019; Sobel et al. 2011).

The geology, topography, climate, and lack of economic diversity in the insular Caribbean make drought one of the most frequent climate hazards, resulting in economic losses and water shortages (Farrell et al. 2010). The annual variability in rainfall together with the physical environment challenge the region’s ability to capture the water during rainy seasons and retain it during dry seasons or drought events, with many of the islands already experiencing problems in meeting water demand during drier periods of the year (Ault 2016; Cashman et al. 2010; Holding et al. 2016).

This work focused on the main island of Puerto Rico as a case study to analyze the role of physical geography in water resources and potential groundwater recharge in insular Caribbean. Puerto Rico is a Caribbean island that rises from sea level to 1,075 m high at the top of the Luquillo Mountains over a distance of only 10–20 km along its east coast (Garcia-Martino et al. 1996). Because the island is exposed to extreme climatic events, such as hurricane and drought, the mountainous landscape introduces another dimension to complexity due to variation in soils, vegetation, and rainfall. The topography allows for orographic rainfall to occur on the windward side of the mountains while the leeward side is drier, with annual rainfall totals over the island ranging from 700 mm in the south to more than 4,000 mm in the east (Garcia-Martino et al. 1996; Hosannah et al. 2019). Moreover, the two major aquifers of Puerto Rico are mostly dependent on direct rainfall for recharge (Mendez-Tejeda et al. 2016), which make them vulnerable to drought with the burgeoning population, industry, tourism, and irrigated agriculture all placing greater demands on water resources.

Therefore, this work is unique by comparing how the different environmental characteristics of Puerto Rico are related to its water balance during a baseline climatology (1981–2010), a recent decade (2010–2019), and several drought years (1991, 1994, 1997, and 2015). The estimation of Puerto Rico water budget and potential groundwater recharge was done by using the new Soil-Water-Balance (SWB2) model Version 2.0 (Westenbroek et al. 2018). Because a drying trend has been already registered in the Caribbean since 1950, and drought is expected to be more frequent and severe in the Caribbean (Cashman et al. 2010; Herrera et al. 2018; Karnauskas et al.

2018), understanding the water balance of Puerto Rico is important to understand where are the areas in the island with less infiltration in order to help local governments to plan for water management. Additionally, this work provided an opportunity to evaluate the performance of a new released and free-access water budget model into a tropical Atlantic island.

3.2 Data and Methods

3.2.1 Study area

Puerto Rico is located in western Tropical Atlantic and extends approximately 180 km from west to east and 65 km from north to south and has a quasi-rectangular shape (with and area of approximately 11,700 km^2). The island is predominantly mountainous (53% of the area), and its maximum altitude is around 1,300 m above sea level. However, most of the northwest coast of Puerto Rico is an area of karst topography (limestone), while the south coast is predominantly formed by discontinuous coastal plain, and they are both divided by a central mountain range extending from east to west called Cordillera Central (Mendez-Tejeda et al. 2016; Miller et al. 1997; Torres-Valcárcel et al. 2014) (Figure 3.1a).

Because of the topography of Puerto Rico, the drainage system of the island is normally radial (from the central highlands to the sea) and "consists of short, deeply incised streams that have steep gradients in the upper reaches" (Miller et al. 1997). Puerto Rico has few perennial streams (along the southern coast), and those rivers' flow requires precipitation and sustained wet periods. Another consequence of the topography is the distribution of annual precipitation. The orographic effect causes variation in annual precipitation in relation to altitude and wind direction over Puerto Rico, with the windward mountainous areas receiving much more rainfall than the leeward side and low-lying coastal areas (Garcia-Martino et al. 1996). Seasonal variation in precipitation also affects runoff, which is greater in Puerto Rico during the rainy seasons (April–November), while little flow occurs during dry season (December–March), with the exception of the larger streams originated in the igneous and volcanic rocks of the interior (Miller et al. 1997).

Most of the precipitation in Puerto Rico returns to the atmosphere through evapotranspiration due to the high average temperatures (Miller et al. 1997). However, some water is stored over the 11 surface-water reservoirs and is used for hydroelectric power generation and irrigation. Some water also infiltrates and enters aquifers as groundwater recharge. Puerto Rico has three important aquifers system, Alluvial Valley Aquifers, the South Coast Aquifer, and the North Coast Limestone Aquifer, which together with the high-water demand in the island make each of them very important as a source of water (Figure 3.1b). The South Coast Aquifer is 70 km long and 3 to 8 km wide and is the most important aquifer in southern Puerto Rico (Mendez-Tejeda et al. 2016), while the North Coast Aquifer is the most extensive and productive fresh-water aquifer on the island (Lugo et al. 2001; Maihemuti et al. 2015). Although the quality of water in the aquifers is normally appropriate for most uses, both the North Coast Limestone Aquifer and the South Coast Aquifer have suffered saline water infiltration (Miller et al. 1997).

The estimated use of water in Puerto Rico is presented in Dieter et al. (2018) according to surface-water and groundwater withdrawals by water-use category, in 2015, in millions of gallons per day. They presented the total water withdrawals by source together with the total population (thousands) to show the most used source and type of water. The total amount of groundwater withdrawal in Puerto Rico represented 22% of the amount of freshwater withdrawal, with 100% of the population served by public supply (Dieter et al. 2018). Considering the public supply and water-use category, irrigation resulted in more withdrawal of both surface and groundwater in Puerto Rico (see more details in Tables 3A and 4A in Dieter et al. (2018)).

3.2.2 The Soil-Water-Balance Model Version 2.0 (SWB2)

This work includes an estimation of the water budget and water availability, measured as net infiltration, to assess the role of physical geography on water resources in Puerto Rico. To accomplish this objective, we used the SWB2 developed by Westenbroek et al. (2018), who applied it to the island of Maui, Hawaii. The SWB2 is an updated code of SWB Version 1.0, which includes an option for additional input data to estimate irrigation amounts, for example, as well as capabilities to allow the use of grids with different spatial extents and projections to be combined without requiring resampling and resizing of the grids. Because this model was applied to another tropical island environment, it was considered to be an appropriate model to this study. Moreover, U.S. Caribbean and Pacific Islands share vulnerabilities related to their isolation, dependence on imports, and dependence on local sources of freshwater, which make the vulnerability to drought similar among them, and different from mainland regions, for reasons including but not limited to saltwater intrusion and sea level rise threatening in their coastal aquifers (Gould et al. 2018).

Before starting to explain the SWB2 model, it is important to define that this model estimates net infiltration instead of groundwater recharge. Although these terms are sometimes used interchangeably, it is critical to understand that net infiltration is the water that has escaped the evapotranspiration sinks of the root zone and can have some portion of which finding its way to the groundwater table, while the groundwater recharge is the water that actually crosses the water table (Healy 2010; Westenbroek et al. 2018). Therefore, this paper will use the term *net infiltration* to refer to the potential groundwater recharge estimation made by the SWB2 model.

The SWB2 uses a modified Thornthwaite and Mather (1957) soil-moisture accounting method to calculate net infiltration at a daily frequency on a grid-by-grid cell basis. It is based on sinks and sources of water within each grid cell based on input climate data and landscape characteristics. A conceptual diagram of SWB2 processes is detailed in Figure 3.2. While running the model, soil moisture is updated every day as the difference between these sources and sinks, and net infiltration is only computed when soil moisture exceeds the field capacity, otherwise it is zero. Equation 1 shows the variables used in this study and explains how the SWB2 quantified net infiltration as recharge below the root zone:

$$NI = R - I - Roff - AET - \Delta S \tag{1}$$

where NI is net infiltration, R is gross precipitation, I is interception, Roff is runoff, AET is actual evapotranspiration, and ΔS is change in soil moisture. Both I and ΔS are considered storage/reservoir within the SWB2 model. The model provides all its outputs in units of inches, converted to SI units here. The SWB2 model outputs grid cell resolution was defined as 300 m.

In this study, we used the following datasets as inputs for the SWB2 model: daily gridded climate data from Daymet (Version 3) at 1 km resolution (precipitation, maximum temperature, and minimum temperature) from 1980 to 2019; hydrologic soil types and available water soil capacity (AWC, 0 to 100 cm) from Gridded Soil Survey Geographic (gSSURGO) Database at 10 m resolution; and two land use and land cover (LULC) data at 30 m resolution, one representing 2001 LULC from National Land Cover Database, and the other for 2010 LULC from NOAA Office for Coastal Management (NOAA/OCM). All the non-transient SWB2 input data are shown in Figure 3.3. Daymet Version 3 was used instead of Version 4 because preliminary analysis indicated the Version 3 performed better in Puerto Rico when compared to observed runoff (Jazlynn Hall, Columbia University, pers. comm.).

Before we describe in more details the parameters used to run the SWB2 model, it is important to explain that this study ran the model for two different periods: the baseline climatology (1981–2010), and the recent decade (2010–2019). This separation was performed to create a climatology reference period (baseline) and be able to compare it with the outputs of the recent decade to look for differences (if any) in their water budget and net infiltration. To account for possible differences in LULC in Puerto Rico, we ran the baseline climatology using LULC from 2001, and the recent decade with an updated LULC from 2010. The differences among those LULC classes are seen in Figure 3.3.

The SWB2 model requires that gross precipitation (R) exceeds the assigned interception (I) before it assumes that net precipitation reached the ground (Harlow and Hagedorn 2018; Westenbroek et al. 2018). Thus, we determined interception amounts for the different types of LULC based on previous studies (Harlow and Hagedorn 2018), and defined as growing season the period correspondent to the rainy seasons in Puerto Rico (April–November) (Table 3.1). The model estimates direct runoff using the curve number method for the different LULC classes and hydrologic soil groups. We assigned curve numbers based on published values (Huffman et al. 2011; Kent 1973; Westenbroek et al. 2018) and presented in Table 3.2. Soil types A, B, C, D, A/D, B/D, and C/D are original from the gSSURGO dataset, while the soil types W and ROut correspond to *water* and *rock outcrop* categories created by the authors to account for gaps within gSSURGO dataset. Therefore, we assigned soil type W for all the landscapes related to water and wetlands (e.g., riverwash, alluvial land, and open water), and assigned type ROut to all the rock outcrop and rock land. For grid cells with no data available, we assigned soil type C, which corresponds to the main soil type in the region (i.e., silty clay loam) according to local experts (Eric Harmssen, University of Puerto Rico-Mayagüez, pers. comm.). For urban land, we assigned soil type C/D due to its lower permeability.

SWB2 avoids the overestimation of net infiltration by allowing the user to assign maximum infiltration rates to specify the maximum amount of daily recharge for each hydrologic soil types (Table 3.3). After reaching the maximum daily net infiltration, the remaining water is classified as rejected net infiltration and it is assumed to find its way to some surface water feature. Therefore, the total runoff (Roff) is the sum of the direct runoff and the rejected net infiltration. In this study, we used the same maximum infiltration rates as used by Westenbroek et al. (2018).

Additionally, three possible potential evapotranspiration (PET) estimation methods are available in the SWB model, including Hargreaves-Samani method used in this study (Hargreaves and Samani 1985), which is considered a simplified version of FAO Penman-Monteith method (not included in the model). The Hargreaves-Samani method required as input spatially distributed minimum and maximum daily temperature and we used gridded data from Daymet (Version 3). By knowing the PET, the SWB2 model can estimate actual ET (AET) as a function of PET, net precipitation, and the current soil moisture amount for each grid cell as follows: (a) when net precipitation – PET ≥ 0, then AET = PET; (b) when net precipitation – PET ≤ 0, then AET is equal to the amount of water that can be extract from the soil via AET considering the computed values of soil moisture retention tables of Thornthwaite and Mather (1957) and modified by Westenbroek et al. (2010). Additionally, to use the Thornthwaite-Mather function, the SWB2 model needed to estimate the maximum soil moisture storage capacity, which was computed in this study as a product of the AWC data (from gSSURGO) multiplied by the root depth of each hydrologic soil type, which were defined based on the values reported by Westenbroek et al. (2018) (Appendix A).

Finally, the SWB2 model requires an initial amount of soil moisture to be able to calculate potential soil saturation and net infiltration or evapotranspiration of day 1, which was determined using the reference value used to run the SWB2 for Maui, Hawaii (Westenbroek et al. 2018). However, to guarantee a better estimation of soil moisture, we ran the SWB2 model for a warmup period of at least one year prior the period of analysis. The detailed control files including all the parameters used to run the SWB2 model for Puerto Rico are provided in Appendix B.

3.2.3 Drought years

After defining the baseline climatology (1981–2010) and the recent decade (2010–2019) to run the SWB2 model, we used the annual average rainfall to select the drought years. We used the input rainfall data averaged over year to select the four years with lowest annual average rainfall amounts for Puerto Rico, representing 10% of the period of analysis. For Puerto Rico, the most intense drought years were 1994, 1997, 1991, and 2015 (in descending order). Then, we compared those years against the drought metric values of the self-calibrated Palmer Drought Index (scPDSI) results from Moraes and Mote (in preparation, Chapter 2) to check if they were part of the driest years. The results indicated that the four drought years selected here were also part of the top six years of drought in Puerto Rico according to scPDSI values.

Then, we averaged the drought years SWB2 outputs during this period to create drought years water budget annual maps. In this way, we could compare the difference in spatial distribution of net infiltration over Puerto Rico during the baseline climatology (1981–2010) and the drought years to analyze where within the island the lack of water was greater when drought events occurred.

3.2.4 Model evaluation

Several methods are used to assess water budget models outputs based on the availability of data. In this study, we assessed the SWB2 outputs in two ways: 1) by comparing SWB2 against an existing water budget model for Puerto Rico, the GOES-PRWEB (Mecikalski and Harmsen 2019); 2) by comparing SWB2 to observed watershed streamflow from stream gauges of the US Geological Survey (USGS).

In Figure 3.4 we presented the comparisons between the SWB2 model and the GOES-PRWEB model. Because the GOES-PRWEB model started its analysis in Puerto Rico only in 2009, we compared the decade of data in which both models overlapped, from 2009 to 2019. Rainfall and runoff comparisons (Figure 3.4 b,c) both demonstrated a positive correlation between SWB2 and GOES_PRWEB models of +0.6 and +0.5, respectively. However, only rainfall correlation was statistically significant (p=0.10), while the relationship between models' runoff was not statistically significant. From 2009 to 2014, the rainfall input from SWB2 presented at least 30% more annual average rainfall than the GOES-PRWEB model. Although further investigation is needed to assess which rainfall input data was more accurate (Daymet Version 3 used in SWB2, or NOAA's Advanced Hydrologic Prediction Service (AHPS) used in GOES_PRWEB), both models rainfall amounts from 2015 to 2019 are in good agreement, which includes at least two extreme events: the intense drought of 2015 and hurricanes Irma and Maria in 2017. The models' correlation for AET was +0.5, which is statistically significant (p=0.10), although SWB2 seemed to overestimate AET when compared to GOES_PRWEB. Finally, the correlation between the SWB2 and GOES_PRWEB net infiltration was very strong (+0.8) and statistically significant (p=0.01). Therefore, considering that the models used different approaches to estimate water budget as well as different input data sources, the statistically significant correlation together with the similarities among models' results of annual net infiltration suggest that they should be both considered as valid options to estimate net infiltration in Puerto Rico.

We also analyzed the model performance in comparison with observed streamflow data from the USGS. The watersheds selection in Puerto Rico was based on their spatial distribution over the island and the availability of data that overlapped the most with our period of study (1981–2019). The following watersheds were included in this study (from larger to smaller): Manati (330.7 km^2), Guanajibo (310.5 km^2), Cibuco (226.8 km^2), Fajardo (38.3 km^2), and Espiritu Santo (22.5 km^2) (Figure 3.5). From the SWB2 model, we used *Roff* (runoff + rejected net infiltration) and converted the model outputs to streamflow (m^3 s^{-1}) to create the simulated data and compare it with the observation. In the observation data, we performed base flow separation through the Web based Hydrograph Analysis Tool (WHAT) system, which used Eckhardt filter method and was tested to provide more consistent results than a manual separation of base flow (Lim et al. 2005). For all watersheds analyzed, we selected the parameter "perennial streams with hard rock aquifers" since all of them are located in the mountainous area of the island.

Finally, we compared the simulated versus observed direct runoff by running three model performance statistical tests commonly used in previous studies (Ang and Oeurng 2018; Kumar et al. 2017; Moriasi et al. 2007), which are the Nash-Sutcliffe efficiency (NSE), the RMSE-observations standard deviation ratio (RSR), and the percent bias (PBIAS). Because we have used different LULC to run the SWB2 for the baseline climatology (1981–2010) and the recent decade (2010–2019) for Puerto Rico, we ran the statistical tests separately for each period of analysis. The definition of each model performance test is summarized below and their reference numbers are presented in Table 3.4 (more details are available in Moriasi et al. (2007)):

- NSE: indicates how well the plot of observed versus simulated data fits the 1:1 line by a normalized statistic that determines the relative magnitude of the residual variance ("noise") compared to the measured data variance ("information"). NSE ranges from $-\infty$ and 1.0 (1 inclusive), where 1.0 is the optimal value. Values between 0.0 and 1.0 are viewed as acceptable levels of performance.
- RSR: standardizes RMSE, which is one of the commonly used error index statistics, using the observations standard deviation. RSR is calculated as the ratio of the RMSE and standard deviation of measured data. It varies from the optimal value of 0, which indicates zero residual variation and perfect model simulation, to a large positive value. Therefore, the lower the RSR the better the model simulation.
- PBIAS: measures the average tendency of the simulated data to be larger or smaller than the observed data. The optimal value is 0.0, with low-magnitude values indicating accurate model simulation. Positive values mean model underestimation bias, and negative values mean model overestimation bias.

The timeseries presented in Figure 3.6 and Figure 3.7 show the comparison of the monthly average simulated versus observed direct runoff for Puerto Rico during the baseline climatology and recent decade, respectively. Overall, the model shows consistency over time in better predicting peak flows, mainly in the larger area watersheds, while it underestimated most of the low flows. In the small watersheds located in the Luquillo Mountains, such as Fajardo and Espiritu Santo, the model slightly underestimated the flow over time. Figure 3.8 shows both scenarios together and reinforce that the model simulated better average and peak flows mainly for Manati, Cibuco and Guanajibo, but it underestimated low flows, while for Fajardo and Espiritu Santo basins the model is overall underestimating the flow. However, the relationship between the simulated and observed data were very strong and statistically significant ($p=0.01$) for all the watersheds, with correlation coefficient $\geq +0.8$, except for Manati in the recent decade that presented a correlation coefficient of +0.7.

Moreover, the model performance statistics for Puerto Rico (Table 3.5) indicated that for the baseline climatology (1981–2010) the best simulation occurred in Guanajibo with both NSE (0.75) and RSR (0.50) rating as good model performance, while its PBIAS indicated the model has a very good performance with an overestimation of only 2.9% of the flow. Cibuco came next, with a similar model performance indicating good rate for NSE (0.71) and RSR (0.54) and very good for PBIAS (+8.2%), while the simulation of direct runoff for Manati was at satisfactory rate in all model performance statistics (NSE = 0.52, RSR = 0.69, PBIAS = -23.5%). For the smaller area basins, SWB2 was very close to satisfactory performance for Fajardo's NSE (0.45) and RSR (0.74), but it did not have the satisfactory performance for Espiritu Santo. In the recent decade, on the other hand, the SWB2 performed slightly better for Fajardo and Espiritu Santo, but slightly worse for Manati, Cibuco, and Guanajibo. In fact, Fajardo simulation in the recent decade presented a satisfactory NSE (0.60) and RSR (0.63), with a PBIAS indicating the model underestimated only 34% of the flow (Table 3.5). For Guanajibo and Cibuco, the model performed very similarly and kept the good NSE and RSR, and very good PBIAS, while Manati was slightly below the satisfactory performance. Overall, Espiritu Santo was the watershed simulation with the worst performance when comparing all the statistics tests and periods, which was expected since it is the smaller watershed analyzed here.

These slightly better performance of the model in the larger watersheds during the baseline climatology (1981–2010) than in the recent decade (2010–2019) may be related to the fact that the Caribbean, in general, has been presenting a negative trend in drought index indicating more drought events (Herrera and Ault 2017; Herrera et al. 2018). Because the model did not perform well reproducing the low flows in Puerto Rico, we hypothesize that the increase in the occurrence and intensity in drought events may have affected the overall model performance in the recent decade. On the other hand, the improvement in how SWB2 performed for the smaller watersheds in the Luquillo Mountains in the recent decade could be related to the increase in data availability and equipment installed to monitor the tropical rainforest, due to research projects such as the Long-Term Ecological Research (LTER). Therefore, more data available recently could probably helped to improve the accuracy of the rainfall input data that uses updated version of Global Historical Climate Network (GHCN) daily data (Thornton et al. 2017), which also improved the SWB2 model simulation in Fajardo and Espiritu Santo. However, because direct runoff is directly related to rainfall, we believe that the accuracy of the Daymet rainfall data and its relatively coarse spatial resolution of 1 km may have a larger effect in a smallest watershed like Espiritu Santo, when compared to the other basins. This basin was served with less than 22 grid cells of rainfall data, which is a coarse resolution for the accuracy and analysis of rainfall needed in a steep slope terrain located in the Luquillo Mountains.

Moreover, the basins where the model performed better, such as Manati, Cibuco, Guanajibo, and Fajardo, all have a large portion of soil type “C” (e.g., silty clay loam), which is the most common soil type in Puerto Rico. This could be an indication that the SWB2 model performs satisfactorily for most of the areas in the island. Although we recommend caution interpreting the results of the SWB2 model mainly for areas located in the steep slope of the Luquillo Mountains, where the model is mostly underestimating streamflow, we believe the model has performed very well in Puerto Rico without the need of calibration, and it should be considered as an option for future studies interested in water budget modeling in the island.

3.3 Results and Discussion

3.3.1 Baseline climatology *versus* recent decade

Annual net infiltration in Puerto Rico had a similar spatial distribution when comparing the baseline climatology (1981–2010) and the recent decade (2010–2019). In Figure 3.9 (a) and Figure 3.10 (a), the estimated net infiltration was greater in the central-west and northern portion of the island ranging from 600–900 mm $year^{-1}$ (baseline) to 700–1000 mm $year^{-1}$ (recent decade). The greatest net infiltration occurred in eastern Puerto Rico, in lower topographic areas of the Luquillo Mountains/El Yunque National Forest, where it reached values greater than 1500 mm $year^{-1}$ during both periods of analysis. When examining the other water budget elements, we see that central and eastern Puerto Rico were areas with greater values of actual ET and runoff, when compared to other areas within the island, but they were also the areas with the greatest annual rainfall ($\geq$ 2500 mm $year^{-1}$). Therefore, the abundant rainfall in those areas provided extra water available for net infiltration. Another characteristic of the areas with greater net infiltration in Puerto Rico is that they are in the heavily vegetated mountainous areas of the island (i.e., Cordillera Central and Luquillo Mountains) and have soil types B and C with greater infiltration rates (Figure 3.3 c). Southern Puerto Rico, on the other side, was where the lowest amount of net infiltration occurred in both periods. That region is known for its dry climate, and we can see that while the annual rainfall was $\leq$ 1000 mm $year^{-1}$, the annual AET was as high as in the rest of the island (~ 750 mm $year^{-1}$), which contributed to its lower annual net infiltration ($\leq$ 200 mm $year^{-1}$).

When comparing the drier south with the wetter east and central Puerto Rico, the role of the mountains as well as the importance of vegetation on water cycle are evident. South Puerto Rico is known as a drier region and based on its humidity, annual precipitation, and PET it was classified as “dry forest” (Holdridge 1967). The lower humidity there is related to its geographic location on the leeward side of the Central Mountain Range (i.e., Cordillera Central), which creates a shield blocking the Atlantic moisture and making the south drier than other regions of Puerto Rico (Torres-Valcárcel et al. 2014). Moreover, the presence of soil type D with lower infiltration rates, as well as having more cultivated crops land than forests (Figure 3.3), could also contributed to the lower rates of net infiltration in the south.

In the Cordillera Central and in the Luquillo Mountains, on the other hand, the orographic uplift of the northeasterly winds coming from the Atlantic Ocean results in greater rainfall that makes these regions wetter than the rest of the island (Hosannah et al. 2019; Sobel et al. 2011). Additionally, these mountains are covered by vegetation, with the Luquillo Mountains being the location of the El Yunque National Forest. The presence of forests can affect the water cycle through their high absorption of solar radiation, due to low albedo, resulting in energy available for evapotranspiration of water, cloud formation and possible showers (Scheffer et al. 2005).

Although the spatial distribution of net infiltration and the other water budget variables are similar between the baseline and the recent decade, there were some important differences in the amount of water distributed over the island during those periods. The changes become clear when we calculate the difference between the recent decade minus the baseline climatology (Figure 3.11). In central and west areas of Puerto Rico, net infiltration was at least 250 mm year^{-1} greater in the recent decade than in the baseline climatology, while AET was similar, and runoff increased in the recent decade ($\geq$ 100 mm year^{-1}). These differences could be explained by the increase in rainfall in most of the island, with central-west region receiving at least 400 mm year^{-1} more annual rainfall in the recent decade than in the baseline climatology. However, the opposite occurred in the Luquillo Mountains/El Yunque National Forest area, where less rainfall was registered from 2010–2019 ($\leq$ -250 mm year^{-1}), followed by less runoff ($\leq$ -200 mm year^{-1}), and less AET ($\leq$ -50 mm year^{-1}). Consequently, net infiltration decreased in eastern Puerto Rico in the recent decade ($\leq$ -100 mm year^{-1}).

In Eastern Puerto Rico, the decrease in rainfall in the recent decade may be influenced by the Saharan Air Layer (SAL) intrusion in the island. In 2015, for example, the Caribbean registered the highest dust concentration from 1980 to 2016, while an increase trend in dust mass concentration have been reported since 1991 (Hosannah et al. 2019). It is known that SAL peaks from late June to mid-August and can propagate westward across the Atlantic Ocean bringing anomalously hot, dry air in the low to middle troposphere (around 700 hPa), producing thermodynamically stable conditions and limiting rainfall in the insular Caribbean, in general, and in Puerto Rico, in particular (Kuciauskas et al. 2018; Mote et al. 2017). Therefore, with the increase in dust concentration in the recent decade the orographic effect that plays an important role in keeping eastern Puerto Rico wetter than most of the island may have been suppressed.

However, local mechanisms should also be investigated to understand the variability in precipitation over Puerto Rico. The increase in rainfall in central-west Puerto Rico in the recent decade, for example, can be related to local island processes such as surface heating, orographic uplift, and sea breeze trade-wind convergence that can overcome drought events and the SAL episodes (Hosannah et al. 2019). These local variations in precipitation over Puerto Rico were well represented during the 2015 drought event, when the east was hardest affected by drought (Miller and Ramseyer 2020; Mote et al. 2017) while the west side had some sites registering positive precipitation anomalies (Hosannah et al. 2019).

These changes in rainfall together with the changes in LULC in Puerto Rico may also affect the difference in net infiltration occurred between the baseline climatology and the recent decade. In Figure 3.3 (a, b), we see the reduction in herbaceous category over the island, from 2001 to

2010 LULC, with the increase in cultivated crops in the central area instead. Greater rainfall in central Puerto Rico and less herbaceous vegetation to intercept the water allowed an increase in net infiltration. On the other hand, the decrease in herbaceous and the increase in developed land in eastern Puerto Rico, together with the decrease in rainfall, may have contributed to the decrease in net infiltration occurring there in the recent decade.

Finally, when analyzing the temporal distribution of the water budget components in Puerto Rico (Figure 3.12), we can see that all the greatest values of rainfall occurred in the recent decade: in 2017, when the island was hit by hurricanes Irma and Maria, followed by 2010, and 2011. Among the years with the lowest annual average rainfall, 1994 could be highlighted in the baseline climatology, and 2015 in the recent decade. These years were previously compared as two intense drought events in Puerto Rico (Mote et al. 2017), and the water budget here suggested they also share in common a water deficit occurring in the prior year, indicating that an imbalance in water before a year with low rainfall are ingredients that result in intense droughts.

3.3.2 Drought years *versus* baseline climatology

We selected 1994, 1997, 1991, and 2015 (in descending order) based on criteria explained in the methods section to represent drought years. Figure 3.13 shows the annual spatial distribution of the water budget components during those drought years and indicated much smaller area as well as lower values of net infiltration when compared to the baseline climatology. During drought years, Puerto Rico had only small areas of net infiltration still occurring in the central-west of the island, with values between 300–500 mm $year^{-1}$, and in the lower topographic areas of Luquillo Mountains/El Yunque National Forest (≤ 800 mm $year^{-1}$). Most of the island, conversely, had very low values of net infiltration (≤ 200 mm $year^{-1}$). Most of southern Puerto Rico received less than 700 mm $year^{-1}$ of rainfall while a similar amount of water was lost through AET (Figure 3.13 b,c), which resulted in little water for net infiltration ($\leq$ 100 mm year^{-1}). The northern area of Puerto Rico had also suffered with less precipitation and high AET, resulting in infiltration concentrated in a small area.

Overall, the island had much less net infiltration during drought years with areas such as the south close to 0 mm year^{-1}. When analyzing the relationship between rainfall, runoff, and AET over the island during the drought years, it is also possible to see that at least two thirds of the rainfall was withdrawal by AET, and the remaining one third was divided between runoff and net infiltration. Past studies have suggested that the high values of AET are one of the primary reasons for the lack of surface water availability, the vulnerability to drought, and the changes in groundwater recharge in the small tropical islands (Gamble 2004; Holding et al. 2016).

The entire island of Puerto Rico had a reduction in net infiltration of at least -150 mm year^{-1} during drought years, except for some rock outcrops located in the north of the island which showed no difference (Figure 3.14). However, the areas more affected by drought years were parts of central and northern Puerto Rico as well as the Luquillo Mountains, where the reduction in net infiltration was more than 400 mm year^{-1} below baseline period. Central and eastern Puerto Rico were areas where the greatest departure in precipitation occurred ($\leq$ -700 mm year^{-1}), together with the reduction of the runoff ($\leq$ -400 mm year^{-1}). Although AET mostly decreased over the island during drought years, central-west and eastern Puerto Rico registered similar amounts of AET when compared to the baseline climatology. Together with large reduction in rainfall, this could explain why central-west and eastern Puerto Rico had the greatest difference in net infiltration during drought years.

We know that for drought years such as 1994 and 2015, one of the reasons for the greater reduction in rainfall in eastern Puerto Rico was the intrusion of the SAL (Miller and Ramseyer

2020; Mote et al. 2017), as previously discussed. The inhibition of rainfall produced by SAL was likely more intense over the mountainous regions of Puerto Rico due to the stable thermodynamic conditions that suppressed the orographic uplift, resulting in less local rainfall. Additionally, those two drought years were also related with positive phase of the North Atlantic Oscillation (NAO) occurring the winter preceding the SAL intrusion and the drought event (Mote et al. 2017), which contribute to stronger North Atlantic subtropical high (NAHP) an stronger trader winds over Tropical North Atlantic that could have helped to bring more dust from SAL events toward Puerto Rico. The greater intensity of 2015 drought in eastern Puerto Rico was registered in other studies (Álvarez-Berríos et al. 2018; Mote et al. 2017).

Additionally, it is important to highlight the potential impacts of drought on Puerto Rico aquifers. The area in northern Puerto Rico where net infiltration reduction occurred was where the North Coast Aquifer is located (Figure 3.1 b), which indicates a substantial reduction in groundwater recharge during drought events. The North Coast Aquifer is considered the most extensive and productive fresh-water aquifer on the island, with its groundwater serving an important source for local ecosystems and for public supply of freshwater (Lugo et al. 2001; Maihemuti et al. 2015; Padilla et al. 2011). Therefore, the reduced rainfall in north and central Puerto Rico during drought years (Figure 3.14 b) may directly affect the recharge of the North Coast Aquifer, because parts of this aquifer is almost exclusively recharged by direct rainfall, while other areas are recharged both by direct rainfall and the streams from Cordillera Central (on the volcanic rocks) that infiltrate underground when they cross onto the karst rocks (Mendez-Tejeda et al. 2016).

Although the difference in net infiltration in southern Puerto Rico were smaller than the rest of the island ($\leq$ -100 mm year^{-1}), when comparing drought years and the baseline climatology, this area is where the South Coast Aquifer is located. According to Mendez-Tejeda et al. (2016), this aquifer is recharged both by direct rainfall and from the streams that flow out of the mountains of the Cordillera Central. Therefore, the impacts of drought in the South Coast Aquifer recharge may come not only from the reduction in local rainfall and net infiltration, but also from the decrease rainfall felt in central Puerto Rico, which affected the river's streamflow in the mountains. Southeastern Puerto Rico was classified as the area of the island most exposed to any classification of drought from 2000 to 2016 (Álvarez-Berríos et al. 2018), while some studies indicated that the South Coast Aquifer has already been suffering with lower recharges and high demand of groundwater in the recent decade (Harmsen 2019; Torres-Gonzalez and Rodriguez 2016). Moreover, the South Coast Aquifer's groundwater was the principal source of potable water for cities in the south coast of Puerto Rico, as well as primary source of water for agricultural irrigation (Torres-Gonzalez and Rodriguez 2016). Therefore, if there is no groundwater availability there during drought events, when surface water is normally unavailable, Puerto Rico would need to rely on desalinization. This creates additional problems as desalinization is energy intense and based on the use of fossil fuels; increased use of desalinization would increase air pollution and emissions of greenhouse gasses in the island (Mendez-Tejeda et al. 2016).

3.4 Conclusions

This study analyzed how the physical geography of Puerto Rico can impact the island's water budget and its net infiltration during three different periods: the baseline climatology (1981–2010), the recent decade (2010–2019), and drought years (1991, 1994, 1997, and 2015).

The results indicated that central west, north, and eastern Puerto Rico are the areas where more net infiltration occurred over the island, both during the baseline climatology and the recent decade. The greater net infiltration in mountainous and highly vegetated areas of the island, such as the Cordillera Central and the Luquillo Mountains, suggested the important role of topography in creating orographic rainfall, and of vegetation as a source of moisture. The presence of the soil types B and C, with higher rates of infiltration, may have also contributed to the greater amount of net infiltration in those areas. However, changes in rainfall amounts in the recent decade have affected the net infiltration. While central west and northern Puerto Rico received more rainfall followed by greater net infiltration in the recent decade, the east registered a decrease in both rainfall and net infiltration, which could be a consequence of large-scale atmospheric circulation mechanisms, such as the SAL intrusion.

On the other side, southern Puerto Rico had lower net infiltration in both periods of analysis, because of its drier climate when compared to the rest of the island. The location of the south, on the rain shadow side of the Cordillera Central, together with the presence of more D soil type (with lower infiltration rates), and greater areas of cultivated crops than heavy vegetation, may have all combined to result in an area with lower net infiltration.

During drought years, the whole island reduced its net infiltration due to drastically reduction in annual rainfall amounts. The greatest reductions in net infiltration occurred in the central west and eastern Puerto Rico, which could impact the tropical forest and its soil moisture, as well as in parts of the north, where the most productive fresh-water aquifer is located (i.e., the North Coast Aquifer). In southern Puerto Rico, although the difference in net infiltration during drought events was less dramatic than in other areas of the island, it could still aggravate the situation of the South Coast Aquifer, which has already been suffering with lower recharges and high demand of groundwater in the recent decade.

Because these findings are the first that we know of to highlight the role of physical geography on Puerto Rico's water budget and net infiltration while comparing the baseline climatology, the recent decade, and drought years, we expect they will be useful to help local government to plan for water management and better prepare for drought events. The use of SWB2, a new released and open-access water budget model from the USGS, was also important to test the performance of the model in a tropical Atlantic island. The fact that the model performed satisfactorily, and in some case much better, for watersheds spatially distributed over Puerto Rico indicated that SWB2 is an excellent tool for water-budget analysis even without calibration. Because we ran the model for the entire island in this work, instead of for specific watersheds, calibration would be a challenge due to the heterogeneity of the island environment that would not allow for a calibration that improved the model islandwide.

The authors note the limitations of the SWB2 model. Therefore, we suggest that future work should test the SWB2 model performance in Puerto Rico using different model parameters we have used here, as well as adding input data we did not find by the time of this research, such as fog interception or irrigation, that could help to improve the model estimation of net infiltration. The application of the SWB2 model in other Caribbean islands would also be interesting and allow for the comparison of SWB2 performance in different areas of the insular Caribbean.

Acknowledgments

The authors thank MSc. Lucas Favero for the support provided with watershed evaluation and SWB2 analysis, as well as with valuable suggestions that helped to improve this manuscript; Stephen Westenbroek for creating the SWB2 (https://pubs.er.usgs.gov/publication/tm6A59) and providing technical support for model execution; and MSc. Ayan Fleischmann for helping with

MatLab coding. The authors also thank the NSF Luquillo Long-Term Ecological Research Program (DEB1239764) and NOAA Modeling, Analysis, Predictions and Projections (MAPP) grant (NA20OAR4310415) for the funding provided, the National Aeronautics and Space Administration (NASA) Earth Data for Daymet data availability (https://daymet.ornl.gov/), the U.S. Geological Survey for Puerto Rico streamflow data (https://waterdata.usgs.gov/pr/nwis/rt), the U.S. Department of Agriculture Geospatial Data Gateway (https://datagateway.nrcs.usda.gov/) for the Gridded Soil Survey Geographic (gSSURGO) Database for hydrologic soil types and available water soil capacity data, and the National Land Cover Database for the 2001 land use and land cover (LULC) data (https://www.mrlc.gov/data/nlcd-2001-land-cover-puerto-rico), as well as NOAA Office for Coastal Management (NOAA/OCM) for 2010 LULC (https://coast.noaa.gov/digitalcoast/data/). Finally, we thank Dr. Eric Harmsen for the GOES-PRWEB model data (https://pragwater.com/goes-puerto-rico-water-and-energy-balance-goes-web-algorithm/) and thoughtful discussion about the model outputs.

3.5 References

Álvarez-Berríos, N. L., S. Soto-Bayó, E. Holupchinski, S. J. Fain, and W. A. Gould, 2018: Correlating drought conservation practices and drought vulnerability in a tropical agricultural system. *Renewable Agriculture and Food Systems*, **33,** 279-291.

Ang, R., and C. Oeurng, 2018: Simulating streamflow in an ungauged catchment of Tonlesap Lake Basin in Cambodia using Soil and Water Assessment Tool (SWAT) model. *Water Science*, **32,** 89-101.

Ault, T., 2016: Island water stress. *Nature Climate Change*, **6,** 1062-1063.

Cashman, A., L. Nurse, and C. John, 2010: Climate change in the Caribbean: the water management implications. *The Journal of Environment & Development*, **19,** 42-67.

Dieter, C. A., and Coauthors, 2018: Estimated use of water in the United States in 2015141134233X.

Farrell, D., A. Trotman, and C. Cox, 2010: Drought early warning and risk reduction.

Gamble, D. W., 2004: Water resource development on small carbonate islands: solutions offered by the Hydrologic Landscape concept. *WorldMinds: Geographical Perspectives on 100 Problems: Commemorating the 100th Anniversary of the Association of American Geographers 1904–2004*, D. G. Janelle, B. Warf, and K. Hansen, Eds., Springer Netherlands, 503-507.

Garcia-Martino, A. R., G. S. Warner, F. N. Scatena, and D. L. Civco, 1996: Rainfall, runoff and elevation relationships in the Luquillo Mountains of Puerto Rico. *Caribbean Journal of Science*, **32,** 413-424.

Geoghegan, T., and Y. Renard, 2002: Beyond community involvement: lessons from the insular Caribbean. *Parks*, **12,** 16-27.

Hargreaves, G. H., and Z. A. Samani, 1985: Reference crop evapotranspiration from temperature. *Applied engineering in agriculture,* **1,** 96-99.

Harlow, J., and B. Hagedorn, 2018: SWB Modeling of groundwater recharge on Catalina Island, California, during a period of severe drought. *Water*, **11,** 58.

Harmsen, E. W., 2019: Puerto Rico South Coast Aquifer recharge analysis. *Press conference presentation*.

Healy, R. W., 2010: *Estimating groundwater recharge.* Cambridge University Press.

Hendry, M. D., 1996: The geological legacy of small islands at the Caribbean-Atlantic boundary. *Coastal and Estuarine Studies***,** 205-224.

Herrera, D., and T. Ault, 2017: Insights from a new high-resolution drought atlas for the Caribbean spanning 1950–2016. *Journal of Climate*, **30,** 7801-7825.

Herrera, D. A., T. R. Ault, J. T. Fasullo, S. J. Coats, C. M. Carrillo, B. I. Cook, and A. P. Williams, 2018: Exacerbation of the 2013–2016 Pan-Caribbean drought by anthropogenic warming. *Geophysical Research Letters*, **45,** 10,619-610,626.

Holding, S., D. M. Allen, S. Foster, A. Hsieh, I. Larocque, J. Klassen, and S. C. Van Pelt, 2016: Groundwater vulnerability on small islands. *Nature Climate Change*, **6,** 1100-1103.

Hosannah, N., J. E. González, C. Lunger, and D. Niyogi, 2019: Impacts of local convective processes on rain on the Caribbean island of Puerto Rico. *Journal of Geophysical Research: Atmospheres*, **124,** 6009-6026.

Huffman, R. L., D. D. Fangmeier, W. J. Elliot, S. R. Workman, and G. Schwab, 2011: *Soil and water conservation engineering.* American Society of Agricultural and Biological Engineers St. Joseph.

Jury, M. R., 2020: Resolution-dependent perspectives on Caribbean hydro-climate change. *Hydrology*, **7,** 93.

Karnauskas, K. B., C.-F. Schleussner, J. P. Donnelly, and K. J. Anchukaitis, 2018: Freshwater stress on small island developing states: population projections and aridity changes at 1.5 and 2 °C. *Regional Environmental Change*, **18,** 2273-2282.

Kent, K., 1973: A method for estimating volume and rate of runoff in small watersheds.

Kuciauskas, A. P., P. Xian, E. J. Hyer, M. I. Oyola, and J. R. Campbell, 2018: Supporting weather forecasters in predicting and monitoring Saharan Air Layer dust events as they impact the Greater Caribbean. *Bulletin of the American Meteorological Society*, **99,** 259-268.

Kumar, N., S. K. Singh, P. K. Srivastava, and B. Narsimlu, 2017: SWAT Model calibration and uncertainty analysis for streamflow prediction of the Tons River Basin, India, using Sequential Uncertainty Fitting (SUFI-2) algorithm. *Modeling Earth Systems and Environment*, **3,** 30.

Lim, K. J., B. A. Engel, Z. Tang, J. Choi, K. S. Kim, S. Muthukrishnan, and D. Tripathy, 2005: Automated web GIS based hydrograph analysis tool, WHAT 1. *JAWRA Journal of the American Water Resources Association*, **41,** 1407-1416.

Lugo, A. E., and Coauthors, 2001: Puerto Rican karst-a vital resource.

Maihemuti, B., R. Ghasemizadeh, X. Yu, I. Padilla, and A. N. Alshawabkeh, 2015: Simulation of regional karst aquifer system and assessment of groundwater resources in Manati-Vega Baja, Puerto Rico. *Journal of Water Resource and Protection*, **07,** 909-922.

Martinez, C., L. Goddard, Y. Kushnir, and M. Ting, 2019: Seasonal climatology and dynamical mechanisms of rainfall in the Caribbean. *Climate Dynamics*.

Mecikalski, J. R., and E. W. Harmsen, 2019: The use of visible geostationary operational meteorological satellite imagery in mapping the water balance over Puerto Rico for water resource management. IntechOpen.

Mendez-Tejeda, R., R. Richards, and A. Emiliano, 2016: Analysis of groundwater in Puerto Rico, **4,** 68-76.

Miller, J. A., R. Whitehead, D. S. Oki, S. B. Gingerich, and P. G. Olcott, 1997: Ground water atlas of the United States: Segment 13, Alaska, Hawaii, Puerto Rico, and the US Virgin Islands0607881267.

Miller, P. W., and C. A. Ramseyer, 2020: Did the Climate Forecast System anticipate the 2015 Caribbean drought? *Journal of Hydrometeorology*, **21,** 1245-1258.

Moriasi, D. N., J. G. Arnold, M. W. Van Liew, R. L. Bingner, R. D. Harmel, and T. L. Veith, 2007: Model evaluation guidelines for systematic quantification of accuracy in watershed simulations. *Transactions of the ASABE*, **50,** 885-900.

Mote, T. L., C. A. Ramseyer, and P. W. Miller, 2017: The Saharan Air Layer as an early rainfall season suppressant in the Eastern Caribbean: The 2015 Puerto Rico drought. *Journal of Geophysical Research: Atmospheres*, **122**.

Padilla, I., C. Irizarry, and K. Steele, 2011: Historical contamination of groundwater resources in the north coast karst aquifers of Puerto Rico. *Rev Dimens*, **3,** 7-12.

Scheffer, M., M. Holmgren, V. Brovkin, and M. Claussen, 2005: Synergy between small- and large-scale feedbacks of vegetation on the water cycle. *Global Change Biology*, **11,** 1003-1012.

Sobel, A. H., C. D. Burleyson, and S. E. Yuter, 2011: Rain on small tropical islands. *Journal of Geophysical Research*, **116**.

Thornthwaite, C. W., and J. R. Mather, 1957: Instructions and tables for computing potential evapotranspiration and the water balance.

Thornton, M.M., P.E. Thornton, Y. Wei, R.S. Vose, and A.G. Boyer, 2017: Daymet: station-level inputs and model predicted values for North America, Version 3. ORNL DAAC, Oak Ridge, Tennessee, USA. https://doi.org/10.3334/ORNLDAAC/1391

Torres-Gonzalez, S., and J. M. Rodriguez, 2016: Hydrologic conditions in the South Coast aquifer, Puerto Rico, 2010–15. Report 2015-1215.

Torres-Valcárcel, Á., J. Harbor, C. González-Avilés, and A. Torres-Valcárcel, 2014: Impacts of urban development on precipitation in the tropical maritime climate of Puerto Rico. *Climate*, **2,** 47-77.

Westenbroek, S. M., J. A. Engott, V. A. Kelson, and R. J. Hunt, 2018: SWB Version 2.0—A soil-water-balance code for estimating net infiltration and other water-budget components. Report 6-A59.

Westenbroek, S. M., V. A. Kelson, W. R. Dripps, R. J. Hunt, and K. R. Bradbury, 2010: SWB-A modified Thornthwaite-Mather soil-water-balance code for estimating groundwater recharge. Report 6-A31.

Table 3.1 – Puerto Rico interception values (mm day^{-1}) for growing season (wet) and non-growing season (dry) based on different types of land use and land cover (LULC) used as input in the Soil Water Balance Model 2 (SWB2). First day of growing season started in April and ended in November, following the rainy seasons.

LULC	**Interception**	
	Growing	**Nongrowing**
High Intensity Developed	0.00	0.00
Medium Intensity Developed	0.51	0.25
Low Intensity Developed	0.51	0.25
Developed, Open Space	0.00	0.00
Cultivated Crops	3.81	3.81
Pasture/Hay	2.03	0.76
Grassland/Herbaceous	2.03	0.76
Mixed Forest	5.08	5.08
Shrub/Scrub	3.81	3.81
Palustrine Forested Wetland	5.08	5.08
Palustrine Scrub/Shrub Wetland	3.81	3.81
Palustrine Emergent Wetland	0.51	0.25
Estuarine Forested Wetland	5.08	5.08
Estuarine Scrub/Shrub Wetland	3.81	3.81
Estuarine Emergent Wetland	0.51	0.25
Unconsolidated Shore	0.00	0.00
Bare Land	0.00	0.00
Open Water	0.00	0.00
Palustrine Aquatic Bed	0.00	0.00
Estuarine Aquatic Bed	0.00	0.00

Source: Harlow and Hagedorn (2018)

Table 3.2 – Puerto Rico Curve Numbers (CN) used for land use and land cover (LULC) and hydrologic soil groups (1 to 9) as input in the Soil Water Balance Model 2 (SWB2). Hydrologic soil group numbers correspond to soil types as follows: B (1), C (2), A (3), C/D (4) D (5), B/D (6), W (7), ROut (8), and A/D (9).

LULC	**CN_1**	**CN_2**	**CN_3**	**CN_4**	**CN_5**	**CN_6**	**CN_7**	**CN_8**	**CN_9**
High Intensity Developed	92	94	89	95	95	94	70	95	93
Medium Intensity Developed	85	90	77	91	92	87	70	95	85
Low Intensity Developed	78	85	67	87	89	84	70	95	79
Developed, Open Space	69	79	49	82	84	75	70	95	65
Cultivated Crops	61	74	39	77	80	71	70	95	62
Pasture/Hay	61	74	39	78	80	71	70	95	62
Grassland/Herbaceous	61	74	39	77	80	71	70	95	62
Mixed Forest	55	70	30	74	77	65	70	95	56
Shrub/Scrub	56	70	35	74	77	65	70	95	59
Palustrine Forested Wetland	55	70	30	74	77	65	70	95	56
Palustrine Scrub/Shrub Wetland	56	70	35	74	77	65	70	95	59
Palustrine Emergent Wetland	58	71	30	74	78	68	70	95	56
Estuarine Forested Wetland	55	70	30	74	77	65	70	95	56
Estuarine Scrub/Shrub Wetland	56	70	35	74	77	65	70	95	59
Estuarine Emergent Wetland	58	71	30	74	78	68	70	95	56
Unconsolidated Shore	70	70	70	70	70	70	70	70	70
Bare Land	83	88	74	89	90	85	70	95	82
Open Water	70	70	70	70	70	70	70	95	70
Palustrine Aquatic Bed	70	70	70	70	70	70	70	95	70
Estuarine Aquatic Bed	70	70	70	70	70	70	70	95	70

Source: Huffman et al. (2011), Kent (1973), and Westenbroek et al. (2018).

Table 3.3 – Maximum net infiltration rates (mm day^{-1}) for Puerto Rico hydrologic soil groups used as input into the Soil Water Balance Model 2 (SWB2).

Hydrologic Soil Type	**Max_infilintration**
A	101.60
B	15.24
C	6.10
D	3.05
A/D	101.60
B/D	3.05
C/D	3.05
W	0.76
ROut	0.25

Source: Westenbroek et al. (2018).

Table 3.4 – General performance ratings for recommended statistics tests to analyze the Soil Water Balance 2 (SWB2) model performance to estimate direct runoff. RSR corresponds to the RMSE-observations standard deviation ratio, NSE is the Nash-Sutcliffe efficiency, and PBIAS is the percent bias test.

Performance Rating	**RSR**	**NSE**	**PBIAS (%)**
Very Good	$0.00 \leq RSR \leq 0.50$	$0.75 < NSE \leq 1.00$	$PBIAS < \pm10$
Good	$0.50 < RSR \leq 0.60$	$0.65 < NSE \leq 0.75$	$\pm10 \leq PBIAS < \pm15$
Satisfactory	$0.60 < RSR \leq 0.70$	$0.50 < NSE \leq 0.65$	$\pm15 \leq PBIAS < \pm25$
Unsatisfactory	$RSR > 0.70$	$NSE \leq 0.50$	$PBIAS \geq \pm25$

Source: Adapted from Moriasi et al. (2007).

Table 3.5 – Statistical tests for SWB2 model performance for Puerto Rico during the baseline climatology (1981–2010) and the recent decade (2010–2019). The performance rates are highlighted as follows: satisfactory performance is in yellow, good performance is in green, and very good performance is in blue, all according Moriasi et al. (2007). Gray values are almost satisfactory performance.

Puerto Rico

Monthly Direct Runoff 1981–2010, LULC 2001

Watershed	**Manati**	**Guanajibo**	**Cibuco**	**Fajardo**	**Espiritu Santo**
PBIAS (%)	-23.5	2.9	8.2	43.5	50.3
NSE	0.52	0.75	0.71	0.45	0.28
RSR	0.69	0.50	0.54	0.74	0.85

Monthly Direct Runoff 2010–2019, LULC 2010

Watershed	**Manati**	**Guanajibo**	**Cibuco**	**Fajardo**	**Espiritu Santo**
PBIAS (%)	-39.9	-8.8	-0.6	34.0	40.7
NSE	0.35	0.66	0.69	0.60	0.34
RSR	0.81	0.58	0.56	0.63	0.81

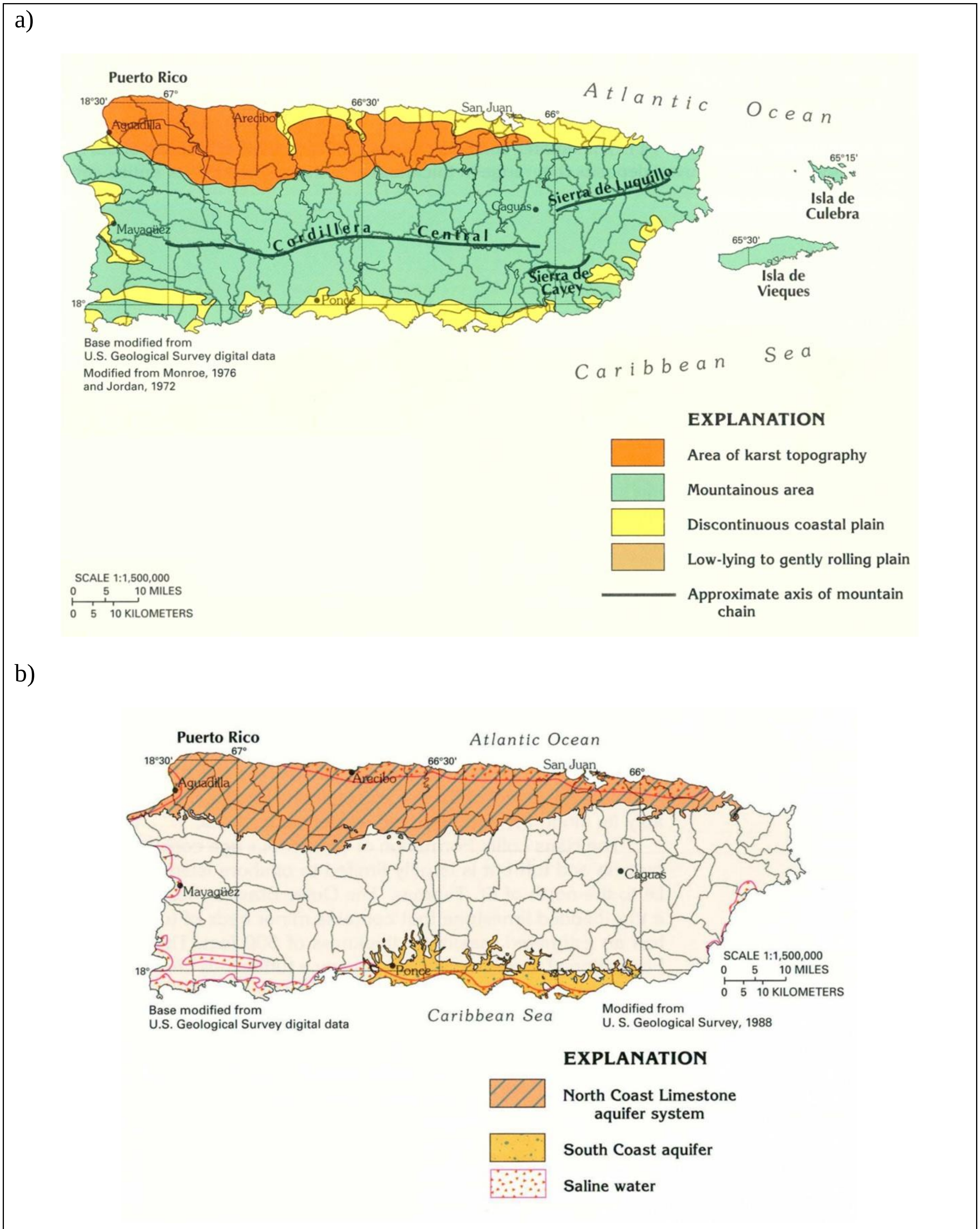

Figure 3.1 – Puerto Rico (a) physical geography and geology, (b) aquifers and coastal saline water intrusion. Source: Miller et al. (1997).

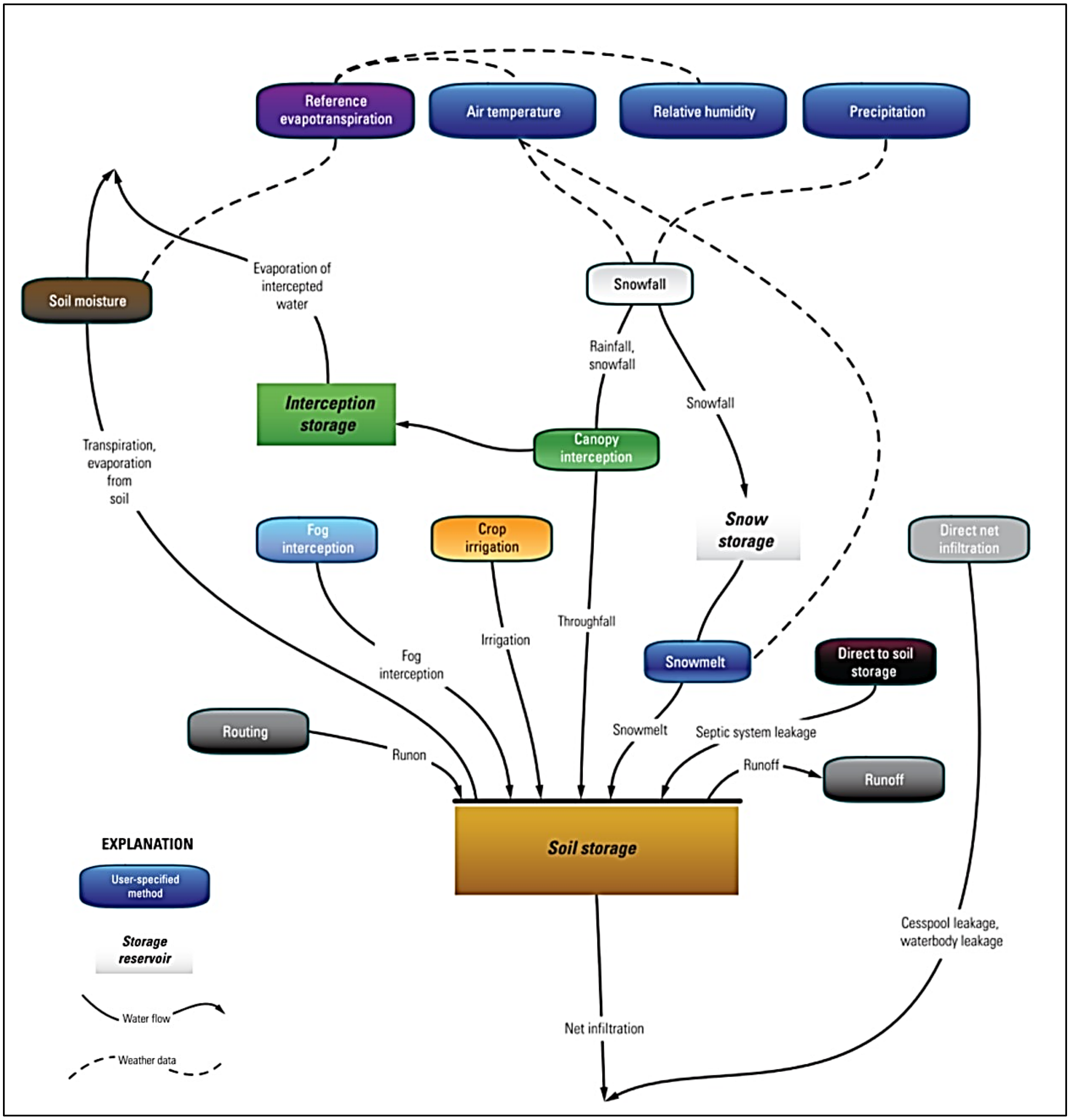

Figure 3.2 – Conceptual diagram of Soil-Water-Balance (SWB2) model storage reservoirs and processes. Source: Westenbroek et al. (2018).

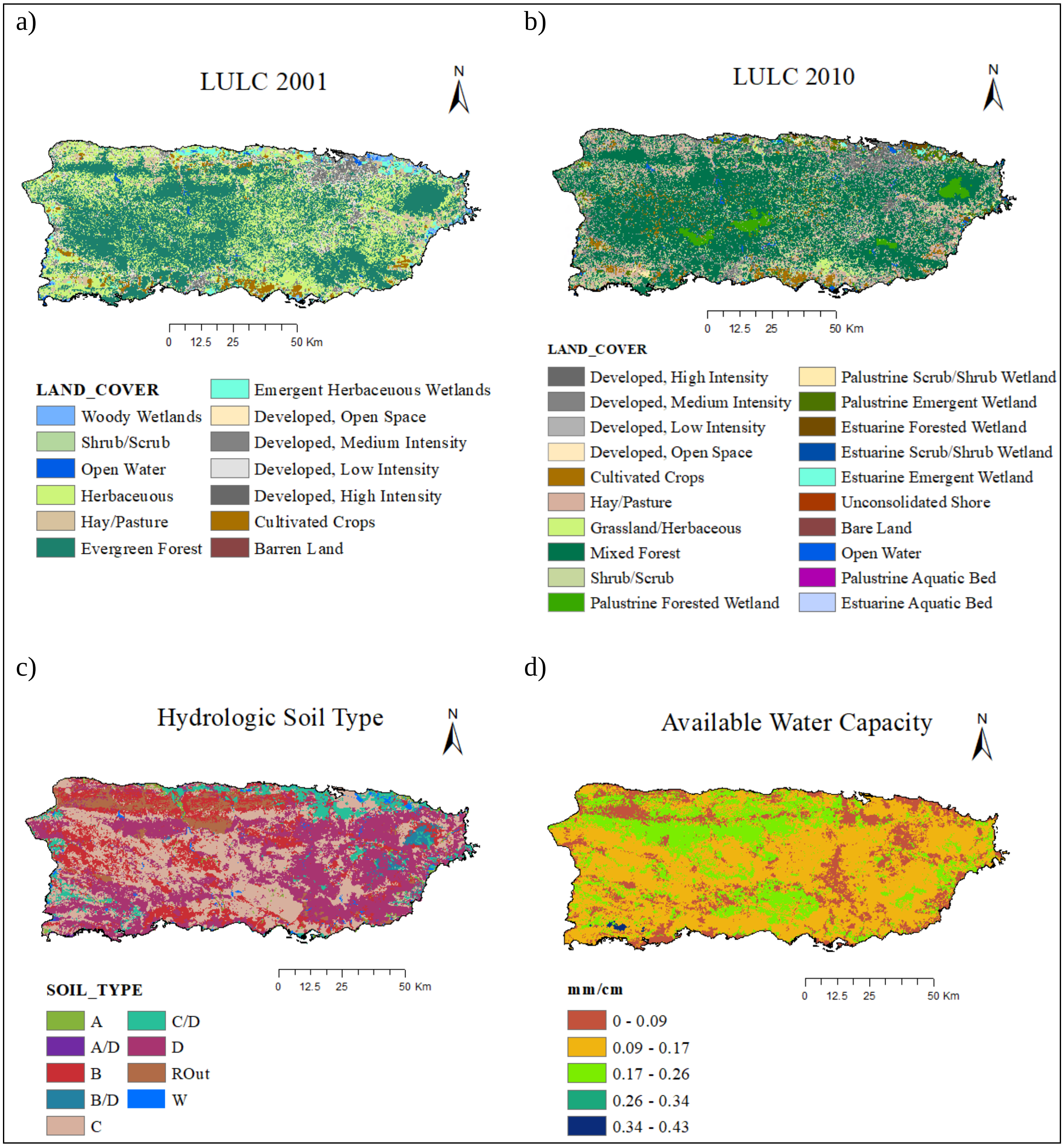

Figure 3.3 – SWB non-transient inputs for Puerto Rico showing spatial distribution of (a) land use and land cover 2001, (b) land use and land cover 2010, (c) hydrologic soil groups, and (d) available water capacity (averaged over the first 100 cm of soil depth).

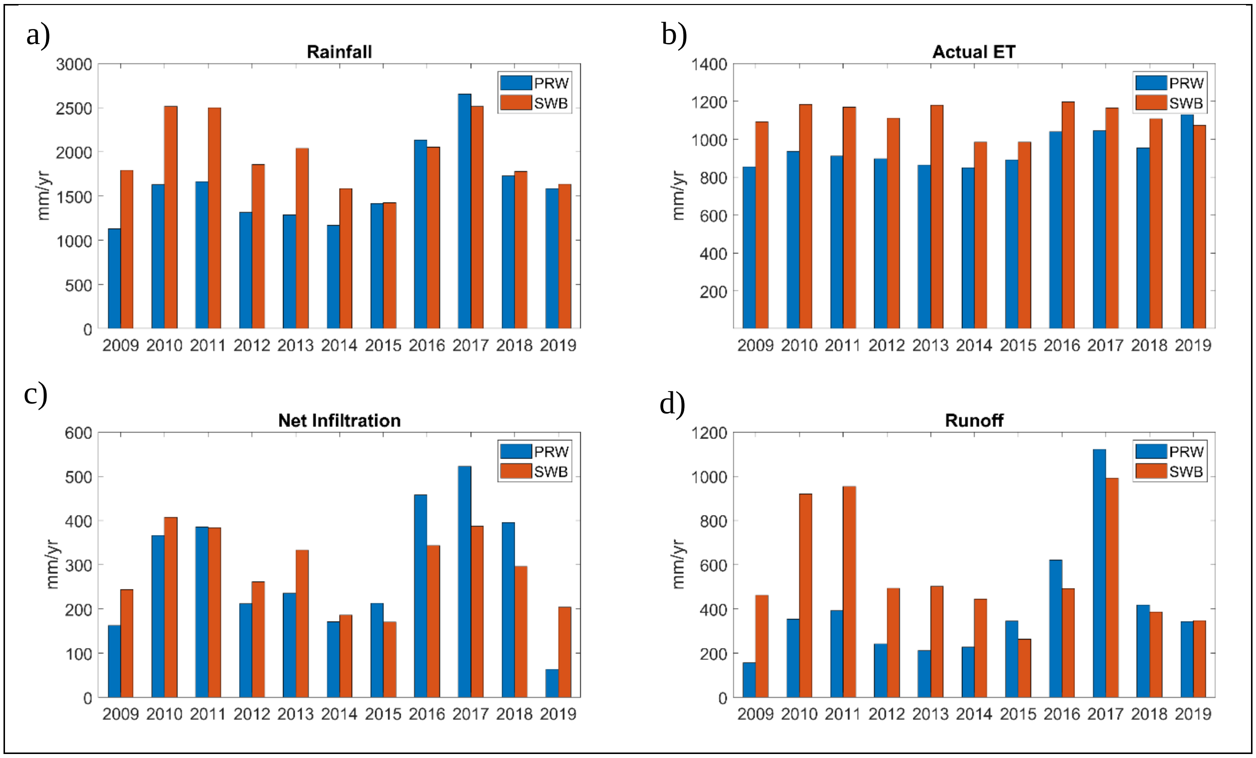

Figure 3.4 – The comparison between SWB2 (in orange) and GOES-PRWEB (in blue) models' outputs annual totals (mm year^{-1}) for (a) actual evapotranspiration (ET), (b) net infiltration, (c) rainfall, and (d) runoff, from 2009 to 2019.

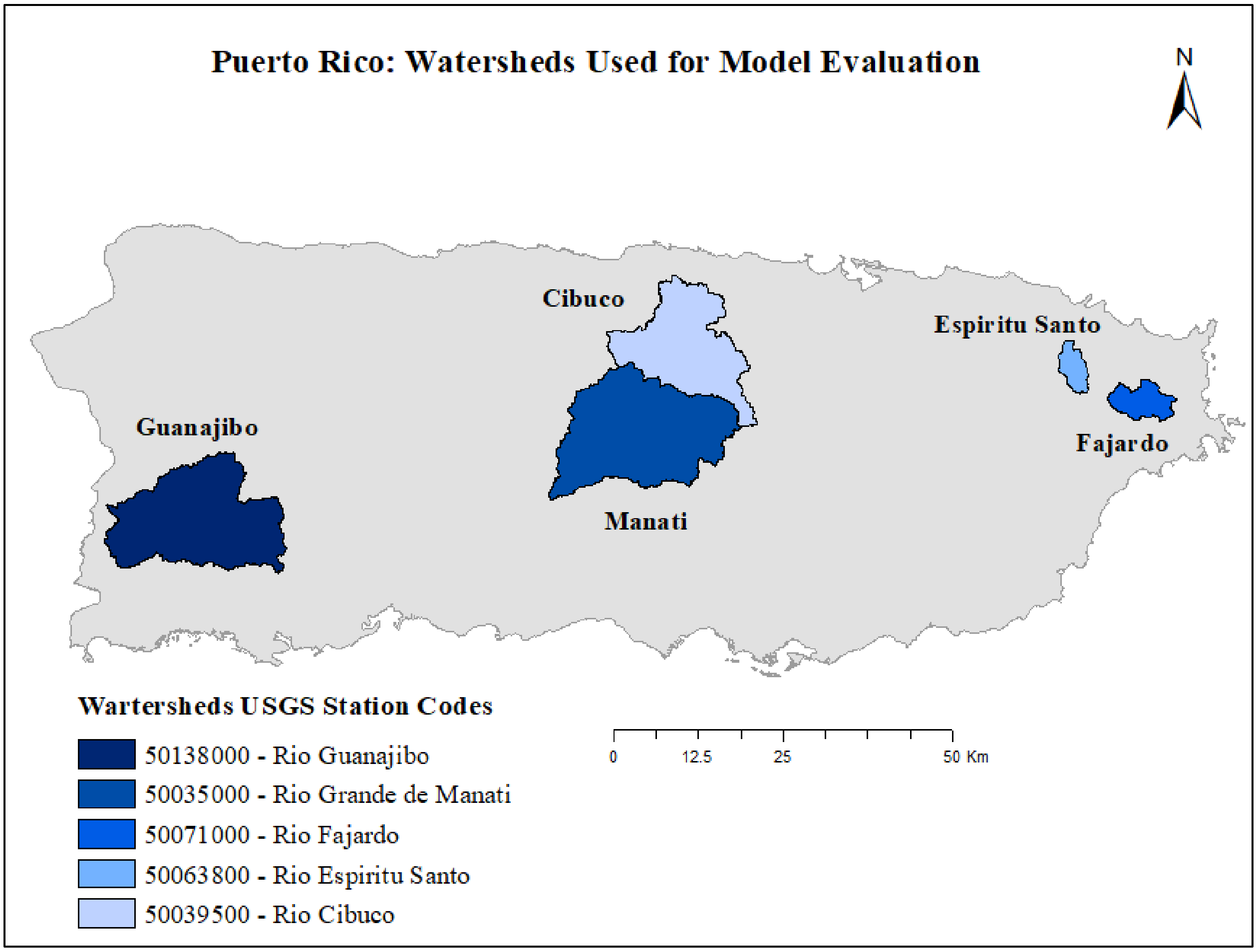

Figure 3.5 – Watersheds select from the U.S. Geological Survey for the SWB2 model evaluation in Puerto Rico. From larger to smaller area, the watersheds are: Manati (330.7 km^2), Guanajibo (310.5 km^2), Cibuco (226.8 km^2), Fajardo (38.3 km^2), and Espiritu Santo (22.5 km^2).

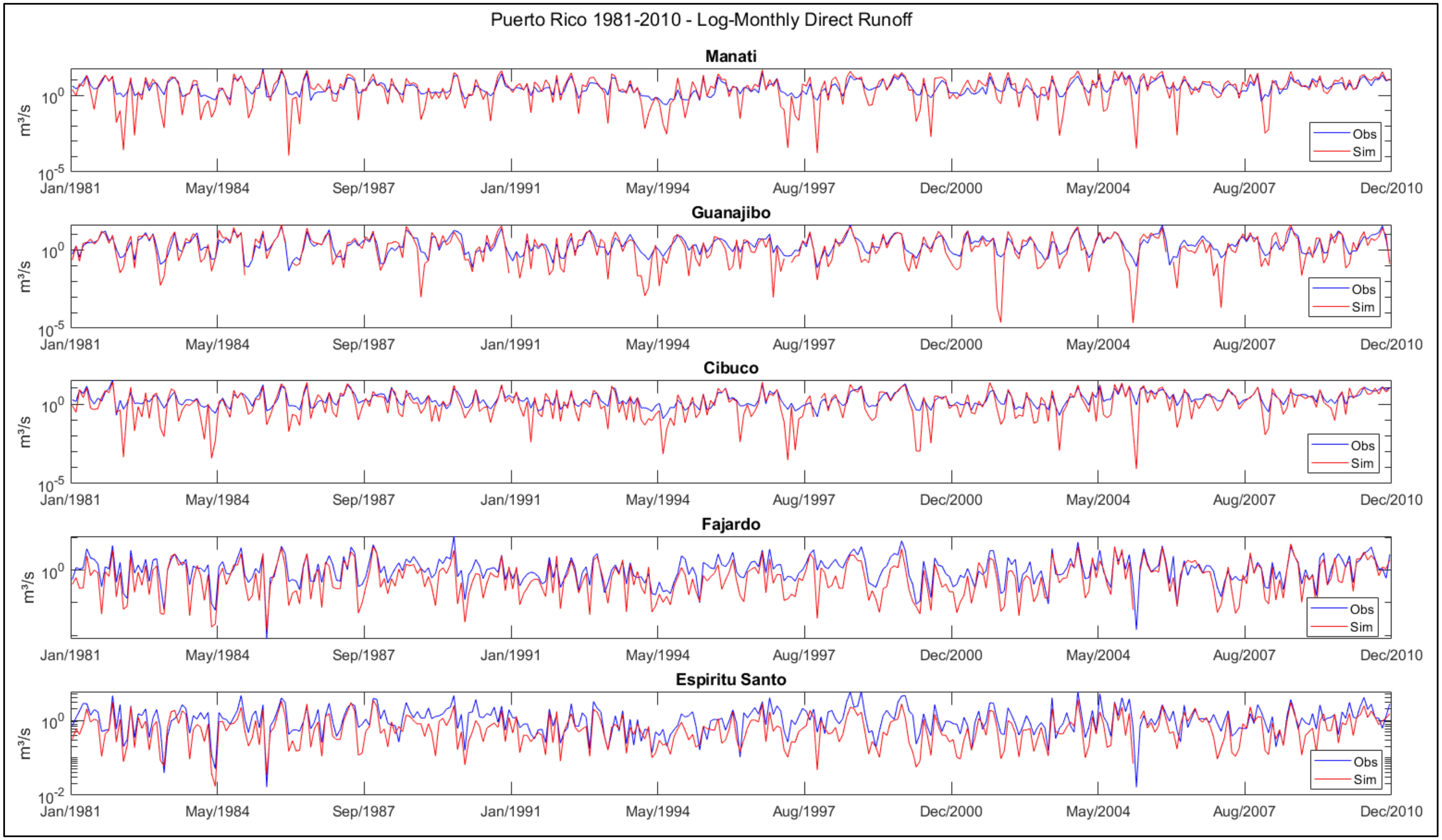

Figure 3.6 – Puerto Rico watersheds analysis comparing monthly direct runoff from SWB2 simulation (red) and USGS observed data (blue) during the baseline climatology (1981–2010).

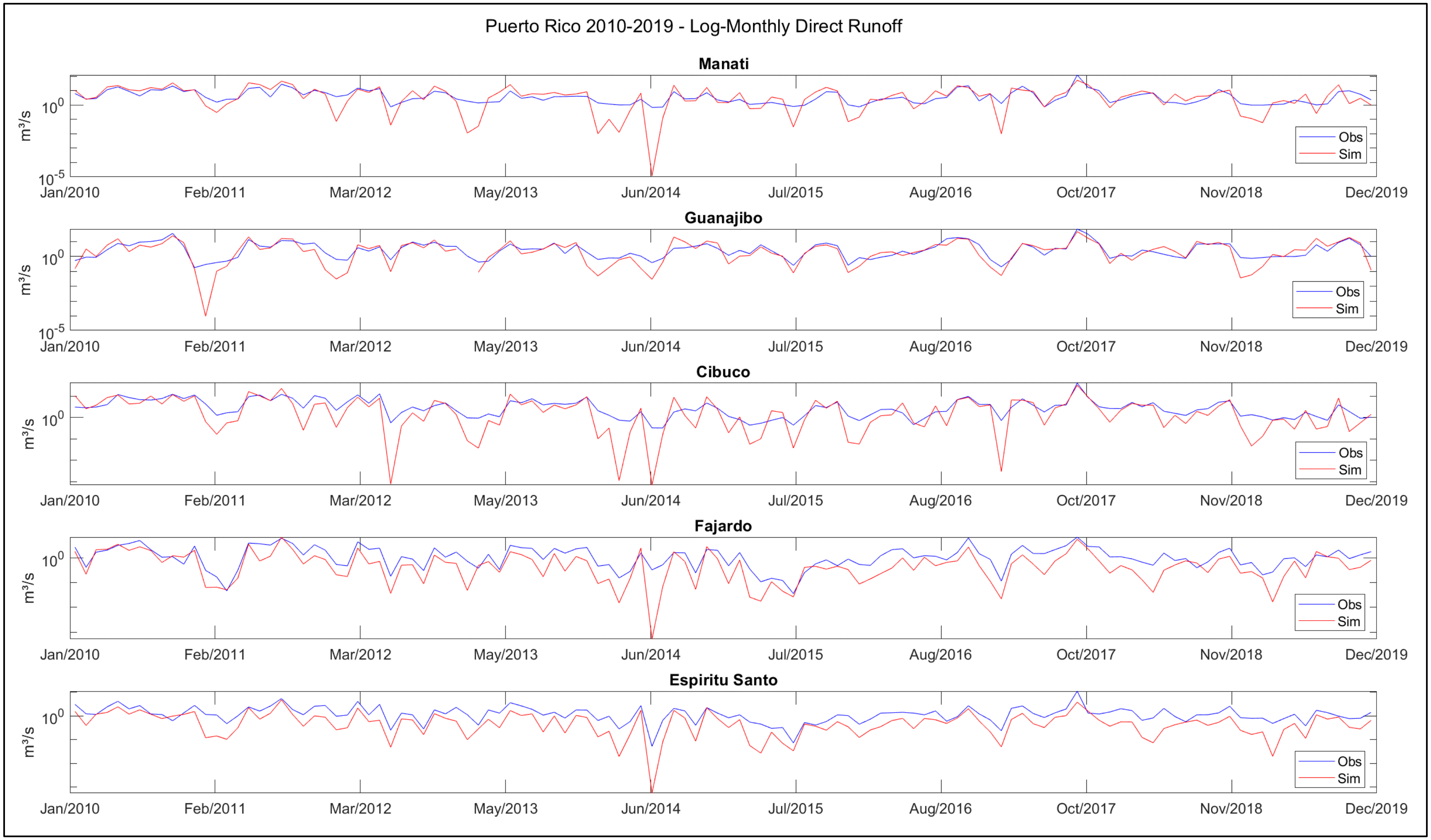

Figure 3.7 – Puerto Rico watersheds analysis comparing monthly direct runoff from SWB2 simulation (red) and USGS observed data (blue) during the recent decade (2010–2019).

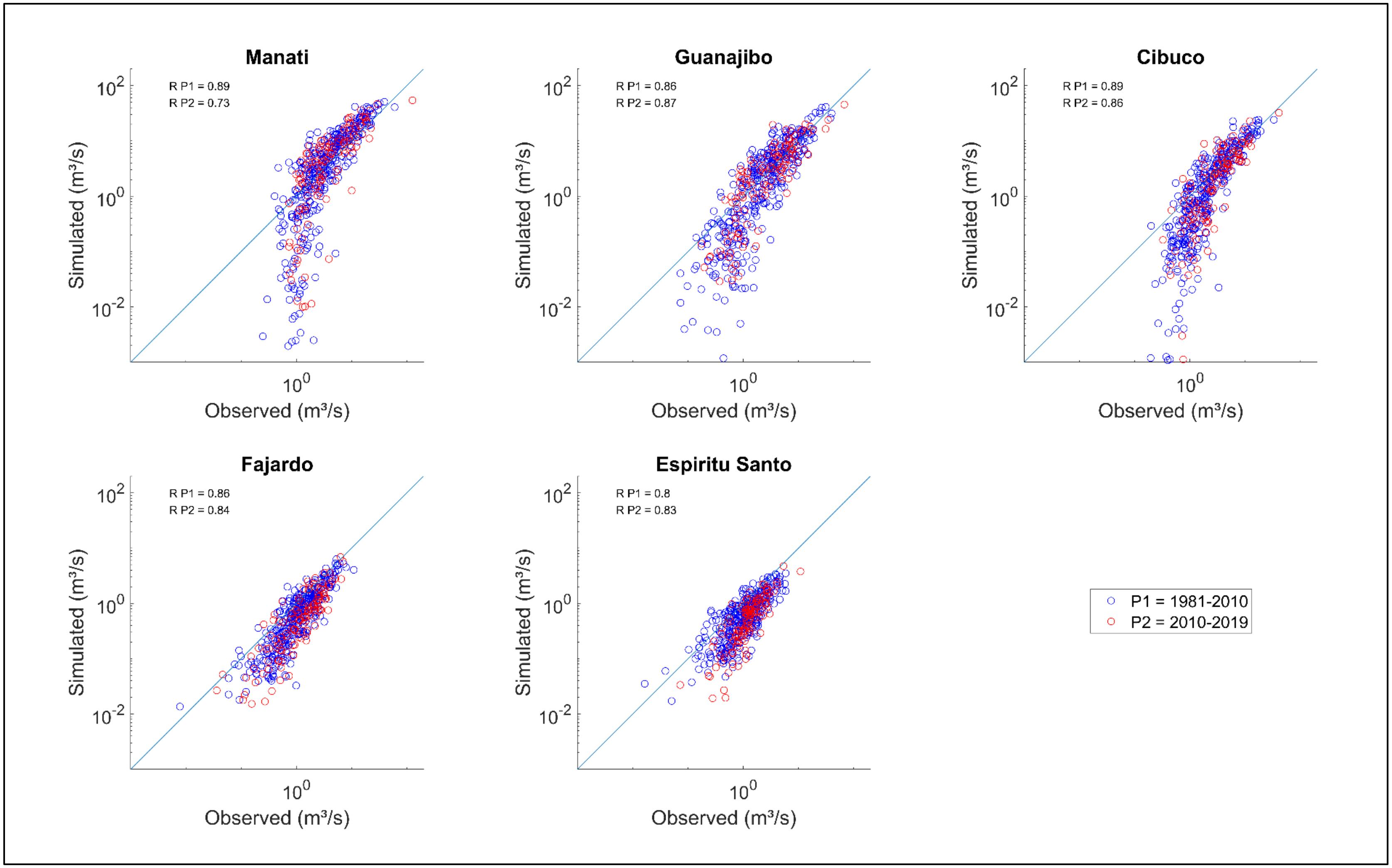

Figure 3.8 – Puerto Rico watershed analysis of SWB2 (simulated) *versus* USGS (observed) direct runoff relationship. The blue dots are the baseline climatology (1981–2010) and the red dots are the recent decade (2010–2019). The R values indicate the correlation coefficient between the simulated and observed data.

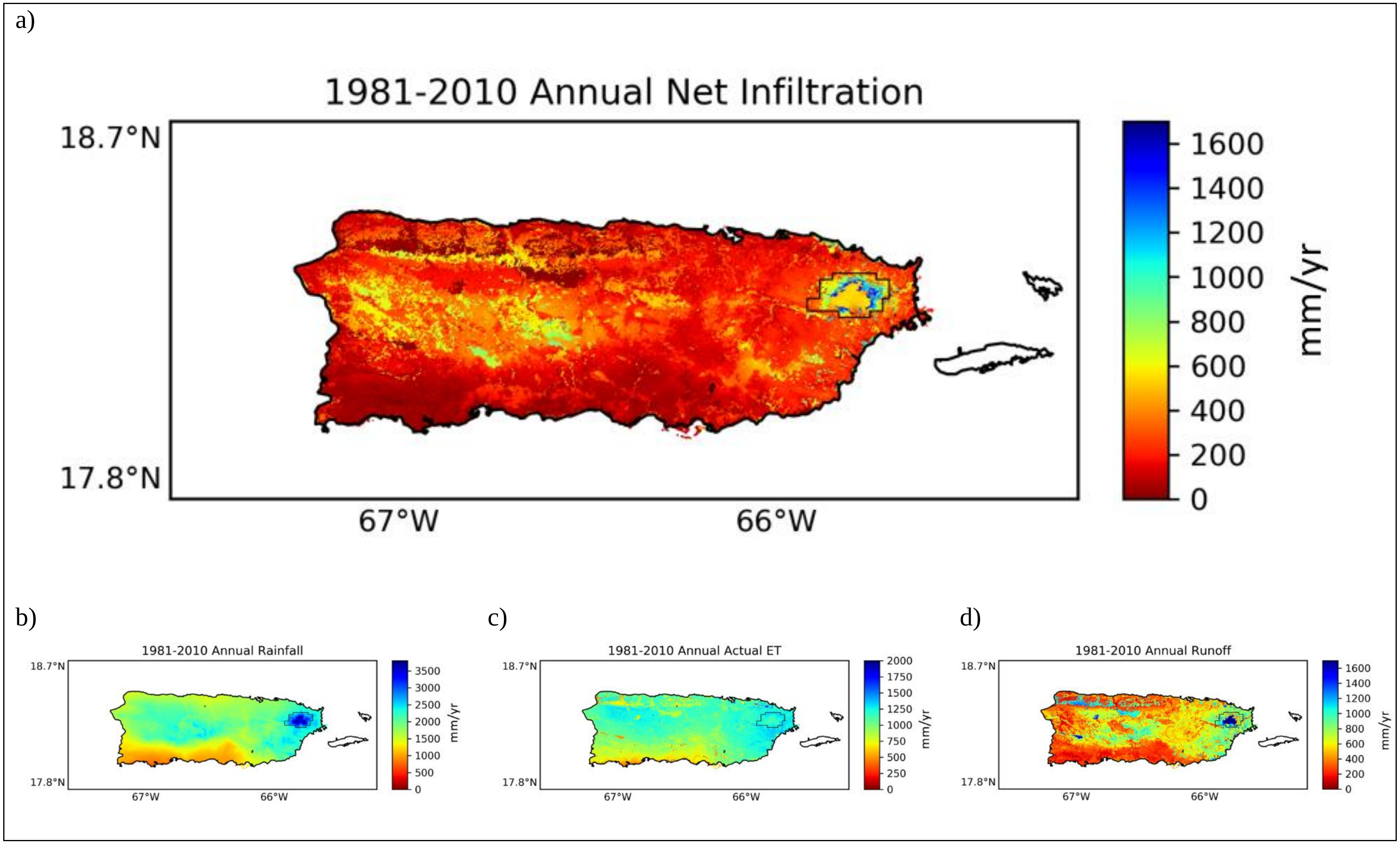

Figure 3.9 – Puerto Rico annual values of water budget components during the baseline climatology (1981–2010): (a) net infiltration, (b) rainfall (gross precipitation), (c) actual ET, and (d) runoff. The black contour in northeastern Puerto Rico highlights the location of the Luquillo Mountains/El Yunque National Forest area.

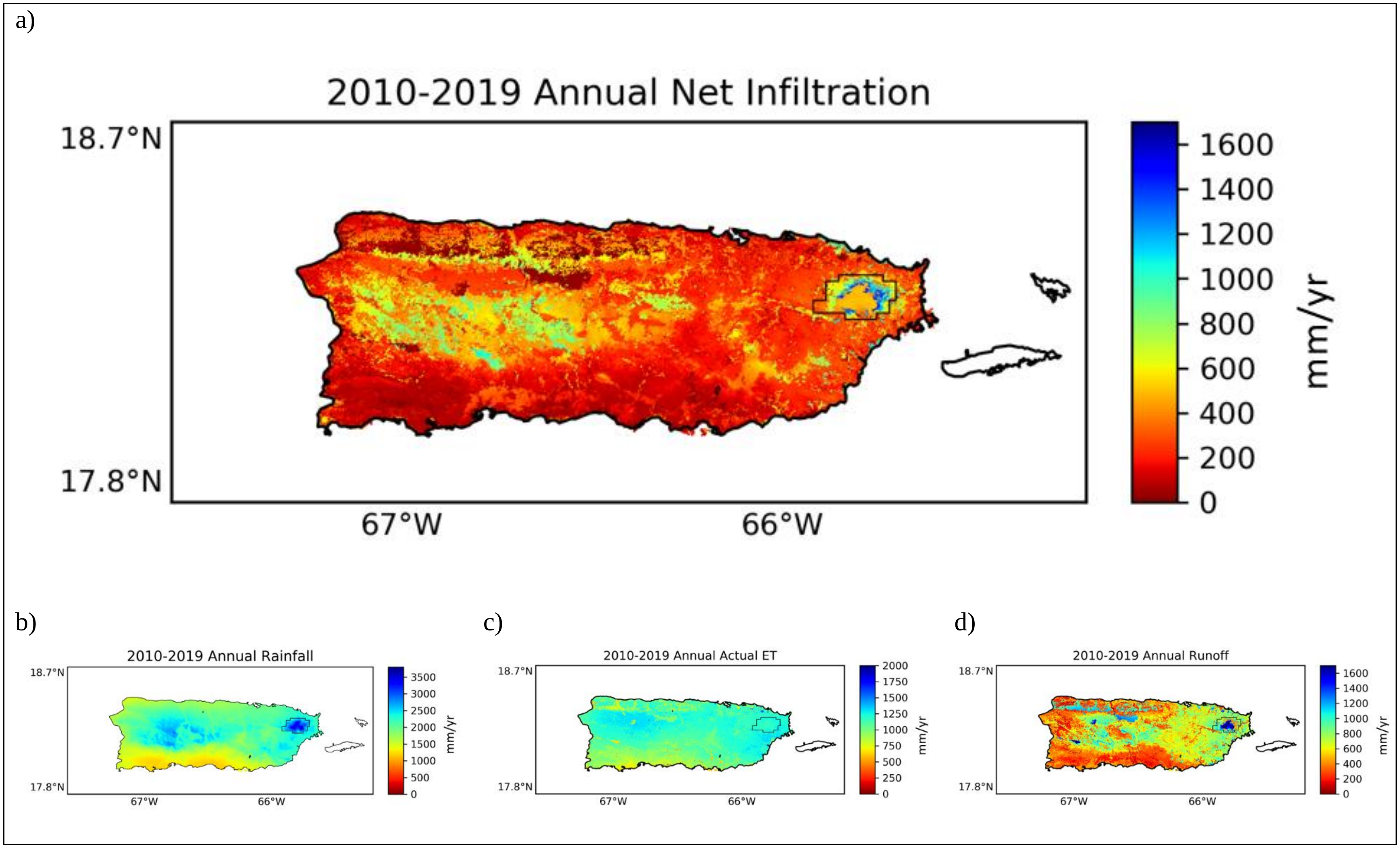

Figure 3.10 – Puerto Rico annual values of water budget components during the recent decade (2010–2019): (a) net infiltration, (b) rainfall (gross precipitation), (c) actual ET, and (d) runoff. The black contour in northeastern Puerto Rico highlights the location of the Luquillo Mountains/El Yunque National Forest area.

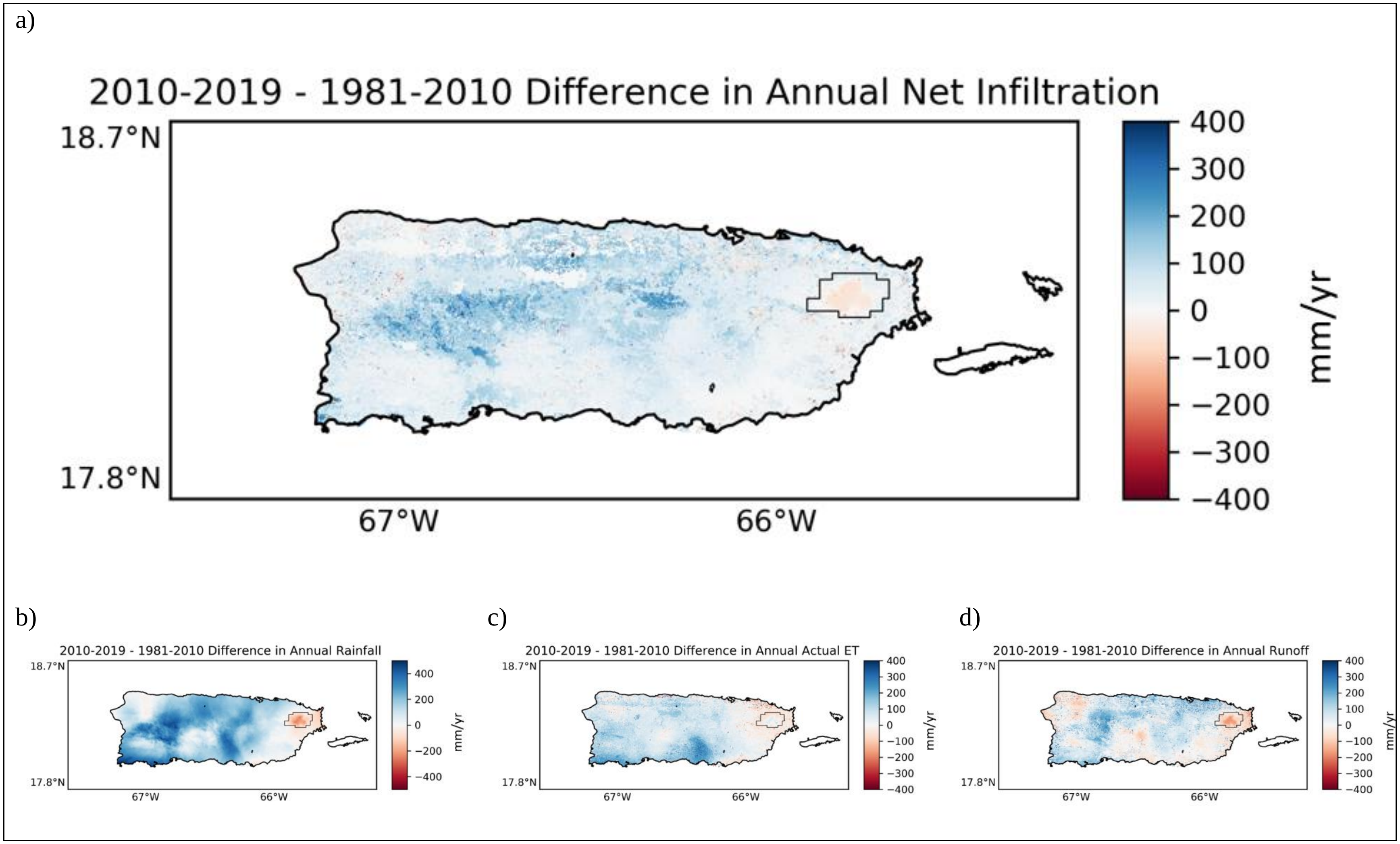

Figure 3.11 – Difference between recent decade *minus* baseline climatology for Puerto Rico annual values of water budget components: (a) net infiltration, (b) rainfall (gross precipitation), (c) actual ET, and (d) runoff. The black contour in northeastern Puerto Rico highlights the location of the Luquillo Mountains/El Yunque National Forest area.

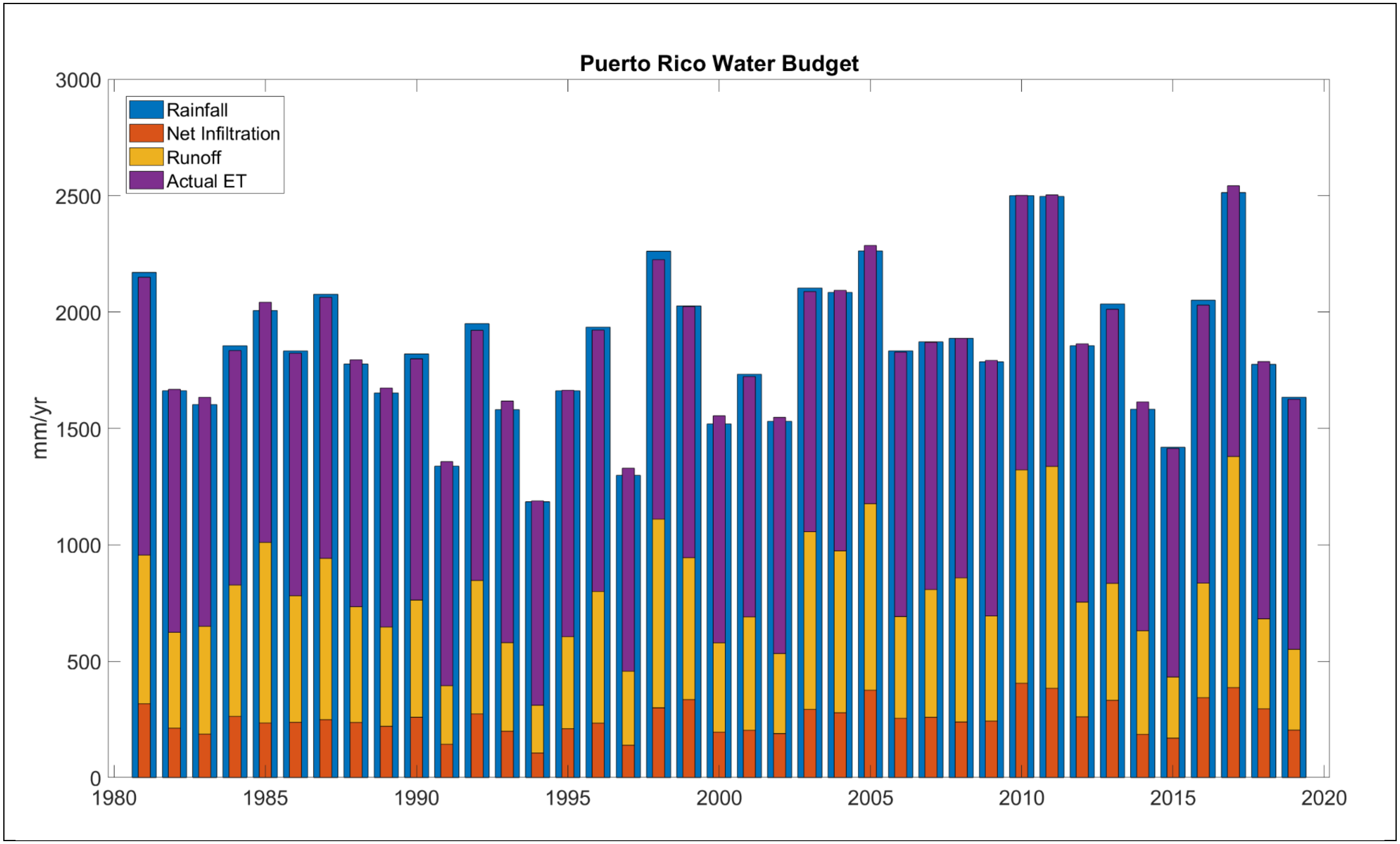

Figure 3.12 – Water budget components annual values for Puerto Rico from 1981–2019. The blue bars in the background correspond to the rainfall (the input of water), while the other colored bars in the front correspond to withdrawal of water: actual ET (in purple), runoff (in yellow), and net infiltration (in orange).

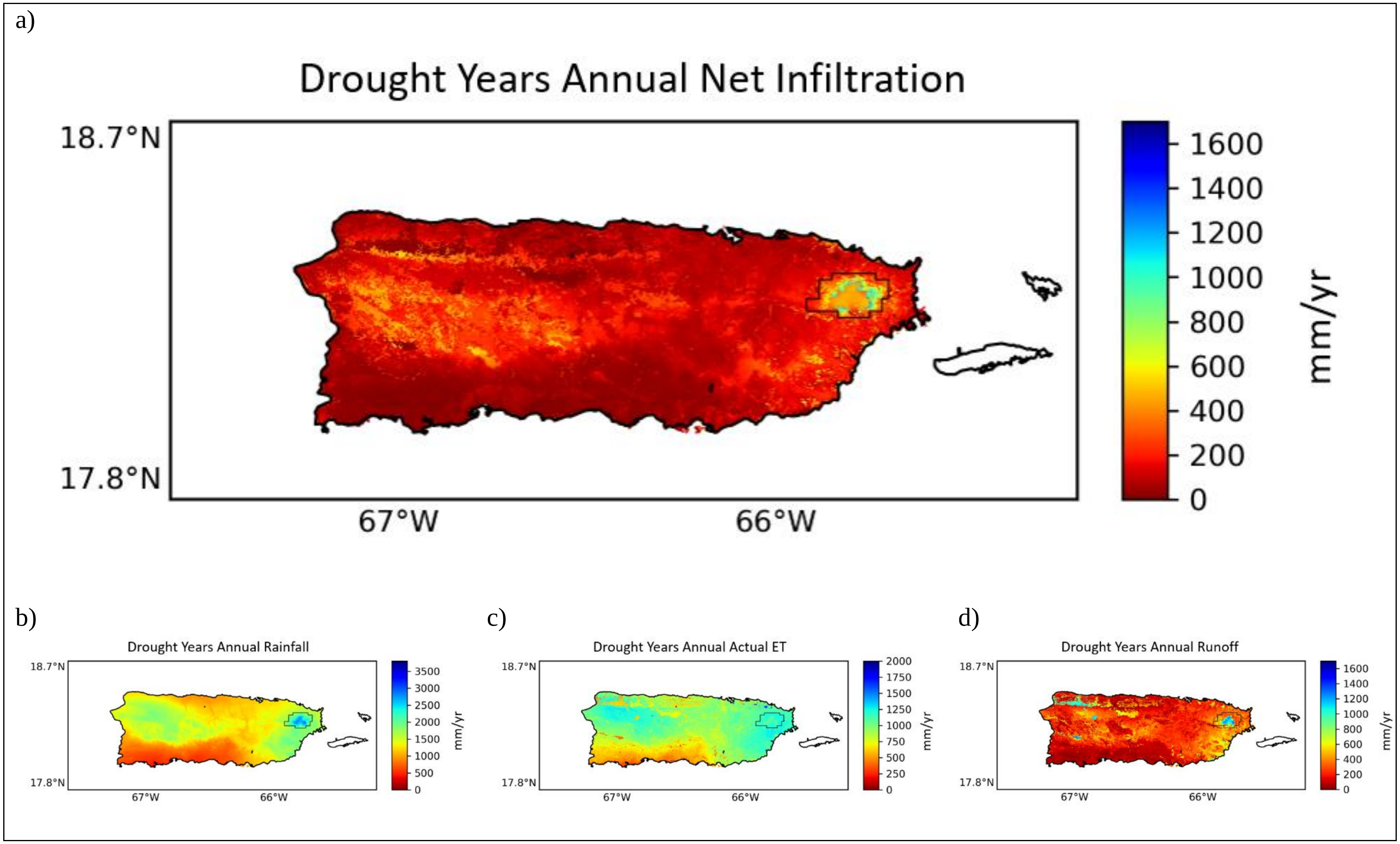

Figure 3.13 – Puerto Rico annual values of water budget components during drought years (1991, 1994, 1997, and 2015): (a) net infiltration, (b) rainfall (gross precipitation), (c) actual ET, and (d) runoff. The black contour in northeastern Puerto Rico highlights the location of the Luquillo Mountains/El Yunque National Forest area.

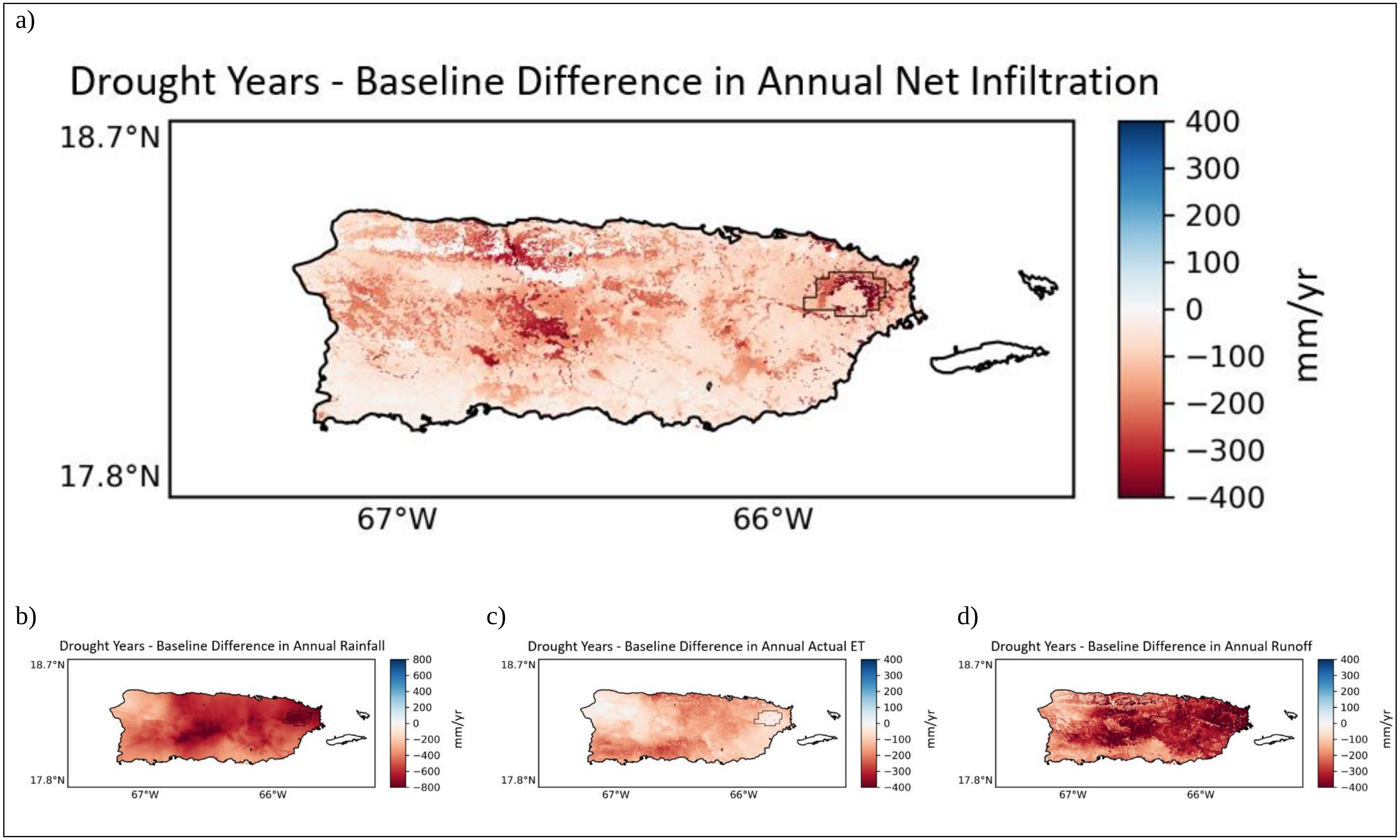

Figure 3.14 – Difference between drought years *minus* baseline climatology for Puerto Rico annual values of water budget components: (a) net infiltration, (b) rainfall (gross precipitation), (c) actual ET, and (d) runoff. The black contour in northeastern Puerto Rico highlights the location of the Luquillo Mountains/El Yunque National Forest area.

4 THE EFFECTS OF PROJECTED CLIMATE CHANGE ON CROP WATER AVAILABILITY IN THE U.S. CARIBBEAN[3]

[3] Moraes, F.D.S, C. Ramseyer, and D. Gamble. The Effects of Projected Climate Change on Crop Water Availability in the U.S. Caribbean. To be submitted to *Climatic Change*.

Abstract

Anthropogenic climate change particularly affects the Small Island Developing States (SIDS) (Karnauskas et al. 2018). Recent studies have suggested that farming systems in the Caribbean are vulnerable to climate change, especially changes in temperature and precipitation, due to its relatively high dependence on rainfall. However, there is a paucity of research investigating the local impacts of climate change on agriculture in the U.S. Caribbean. This work evaluated how temperature and precipitation projections could affect water crop need in Puerto Rico (Greater Antilles) and St. Croix (Lesser Antilles). We used Daymet Version 3 climate data to create a baseline climatology (1981–2010), and the Coupled Model Intercomparison Project Phase 6 (CMIP6) to create two future climatologies (2041–2070 and 2071–2100). The Thornthwaite water budget model was used to estimate water deficit, and the CROPRISK model to determine crop suitability for sweet pepper, banana, and plantain. Results indicated that water stress after 2041 is expected to be greater for most of the region during June–August, except for western Puerto Rico, where water deficit will be greater from January–March. For sweet pepper, banana, and plantain agroclimatic suitability, the most water stressed season is projected to be January–July, mainly for southern Puerto Rico and St. Croix. November will be the only month during which all regions and all crops were projected to be highly suitable through the end of the 21st Century. These findings suggested that Puerto Rico and St. Croix crop water stress may be more sensitive to future changes in temperature than changes in precipitation. An understanding of the location and periods most sensitive to water stress and crop suitability should help local governments to better plan for agriculture to mitigate future food insecurity in the U.S. Caribbean.

4.1 Introduction

Anthropogenic climate change particularly affects the Small Island Developing States (SIDS) (Karnauskas et al. 2018). The rainfall variability, the effects of low-frequency atmospheric circulation patterns on rainfall and drought events, as well as the lack of freshwater resources in the insular Caribbean point to its vulnerability to climate change (Ault 2020; Giannini et al. 2001; Karnauskas et al. 2018; Robinson and Wren 2020). Accordingly, predicted increase in temperature, decreased length of the rainy season, increased length of the dry season, more intense rainstorms, and increase in sea level for the Caribbean could result in the reduction of the already scarce water availability due to the increase of evapotranspiration rates, more flooding and aquifer depletion (reduced recharge), and salinity intrusion into groundwater and coastal aquifers (Ault 2016; Cashman et al. 2010; Farrell et al. 2010; Karnauskas et al. 2016; Pulwarty et al. 2010).

Because agricultural activities are dependent on water, this sector can be directly impacted by future drying trends, with smallholder farmers, in particular, being the most dependent upon the amount and timing of annual rainfall (Bates et al. 2008; Curtis et al. 2014). The Caribbean is already facing poverty and food insecurity together with limited land availability, which means that global climate change will further exacerbate the challenges in the agricultural sector (Connell et al. 2020; Trotman et al. 2009). Studies have found farming systems in the Caribbean to be vulnerable to projected climate change, especially changes in temperature and precipitation, due to its relatively high dependence on rainfall (Bates et al. 2008; Cashman et al. 2010; Curtis et al. 2014). Impacts of a drier and warmer Caribbean climate can include, but are not limited to: reduction in plant-available moisture due to increased rates of evapotranspiration, increased spread of some pests and diseases, decrease in crop suitability, and increased stress on food productivity and sustainability (Cashman et al. 2010; Curtis et al. 2014; McGregor et al. 2009).

Among the insular Caribbean nations, Jamaica has been the focus of studies concerning climate change and agriculture due to its large agricultural land areas, and where the livelihood of the rural population largely depends on agriculture (Curtis et al. 2014; Rhiney et al. 2018; Trotman et al. 2009). The sensitivity of crop water stress to 2071–2095 projected temperature and precipitation changes in Jamaica indicated that a warming climate will contribute to larger crop water deficits from November to April, while the drying trend will affect crops from May to October (Curtis et al. 2014). Research has also found that in Puerto Rico, the cultural and economic importance of coffee is also expected to be thread by climate change scenarios (Fain et al. 2018). Temperature and rainfall projections indicated warming and drying trends acceleration after 2040 that could result in the loss of 60–84% of highly suitable growing conditions in top producing municipalities by 2070 (Fain et al. 2018).

Beyond these studies, much of the research on climate change and agriculture has been more general and of regional scope (Ault 2020; Barker 2012; Bates et al. 2008; Farrell et al. 2007; Karnauskas et al. 2018; Neelin et al. 2006; Pulwarty et al. 2010; Trotman et al. 2009), so there is a clear need for more case studies focusing on specific islands within the Caribbean. Additionally, to our knowledge, there is no research comparing the impacts of climate change on agriculture on an island in the Greater and the Lesser Antilles. Therefore, this work used a crop risk model (Batjes 1987) to analyze how water deficit and crop water stress in Puerto Rico (Greater Antilles) and the U.S. Virgin island of St. Croix (Lesser Antilles) can be affected by future temperature and precipitation changes by mid-century (2041–2070) and late-century (2071–2100). For this analysis, we choose to focus on the crops sweet pepper, banana, and plantain due to their agricultural importance to Puerto Rico and St. Croix, as well as to their sensitivity to water deficits.

4.2 Data and Methods

In order to evaluate how temperature and precipitation projections for 2041–2070 and for 2071–2100 can affect water stress and crop suitability in Puerto Rico and St. Croix, a multi-step methodology was developed, which included creating a baseline climatology and two future climatologies, using the Thornthwaite water budget model to estimate potential and actual evapotranspiration used to calculate water deficits, as well as using the CROPRISK model to assess crop suitability in current and future climates. These steps are explained below.

4.2.1 Study area and climate data

The first steps in our analysis were to define the study area, to create the baseline climatology and the two future climatologies. To account for the different climatic regions in Puerto Rico associated with the topography of the island, we divided the island into four basins (North, South, East, West) according to the 8-digit hydrologic units from the U.S. Geological Survey (USGS) (Figure 4.1). These four basins were then used to clip the climatological data for Puerto Rico and to perform the water stress and crop suitability analysis. Because St. Croix is a smaller island (with an area of approximately 220 km^2), and its agriculture is mostly located in the center, we did not divide the island to perform the analysis (Figure 4.1).

For baseline climatology, we used daily gridded weather data from Daymet (Version 3) at 1 km resolution (precipitation, maximum temperature, and minimum temperature) from 1981 to 2010. Daymet data offers gridded estimates of daily weather variables for North America and the U.S. Caribbean distributed from 1 January 1980 to 31 December 2019 (Thornton et al. 2016). The methodology used in the current data set is intended to create spatially continuous gridded products over large regions of complex terrain and to accomplish for the heterogeneous distribution of stations by using an iterative station density algorithm (Thornton et al. 1997). Daymet was previously used in studies analyzing rainfall patterns in the complex terrain of Puerto Rico (Miller et al. 2019; Mote et al. 2017). Daymet Version 3 was used instead of Version 4 because preliminary analysis indicated the Version 3 performed better in Puerto Rico when compared to observed runoff (Jazlynn Hall, Columbia University, pers. comm.). By using Puerto Rico four basins' shapefiles and St. Croix's shapefile, we clipped the Daymet data from each location, averaged precipitation and temperature over the area and created 30-year monthly mean baseline climatology for Puerto Rico (Figure 4.2 and Figure 4.3) and St. Croix (Figure 4.4). Maximum and minimum temperature data from Daymet were averaged to create the 30-year monthly mean temperature for the baseline climatology.

For future climates, we used the Coupled Model Intercomparison Project Phase 6 (CMIP6) and selected the five models that have been regridded to a common grid (100 km). Models included in this analysis were downloaded from https://esgf-node.llnl.gov/search/cmip6/ and are found in Table 4.1. We downloaded and selected both historical (1981–2010) and future (2041–2100) monthly precipitation and surface temperature data from each model. For future data, we downloaded the shared socioeconomic pathway-representative concentration pathway (SSP-RCP) scenario SSP5-8.5, which is an updated version of RCP8.5 in CMIP5 used in Curtis et al. (2014) in a similar study, and refers to the scenario with higher CO_2 emissions by the end of century (O'Neill et al. 2016).

Then, the data was remapped to account for the different grid systems used by the models, even though they have the same resolution. The remapping used the nearest neighbor remapping function (*remapnn*) from Climate Data Operators (CDO) to select the grid cell corresponding to the centroid of each basin in Puerto Rico and of the island of St. Croix (Figure 4.1). We used nearest-neighbor approach since other studies have indicated that this approach does not smooth the extremes of the models (Wang et al. 2019). After that, we concatenated all models and created the 30-year monthly mean surface temperature and precipitation for historical and future climates.

In Figures 4.2, 4.3, and 4.4, we can see that historical precipitation and temperature from CMIP6 models (gray lines) were overestimated when compared to the baseline observations from Daymet (black line), except in May when observed precipitation exceeds the model simulation in almost all regions of analysis. We applied the delta method for climate model bias correction. This method has proved to reduce climate model bias by at least 50–70% and to be effective on preparing the data for assessing impacts of climate change on agriculture (Navarro-Racines et al. 2020). Other studies have shown that the delta method is robust to correct mean climate conditions in other regions (Hawkins et al. 2013; Navarro-Racines et al. 2020), and the method was used to correct our future climate conditions (2041–2070 and 2071–2100) for Puerto Rico and St. Croix. In this bias correction method, a change factor or delta is derived from the CMIP6 models and then applied to the observations (Daymet). The delta is defined as the difference between the 30-year mean of precipitation and temperature in the future and the historical period simulations. Following the approach applied by Navarro-Racines et al. (2020), we calculated the absolute difference for temperature (equation 1), and the proportional differences for precipitation (equation 2), because the relative changes for precipitation avoids negative values when applying the CMIP6 delta values into observed Daymet.

$$\Delta X_i = X_{Fi} - X_{Ci} \tag{1}$$

$$\Delta X_i = \frac{X_{Fi} - X_{Ci}}{X_{Ci}} \tag{2}$$

where, ΔX_i is the delta change, X_{Fi} is the 30-year mean of the climate variable in the future climate, and X_{Ci} is the 30-year mean of the climate variable in the historical climate of the CMIP6 models in the month i.

We then applied the delta (also called anomalies) to the baseline climate from Daymet to get the bias corrected future climatologies. For temperature, we simply added the delta values in degree Celsius to the value from Daymet (equation 3), while for precipitation we used the absolute value of the change relative to the baseline climatology (equation 4) to avoid negative monthly precipitation values (Navarro-Racines et al. 2020).

$$X_{DCi} = X_{OBSi} + \Delta X_i \tag{3}$$

$$X_{DCi} = X_{OBSi} \times (1 + \Delta X_i) \tag{4}$$

where, X_{OBSi} is the baseline climatology from observations (i.e., Daymet), ΔX_i is the delta change calculate in equations 1 and 2, and X_{DCi} is the calculated future climatology of the CMIP6 models in the month i. The observed, simulated, and bias corrected future climatologies can be seen in Figures 4.2, 4.3, and 4.4.

4.2.2 Crop water stress and agroclimatic suitability

After processing the climate data, we performed the sensitivity analysis of water availability in Puerto Rico and St. Croix, followed by the analysis of agroclimatic suitability for specific crops in the islands. For water availability analysis, we used the Thornthwaite Monthly Water Balance Model as developed by the USGS (McCabe and Markstrom 2007), available at https://www.usgs.gov/software/thornthwaite-monthly-water-balance-model. This model was the same used by Curtis et al. (2014) in their study focusing on crop water stress in Jamaica, and is designed to work with tabular monthly climate data used in this study. The input parameters for the model were the same used by Curtis et al. (2014) in their analysis for Jamaica. This model is driven by a graphical user interface in which some parameters can be specified, and the input data are monthly temperature and precipitation from a specific location. The model analyzes the components of the hydrologic cycle according to Thornthwaite (McCabe and Markstrom 2007; Thornthwaite 1948). We ran the model for each one of the four basins of Puerto Rico and the island of St. Croix using the following parameters for the five locations: 18° N as the latitude parameter; 5% as the fraction of precipitation that becomes direct runoff from infiltration-excess overflow; 150 mm as the soil-moisture storage capacity, and the runoff generation as 50% of the surplus water produced after the soil-moisture storage surpasses its capacity (Curtis et al. 2014; McCabe and Markstrom 2007; Wolock and McCabe 1999).

Among the outputs of the water budget model, only the actual evapotranspiration (AET) and potential evapotranspiration (PET) were retained; the difference between those values is the water deficit, also referred here as crop water stress. Past studies suggested that PET – AET is directly related to drought stress in agricultural fields (Curtis et al. 2014; Stephenson 1998). In addition, the water deficit was used to estimate the deficit from maximum crop yield (equation 5) following the crop risk model (CROPRISK) developed by Batjes (1987) for Jamaica:

$$DY = ky(ETC - AET)/ETC \tag{5}$$

where DY is the deficit from maximum crop yield, ky is the yield response factor that indicates the effect of water stress on a crop, and ETC is equal to *kc* x PET, where *kc* is the crop coefficient for the specific growing stage and type of crop, which typically ranges from 0.35 to 1.15 (Curtis et al. 2014). The values of *ky* and *kc* are presented in the next section (4.2.3) together with the crops we chose to analyze in this study.

Finally, we used the deficit from maximum crop yield to establish the agroclimatic suitability classes defined by Batjes (1987). These classes depend on the number of years in which at least 80% and 60% of the crop's maximum yield can be obtained, as following:

- Highly suitable (HiS): when 80% condition of crop's maximum yield is met at least 60% of the years and the 60% condition is met at least 80% of the years.
- Moderately suitable (MoS): when 80% condition of crop's maximum yield is met at least 40% of the years and the 60% condition is met at least 60% of the years.
- Marginally suitable (MaS): when 80% condition of crop's maximum yield is met at least 20% of the years and the 60% condition is met at least 40% of the years.
- Not suitable (NS): when 80% condition of crop's maximum yield is met in less than 20% of the years and the 60% condition is met in less than 40% of the years.

Both crop water stress (PET – AET) and agroclimatic suitability classes were determined on the annual cycle for the baseline climatology (1981–2010), the future climatology representing the mid-century (2041–2070), and the one representing the late-century (2071–2100) for each one of the four basins in Puerto Rico and the island of St. Croix. Through the analysis of these future climatologies, we expect to evaluate the role of temperature and precipitation changes on future agricultural suitability and water stress in both the Greater and Lesser Antilles.

4.2.3 Agricultural data

In Puerto Rico, the most recent census of agriculture from the U.S. Department of Agriculture (USDA 2020a) indicated that the number of farms has decreased from 2012 to 2018, and the number of cropland harvested farms decreased from 10,008 to 4,888, representing a reduction of more than 17,806 hectares. The irrigated land has also decreased its area since 2012 by at least 10,360 hectares, which leaves more than 20,000 hectares of harvested cropland mostly dependent on rainfall.

Puerto Rico's major crops include plantain and banana, which were cultivated in 2,035 and 1,157 farms, respectively, in 2018 (USDA 2020a). Although the numbers of farms cultivating plantain and bananas have decreased since 2012, their economic value is still among the highest, with an average of market value of products sold in 2018 equal to $31,243 per farm for plantain, and to $13,521 per farm for bananas (USDA 2020a). More farms grow peppers than any other vegetable in Puerto Rico, with sweet pepper cultivated at 290 farms in 2018, and other types of peppers cultivated in 62 farms. These numbers also decreased when compared to the 2012 agricultural census, when peppers were cultivated in 603 farms (USDA 2020a). Sweet peppers also lead the vegetables with the majority number of farms (> 100 farms) with a market value of agricultural products sold > $60,000.

On the contrary, St. Croix has quintupled its area of cropland in 10 years, from 106 farms (161 hectares) in 2007 to 336 farms (851 hectares) in 2018. Vegetable represented the largest category of production with sales of $1.1 million (USDA 2020b). Notably, an increase in land irrigated also occurred, from 81 hectares in 2007 to 223 hectares in 2018 (USDA 2020b). Despite this increase, there are still at least 600 hectares of cropland dependent on rainfall.

Among the vegetables produced in St. Croix, peppers also lead the number of farms as the primary crop with a total of 121 farms in 2018 within which more than 20 farms have a market value of agricultural products sold > $10,000. Plantain and bananas are also one of the main fruits cultivated in St. Croix, based on the number of farms. In 2018, 119 farms cultivated plantain and 220 farms cultivated bananas, compared to only 33 farms cultivating plantain and 57 farms cultivating bananas in 2007. The market value of agricultural product sold was > $10,000 for at least 9 plantain and 24 banana farms in St. Croix (USDA 2020b).

On top of the economic value, these crops also have an important cultural value for the islands. For the Puerto Rican community that live either in Puerto Rico or in St. Croix, a particular sweet pepper, locally known as *Ají dulce* (*Capsicum chinense*), is popular and used in culinary seasoning giving characteristic flavor to most Puerto Rican recipes (Palada 2003). The historical significance of banana and plantain for the small islands in the Caribbean also make those crops relevant for our analysis. It is estimated that the production of banana is one of the largest employer of labor and sustained thousands of small farmers in the Caribbean, providing a foundation for the economic viability and social and political stability in the region (Bernal 2020).

Besides the economic and cultural importance of banana, plantain, and sweet pepper, these crops were the widely cultivated across Puerto Rico in 2016, according to the agricultural statistics interactive platform created by the USDA Caribbean Climate Hub (https://caribbeanclimatehub.org/tools-apps/agricultural-statistics/). In 2016, sweet pepper, banana, and plantain were cultivated in at least 148, 156, and 430 neighborhoods, respectively, in Puerto Rico (Figure 4.5). Although we understand the importance of coffee plantation for Puerto Rico, we decided to not include coffee in this analysis because it is not cultivated in St. Croix and a recent study has examined the impact of climate change on coffee in Puerto Rico (Fain et al.

2018). Therefore, we chose to use sweet pepper, banana, and plantain as the crops to analyze the future agroclimatic suitability in Puerto Rico and St. Croix.

4.2.3.1 Crop coefficient (kc) and yield response factor (ky)

The values of *kc* and *ky* used for the CROPRISK model were related to each crop. Sweet pepper *kc* during its mid growth stage is 1.05 and during its late growth stage is 0.90 (Allen et al. 1998; Harmsen et al. 2003; Kisekka et al. 2010). Here we followed the approach of Curtis et al. (2014) and chose a value of 1.0 to represent the harvest time of sweet pepper and avoid negative *DY*s, which is possible with smaller *kc* values. For sweet pepper *ky*, we used a value of 1.10 (Batjes 1987). Because banana and plantain are member of the same crop group, we used the same values of *kc* and *ky* (Allen et al. 1998): *kc* = 1.10, based on the average *kc* for mid and late growth stage for the first and second year of cultivation, and *ky* = 1.27. Water stress increases on a crop with *ky* values greater than one (Curtis et al. 2014), which suggests that sweet pepper, banana, and plantain are all crops with increased sensitivity to water availability.

4.3 Results and Discussion

4.3.1 Temperature and precipitation change

After downloading and processing the climate observations (Daymet) and climate model outputs (CMIP6), this study analyzed how temperature and precipitation of mid-century (2041–2070) and late-century (2071–2100) climatologies will change when compared to the baseline climatology (1981–2010). Figure 4.2 and Figure 4.4 a present the 24-month annual cycle of temperature (ºC) for all the observed and projected climatologies for the four basins in Puerto Rico and for St. Croix, respectively. For observed data (Daymet), the higher monthly average temperature occurred in July–August while for simulated data (CMIP6) the higher temperatures occurred in September–October for both the historical and future climatologies. However, the future climatologies, here called "Delta" to indicate they were bias corrected projections, also peaked in July–August but with temperatures ranging from 1.8 °C to 2.2 °C warmer in 2041–2070 than the baseline climatology in Puerto Rico and St. Croix. For 2071–2100, differences in temperatures ranged from 3.2 °C to 3.7 °C warmer in Puerto Rico and in St. Croix when compared to the baseline climatology.

Among the basins in Puerto Rico, the East basin registered a slightly smaller difference between observed temperature and the two future climatologies in July–August than the rest of the island. This smaller increase in future temperature in eastern Puerto Rico could be related to the presence of the El Yunque National Forest, a tropical rainforest located in the Luquillo Mountains with an area around 100 km^2. The effect of tropical rainforests in controlling temperature is mainly related to their high evapotranspiration demands, which uses the available latent heat, and consequent cloud formation, which decrease incoming solar radiation at the surface (Brovkin 2002; Fetcher et al. 1985; Lawrence and Vandecar 2015). On the other hand, the fact that St. Croix registered the smallest change in temperature between observed and future climatologies, when compared to Puerto Rico basins, could be related to the maritime effect being more efficient in the smaller island climate, resulting in smaller temperature ranges (Granger 1985).

The observed (Daymet) 24-month annual cycle of precipitation (Figure 4.3 and Figure 4.4 b) confirmed the bimodal cycle of rainfall in eastern Caribbean, with two rainy seasons occurring in April–July (Early Rainfall Season) and August–November (Late Rainfall Season), separated by a drier period in June–July (mid-summer dry spell), and a dry season occurring in December–March (Angeles et al. 2010; Curtis and Gamble 2008; Taylor et al. 2002). The mid-summer dry spell is less apparent in East Puerto Rico basin (Figure 4.3 a), probably because this region has local mechanisms of rainfall along the year, such as the orographic effect and the presence of the tropical rainforest (Jury 2020; Ramseyer and Mote 2016; Sobel et al. 2011), that makes it wetter than the rest of the island.

Before bias correction was applied, the CMIP6 models did not represent the bimodal cycle in precipitation. They could not simulate the December–March dry season and the April–July rainy season, while they overestimated the August–November rainy reason in Puerto Rico and in St. Croix. However, after bias correction was applied, the future climatologies are projected to have the same pattern as the observed precipitation. The 2041–2070 precipitation was predicted to have from 54 to 74 mm less precipitation than the baseline climatology, mainly from June to October, in the four basins of Puerto Rico, and 36 mm less in St. Croix over the same period. The greater difference in precipitation is expected to occur between the baseline period and 2071–2100, when West Puerto Rico basin is projected to have 215 mm less precipitation from June to October, and St. Croix 96 mm less precipitation. The only month when projected precipitation was expected to be greater than the observed precipitation was November, which can indicate a future shift in the peak of the hurricane season that currently occurs in September (Kossin 2008; Martinez et al. 2019).

The overall increase in temperature and decrease in precipitation by mid-to-late-century found here was also observed in past studies that used earlier versions of CMIP6 (CMIP5 and CMIP3) to assess crop suitability in Jamaica and Puerto Rico (Curtis et al. 2014; Fain et al. 2018). Although uncertainties still exist, mainly regarding the precipitation projections, those findings using different models and different bias correction methods all pointed to a likely warmer and drier insular Caribbean starting in 2041 if the worst-case CO_2 emission scenario in CMIP6 is not avoided.

4.3.2 Water deficit

The Thornthwaite water budget model was applied to each one of the four basins of Puerto Rico and to St. Croix during the baseline climatology (1981–2010) and the two future climatologies representing the mid-century (2041–2070) and late-century (2071–2100). Using PET and AET outputs from the model, we computed water deficits and crop suitability for each basin and for St. Croix under those three climatologies.

Figure 4.6 shows the annual cycle of crop water stress for the baseline and the two future climatologies. In the baseline climatology, there was almost no crop water stress occurring in East and North Puerto Rico basins during the annual cycle. This is probably related to their greater annual precipitation compared to other basins, due to tropical forest and orographic rainfall discussed earlier. However, some crop water stress was exhibited during dry season (January–March) in West basin, while the most severe crop water stress during the baseline climatology occurred in South Puerto Rico basin and in St. Croix, with highest values in June–July. These months coincided with mid-summer dry spell, when the region experiences its highest temperature and a reduction in precipitation (Figures 4.2, 4.3, and 4.4). South Puerto Rico and St. Croix were the driest regions in the study, but monthly temperatures were as high as the wetter regions, indicating a potential increase in evapotranspiration demand and greater vulnerability to water stress. In fact, South Puerto Rico basin is known as a drier region and was classified as “dry forest” based on its humidity, annual precipitation, and PET (Holdridge 1967). The region is geographically located to the south of the Central Mountain Range, which creates a shield blocking the Atlantic moisture and making the south drier than other regions of Puerto Rico (Torres-Valcárcel et al. 2014).

For the future climates, the overall crop water stress was also highest from June–August, except for the West Puerto Rico basin where the higher values occurred in January–March. This means that even wet regions such as East and North Puerto Rico basins, that are not currently facing water stress during the mid-summer dry spell, will start to have problems with water available for crops during these drier months after 2041. In South Puerto Rico basin and St. Croix, where crop water stress is already occurring in the first half of the year, the late-century climatology suggested as much as double the current water stress during boreal summer in St. Croix and almost three times the water stress in southern Puerto Rico. These climate projections indicate that crop risk in those areas will be high after 2041.

A similar result was found by Curtis et al. (2014), when analyzing the crop water stress for Jamaica by the end of the 21st Century, indicating the mid-summer dry spell as a key component for future regional water stress. They suggest that one of the causes for the mid-summer water stress could be associated with the Caribbean low-level jet (CLLJ), which has its relative maximum in July (Curtis et al. 2014; Gamble and Curtis 2008). The PRECIS regional model simulated the patterns of the CLLJ by the end of the 21st Century and suggested that an intensification of the CLLJ will occur from May to November and reach Jamaica, Hispaniola, Puerto Rico, and the north coast of South America resulting in drier climate for the Caribbean (Taylor et al. 2013). The CLLJ together with the North Atlantic subtropical high (NAHP) are important atmospheric patterns responsible for the current lower values of precipitation during the boreal summer in the Caribbean, transporting moisture from the Caribbean to Central America (Cook and Vizy 2010; Gamble and Curtis 2008; Gamble et al. 2008). The period when CLLJ is projected to be more intense (Taylor et al. 2013) aligned with the months the future climatologies analyzed here projected less precipitation for all the four basins of Puerto Rico and for St. Croix (Figure 4.3 and

Figure 4.4 b). Thus, the intensification of these atmospheric features with climate change can justify the drier mid-summer dry spell and the increase in water stress across those islands.

4.3.3 Crop suitability

After analyzing crop water stress, we ran the CROPRISK model to assess agroclimatic suitability for sweet pepper, banana, and plantain in the four basins of Puerto Rico and St. Croix. We ran the model for each crop and each region over the three periods of analysis. Table 4.2 and Table 4.3 show the suitability classes for each month. The overall results indicate that condition for banana and plantain cultivation will be less suitable than sweet pepper in South and West Puerto Rico basins and in St. Croix by the end of the 21st Century.

When focusing on sweet pepper (Table 4.2) during the baseline climatology, the results indicated this crop as highly suitable over the entire year for East, West, and North Puerto Rico basins, while in South Puerto Rico basin and St. Croix the highly suitable class is limited to August–January and October–January, respectively. During the early rainfall season (April–July), sweet pepper was already moderately suitable for South Puerto Rico basin and marginally suitable for St. Croix from 1981–2010. Future climatologies, starting in 2041, did not change the high suitability of sweet pepper in East and North Puerto Rico, except for July in the northern basin, in which the crop became moderately suitable after 2071. However, a gradual decrease in sweet pepper suitability was evident in West Puerto Rico basin in January–April, when this region is under water stress, and each month reduced at least one suitability class. On the other hand, South Puerto Rico basin presented a drastic change in sweet pepper suitability, mainly from February to August when the crop that used to be moderately suitable during the baseline climatology will becomes unsuitable after 2071. In St. Croix, the decrease of crop suitability occurred first, because sweet pepper will be unsuitable from March to August starting in 2041.

For banana and plantain (Table 4.3), the agroclimatic suitability assessment was even less optimistic. During the baseline climatology, East and North Puerto Rico basins were still highly suitable, but some moderately suitable category will start to occur during the mid-summer dry spell in East basin after 2071. For the North basin, only July is moderately suitable after 2041, while after 2071 this region has a drastic change to not suitable for banana and plantain. In West Puerto Rico basin, suitability also decreased from highly-moderately suitable in baseline climatology to marginally-not suitable in January–March after 2041. However, the drastic decrease in banana and plantain suitability occurs in South Puerto Rico basin, from January to August, where most of the months that used to be moderately-marginally suitable became not suitable. The exception for this region is the hurricane season, from September to November, when crop suitability is high throughout the end of this century. In St. Croix, where banana and plantain are already not suitable to be rainfed from March–August in the baseline climatology, the decrease in suitability expanded to 9 months of the year (January–September) after 2071. The greater decrease in banana and plantain suitability is probably related to the fact that they are more prone to water stress than sweet pepper. As mentioned previously, the *ky* value greater than one indicates crops more sensitive to water availability, and the *ky* for banana and plantain is greater than the one for sweet pepper.

Therefore, the overall crop suitability in the region is predicted to decay during the first half of the year (January–July), affecting the early rainfall season and the two drier seasons agroclimatic suitability. The effects of the crop suitability reduction will be mostly felt in St. Croix and in southern Puerto Rico. On the other hand, November is the only month when all crops, independent of the period and the region, will remain highly suitable. This is most likely due to the increase in precipitation projected by the future climatologies that was previously discussed (Figure 4.3 and Figure 4.4).

These results suggested that temperature increase has a slightly larger impact than precipitation on crop suitability and water stress. While the temperature increase is predicted to occur yearlong, the greater reduction in precipitation is projected to occur only from June to October, which were not the months with the greatest water stress and poorest crop suitability. Similarly to what Curtis et al. (2014) found in Jamaica, the effect of temperature on agriculture suitability was probably related to the projected warming in the boreal winter, which increases the evapotranspiration demand during Caribbean dry season.

4.3.4 Food security and climate change

The results discussed here indicated that southern Puerto Rico and St. Croix, which are already sensitive to water deficit, will face difficulty in keeping crop suitability for sweet pepper, banana, and plantain during most of the annual cycle after 2041. For short rotation crops studied in Jamaica, drought and water deficits are major problems already affecting growth rate, fertilization, and yield (Rhiney et al. 2018), which will also be the case of sweet pepper analyzed here, whose life cycle range from 60 to 90 days. Other studies suggested that important crops such as coffee production would have an estimated reduction in up to 84% of highly suitable growing conditions in top producing municipalities in Puerto Rico by 2070 (Fain et al. 2018).

Therefore, one of the strategies that may be considered to adapt to climate change is finding alternatives to sweet pepper, banana, and plantain, including more drought tolerant crops, such as sweet potato and cassava (Campbell et al. 2011; Curtis et al. 2014). Furthermore, irrigation may also be an option, as parts of the South Puerto Rico basin were already classified as conditional farmland soils, meaning the soils there typically need irrigation (Gould et al. 2017). Another alternative could be to invest in farmer field schools with farmer-centered approaches for collaboration and participation to solve the problems and plan for the future, which may increase the chances for knowledge diffusion and collective action (Tomlinson and Rhiney 2018).

Additionally, it is important to emphasize that agriculture was highlighted as one of the human systems most impacted by climate change at the community level (Robinson and Wren 2020), while results from the Fifth Assessment Report (AR5) of the Intergovernmental Panel on Climate Change (IPCC) indicated that climate change will impact agriculture in the Caribbean mainly due to changes in temperature and water availability (Lincoln Lenderking et al. 2021). Therefore, the reduction in agroclimatic suitability assessed here and in past studies reinforced the likelihood of climate change being a threat to food security in Puerto Rico and St. Croix, because food security depends not only on food availability, but also on food access, utilization, and stability that are all significantly affected by climate change (Lincoln Lenderking et al. 2021; Rhiney et al. 2018).

4.4 Conclusions

This work investigated how future climate can impact water stress and crop suitability for four basins in Puerto Rico (South, North, East, and West) and the island of St. Croix using the CROPRISK model. We created a baseline climatology (1981–2010) and two future climatologies (2041–2070 and 2071–2100) using monthly temperature and precipitation from Daymet data (Version 3) and CMIP6 models ensemble, under the SSP5-8.5 scenario, to investigate future changes in agroclimatic suitability and water deficit. For this analysis we choose to focus on sweet pepper, banana, and plantain due to their agricultural importance to Puerto Rico and St. Croix, as well as their sensitivity to water deficit.

The projected increase in temperature and decrease in precipitation will continually decrease crop suitability and increase water stress over most of Puerto Rico and in St. Croix after 2041. Among the regions, we highlighted South Puerto Rico basin and St. Croix as the most sensitives to the future changes due to their greater water stress and lower crop suitability when compared to the other regions. By 2041, St. Croix will not be suitable for sweet pepper, banana, and plantain at least half of the year, while southern Puerto Rico will follow the same path after 2071. For other regions of Puerto Rico, such as East and North basins, the greater precipitation values and the smaller increase in projected temperature will help them to keep crop suitability and lower water stress for almost the entire year. The exception was for mid-summer dry spell months (June–July), when all regions exhibit the effects of climate change in their water deficits and in banana/plantain crop suitability.

When comparing the results of Puerto Rico and St. Croix, we can see the different impacts of climate change on a Greater and a Lesser Antilles. While Puerto Rico will still have some areas remaining suitable for crops most of the year until the end of this century, St. Croix will suffer more and sooner with water stress and crop suitability, with a chance to have most of the year without the ability to rely on rainfed crops. The differences in island area (St. Croix is at least 50 times smaller than Puerto Rico) and water resources availability can play an important role in defining the islands that are going to feel the consequences of climate change first.

Overall, results indicated that banana and plantain were more sensitive to water deficits then sweet pepper, and that the effects of future climate change on water stress and crop suitability will be worse from January–July. This indicates that the projected temperature increase will have a slightly larger impact than precipitation on crop suitability and water stress in Puerto Rico and St. Croix. While the temperate increase is predicted to occur yearlong, the greater reduction in precipitation was projected to occur only from June to October, which are not the months with the greatest water stress and poorest crop suitability in the islands.

The reduction in crop suitability and greater water stress from January–July also indicated that the two dry seasons and the early rainfall season will be the periods when planning for agriculture will be critical in order to keep crops suitable in the future. Among the options for planning and adaptation, focusing on more drought resistant crops and/or having an irrigation plan at government level could be alternatives. Preserving forested and highly vegetated areas would also be important, as we saw their roles in controlling temperature range and precipitation in eastern Puerto Rico. Moreover, we believe that any effort that helps to reduce the CO_2 emissions should be taken into consideration to prevent a drastic increase in temperature and its consequent impact on SIDS and smallholder farmers.

Additionally, it is important to emphasize that this study is only one possible application of the CROPRISK model. Methods applied here could be replicated using other crops of interest in Puerto Rico and St. Croix, as well as be applied to other areas of study. Therefore, we believe that further investigation is needed to assess the possible impacts of climate change on Puerto Rico and St. Croix's agriculture, as well as to better understand the spatial distribution of those impacts. It would also be important to apply a similar approach to other nations in the insular Caribbean to understand the regional impacts of future climate on crop water stress, and, hopefully, to encourage a regional action/plan to better prepare and adapt to mitigate food insecurity.

Finally, we understand that the outputs from the climate models used here should be interpreted as projected climate trends for an extreme climate change scenario, rather than predictions of future weather. There are still many uncertainties in the climate models, mainly in predicting precipitation changes in the future, that requires caution when interpreting the model outputs.

Acknowledgments

The authors thank Dr. Thomas Mote for providing insightful comments and suggestions that improved this manuscript. The authors also thank the NSF Luquillo Long-Term Ecological Research Program (DEB1239764) for the funding provided, the National Aeronautics and Space Administration (NASA) Earth Data for Daymet data availability (https://daymet.ornl.gov/), the U.S. Geological Survey for the Thornthwaite Water Balance model (https://www.usgs.gov/software/thornthwaite-monthly-water-balance-model), the World Climate Research Programme for the CMIP6 data availability (https://esgf-node.llnl.gov/projects/cmip6/), as well as Christina Chanes and Dr. William Gould for sharing with us some agricultural data from Puerto Rico and St. Croix.

4.5 References

Allen, R. G., L. S. Pereira, D. Raes, and M. Smith, 1998: FAO Irrigation and drainage paper No. 56. *Rome: Food and Agriculture Organization of the United Nations*, **56,** e156.

Angeles, M. E., J. E. Gonzalez, N. D. Ramírez-Beltrán, C. A. Tepley, and D. E. Comarazamy, 2010: Origins of the Caribbean rainfall bimodal behavior. *Journal of Geophysical Research: Atmospheres*, **115**.

Ault, T., 2016: Island water stress. *Nature Climate Change*, **6,** 1062-1063.

Ault, T. R., 2020: On the essentials of drought in a changing climate. *Science*, **368,** 256-260.

Barker, D., 2012: Caribbean agriculture in a period of global change: vulnerabilities and opportunities. *Caribbean Studies*, **40,** 41-61.

Bates, B., Z. Kundzewicz, and S. Wu, 2008: *Climate change and water*. Intergovernmental Panel on Climate Change Secretariat.

Batjes, N., 1987: CROPRISK: A computerized procedure to assess the agro-ecological suitability of land for rainfed annual crops. *Technical Soils Bulletin*.

Bernal, R. L., 2020: The importance of bananas in the Caribbean. *Corporate versus National Interest in US Trade Policy*, Springer, 41-61.

Brovkin, V., 2002: Climate-vegetation interaction. *Journal de Physique IV (Proceedings)*, **12,** 57-72.

Campbell, D., D. Barker, and D. McGregor, 2011: Dealing with drought: small farmers and environmental hazards in southern St. Elizabeth, Jamaica. *Applied Geography*, **31,** 146-158.

Cashman, A., L. Nurse, and C. John, 2010: Climate change in the Caribbean: the water management implications. *The Journal of Environment & Development*, **19,** 42-67.

Connell, J., K. Lowitt, A. Saint Ville, and G. M. Hickey, 2020: Food security and sovereignty in small island developing states: contemporary crises and challenges. *Food Security in Small Island States*, J. Connell, and K. Lowitt, Eds., Springer Singapore, 1-23.

Cook, K. H., and E. K. Vizy, 2010: Hydrodynamics of the Caribbean Low-Level Jet and its relationship to precipitation. *Journal of Climate*, **23,** 1477-1494.

Curtis, S., and D. W. Gamble, 2008: Regional variations of the Caribbean mid-summer drought. *Theoretical and Applied Climatology*, **94,** 25-34.

Curtis, S., D. W. Gamble, and J. Popke, 2014: Sensitivity of crop water need to 2071–95 projected temperature and precipitation changes in Jamaica. *Earth Interactions*, **18,** 1-17.

Fain, S. J., M. Quiñones, N. L. Álvarez-Berríos, I. K. Parés-Ramos, and W. A. Gould, 2018: Climate change and coffee: assessing vulnerability by modeling future climate suitability in the Caribbean island of Puerto Rico. *Climatic Change*, **146,** 175-186.

Farrell, D., L. Nurse, and L. Moseley, 2007: *Managing water resources in the face of climate change: a Caribbean perspective.* UWI.

Farrell, D., A. Trotman, and C. Cox, 2010: Drought early warning and risk reduction.

Fetcher, N., S. F. Oberbauer, and B. R. Strain, 1985: Vegetation effects on microclimate in lowland tropical forest in Costa Rica. *International Journal of Biometeorology*, **29,** 145-155.

Gamble, D. W., and S. Curtis, 2008: Caribbean precipitation: review, model and prospect. *Progress in Physical Geography*, **32,** 265-276.

Gamble, D. W., D. B. Parnell, and S. Curtis, 2008: Spatial variability of the Caribbean mid-summer drought and relation to north Atlantic high circulation. *International Journal of Climatology*, **28,** 343-350.

Giannini, A., M. A. Cane, and Y. Kushnir, 2001b: Interdecadal changes in the ENSO teleconnection to the Caribbean region and the North Atlantic Oscillation. *Journal of Climate*, **14,** 2867-2879.

Gould, W. A., F. H. Wadsworth, M. Quiñones, S. J. Fain, and N. L. Álvarez-Berríos, 2017: Land use, conservation, forestry, and agriculture in Puerto Rico. *Forests*, **8,** 242.

Granger, O. E., 1985: Caribbean climates. *Progress in Physical Geography*, **9,** 16-43.

Harmsen, E., J. Colon Trinidad, C. Lis Arcelay, and D. Cadiz Rodriguez, 2003: Evaluation of percolation and nitrogen leaching from a sweet pepper crop grown on an oxisol soil in Northwest Puerto Rico.

Hawkins, E., T. M. Osborne, C. K. Ho, and A. J. Challinor, 2013: Calibration and bias correction of climate projections for crop modelling: an idealised case study over Europe. *Agricultural and Forest Meteorology*, **170,** 19-31.

Holdridge, L. R., 1967: Life zone ecology. *Life zone ecology.*

Jury, M. R., 2020: Resolution-dependent perspectives on Caribbean hydro-climate change. *Hydrology*, **7,** 93.

Karnauskas, K. B., J. P. Donnelly, and K. J. Anchukaitis, 2016: Future freshwater stress for island populations. *Nature Climate Change*, **6,** 720-725.

Karnauskas, K. B., C.-F. Schleussner, J. P. Donnelly, and K. J. Anchukaitis, 2018: Freshwater stress on small island developing states: population projections and aridity changes at 1.5 and 2 °C. *Regional Environmental Change*, **18,** 2273-2282.

Kisekka, I., K. Migliaccio, M. D. Dukes, J. H. Crane, and B. Schaffer, 2010: Evapotranspiration-based irrigation for agriculture: crop coefficients of some commercial crops in Florida. *EDIS*, **2010**.

Kossin, J. P., 2008: Is the North Atlantic hurricane season getting longer? *Geophysical Research Letters*, **35**.

Lawrence, D., and K. Vandecar, 2015: Effects of tropical deforestation on climate and agriculture. *Nature Climate Change*, **5,** 27-36.

Lincoln Lenderking, H., S.-A. Robinson, and G. Carlson, 2021: Climate change and food security in Caribbean small island developing states: challenges and strategies. *International Journal of Sustainable Development & World Ecology*, **28,** 238-245.

Martinez, C., L. Goddard, Y. Kushnir, and M. Ting, 2019: Seasonal climatology and dynamical mechanisms of rainfall in the Caribbean. *Climate Dynamics*.

McCabe, G. J., and S. L. Markstrom, 2007: A monthly water-balance model driven by a graphical user interface. Report 2007-1088.

McGregor, D., D. Barker, and D. Campbell, 2009: Environmental change and Caribbean food security: recent hazard impacts and domestic food production in Jamaica. *Global change and Caribbean vulnerability: Environment, economy and society at risk***,** 273-297.

Miller, P. W., T. L. Mote, and C. A. Ramseyer, 2019: An empirical study of the relationship between seasonal precipitation and thermodynamic environment in Puerto Rico. *Weather and Forecasting*, **34,** 277-288.

Mote, T. L., C. A. Ramseyer, and P. W. Miller, 2017: The Saharan Air Layer as an early rainfall season suppressant in the Eastern Caribbean: The 2015 Puerto Rico drought. *Journal of Geophysical Research: Atmospheres*, **122**.

Navarro-Racines, C., J. Tarapues, P. Thornton, A. Jarvis, and J. Ramirez-Villegas, 2020: High-resolution and bias-corrected CMIP5 projections for climate change impact assessments. *Scientific Data*, **7**.

Neelin, J. D., M. Münnich, H. Su, J. E. Meyerson, and C. E. Holloway, 2006: Tropical drying trends in global warming models and observations. *Proceedings of the National Academy of Sciences*, **103,** 6110-6115.

O'Neill, B. C., and Coauthors, 2016: The scenario model intercomparison project (ScenarioMIP) for CMIP6. *Geoscientific Model Development*, **9,** 3461-3482.

Palada, M. C. M., Jeanmarie M., and O'Keefe, Daniela 2003: Growth and yield response of Puerto Rican sweet pepper to levels of drip irrigation in the Virgin Islands *Caribbean Food Crops Society, Thirty Ninth Annual Meeting*.

Pulwarty, R. S., L. A. Nurse, and U. O. Trotz, 2010: Caribbean islands in a changing climate. *Environment: Science and Policy for Sustainable Development*, **52,** 16-27.

Ramseyer, C. A., and T. L. Mote, 2016: Atmospheric controls on Puerto Rico precipitation using artificial neural networks. *Climate Dynamics*, **47,** 2515-2526.

Rhiney, K., A. Eitzinger, A. D. Farrell, and S. D. Prager, 2018: Assessing the implications of a 1.5 °C temperature limit for the Jamaican agriculture sector. *Regional Environmental Change*, **18,** 2313-2327.

Robinson, S.-A., and C. Wren, 2020: Geographies of vulnerability: a research note on human system adaptations to climate change in the Caribbean. *Geografisk Tidsskrift-Danish Journal of Geography***,** 1-8.

Sobel, A. H., C. D. Burleyson, and S. E. Yuter, 2011: Rain on small tropical islands. *Journal of Geophysical Research*, **116**.

Stephenson, N., 1998: Actual evapotranspiration and deficit: biologically meaningful correlates of vegetation distribution across spatial scales. *Journal of Biogeography*, **25,** 855-870.

Taylor, M. A., D. B. Enfield, and A. A. Chen, 2002: Influence of the tropical Atlantic versus the tropical Pacific on Caribbean rainfall. *Journal of Geophysical Research: Oceans*, **107,** 10-11-10-14.

Taylor, M. A., F. S. Whyte, T. S. Stephenson, and J. D. Campbell, 2013: Why dry? Investigating the future evolution of the Caribbean Low Level Jet to explain projected Caribbean drying. *International Journal of Climatology*, **33,** 784-792.

Thornthwaite, C. W., 1948: An Approach toward a rational classification of climate. *Geographical Review*, **38,** 55.

Thornton, P. E., S. W. Running, and M. A. White, 1997: Generating surfaces of daily meteorological variables over large regions of complex terrain. *Journal of Hydrology*, **190,** 214-251.

Thornton, P. E., M. M. Thornton, B. W. Mayer, Y. Wei, R. Devarakonda, R. S. Vose, and R. B. Cook, 2016: Daymet: daily surface weather data on a 1-km grid for North America, Version 3. ORNL Distributed Active Archive Center.

Tomlinson, J., and K. Rhiney, 2018: Experiential learning as a tool for farmer engagement and empowerment in a changing regional climate. *Caribbean Quarterly*, **64,** 114-135.

Torres-Valcárcel, Á., J. Harbor, C. González-Avilés, and A. Torres-Valcárcel, 2014: Impacts of urban development on precipitation in the tropical maritime climate of Puerto Rico. *Climate*, **2,** 47-77.

Trotman, A., R. M. Gordon, S. D. Hutchinson, R. Singh, and D. McRae-Smith, 2009: Policy responses to GEC impacts on food availability and affordability in the Caribbean community. *Environmental Science & Policy*, **12,** 529-541.

USDA, U. S. D. o. A., 2020a: 2017 Census of agriculture - Puerto Rico (2018), 230 pp.

——, 2020b: 2017 Census of agriculture - Virgin Islands of the United States (2018) 55 pp.

Wang, A., F. Dominguez, and A. Schmidt, 2019: Extreme precipitation spatial analog: in search of an alternative approach for future extreme precipitation in urban hydrological studies. *Water*, **11,** 1032.

Wolock, D., and G. McCabe, 1999: Effects of potential climatic change on annual runoff in the conterminous United States. *Journal of the American Water Resources Association*, **35,** 341-341,350.

Table 4.1 – Detailed information about the General Circulation Models (GCM) from CMIP6 used in this study.

Acronyms	Expanded Names	Emission Scenario	Origins
CIESM	Community Integrated Earth System Model	SSP5-8.5	Department of Earth System Science, Tsinghua University, Beijing 100084, China
E3SM 1.1	Energy Exascale Earth System Model	SSP5-8.5	LLNL Climate Program, L-103, 7000 East Avenue, Livermore, CA 94550, USA
EC-Earth3	EC-Earth3	SSP5-8.5	EC-Earth consortium, Rossby Center, Swedish Meteorological and Hydrological Institute/SMHI, SE-601 76 Norrkoping, Sweden
EC-Earth3-Veg	EC-Earth3-Veg	SSP5-8.5	
FGOALS-f3-L	FGOALS-f3-L	SSP5-8.5	Chinese Academy of Sciences, Beijing 100029, China

Source: https://wcrp-cmip.github.io/CMIP6_CVs/docs/CMIP6_source_id.html

Table 4.2 – Annual cycle of agroclimatic suitability for sweet pepper in the four basins of Puerto Rico and in St. Croix during the baseline climatology (1981–2010), and the two future climatologies: mid-century (2041–2070) and late-century (2071–2100). Highly suitable class is in green, moderately suitable in yellow, marginally suitable in orange, and not suitable in red.

Sweet Pepper	**East PR**			**North PR**			**West PR**			**South PR**			**St. Croix USVI**		
Month	**1981-2010**	**2041-2070**	**2071-2100**	**1981-2010**	**2041-2070**	**2071-2100**	**1981-2010**	**2041-2070**	**2071-2100**	**1981-2010**	**2041-2070**	**2071-2100**	**1981-2010**	**2041-2070**	**2071-2100**
JAN	HiS	HiS	HiS	HiS	HiS	HiS	HiS	HiS	MoS	HiS	MoS	MaS	HiS	MoS	MaS
FEB	HiS	HiS	HiS	HiS	HiS	HiS	HiS	MoS	MaS	MoS	MaS	NS	MoS	MaS	NS
MAR	HiS	HiS	HiS	HiS	HiS	HiS	HiS	MaS	NS	MaS	NS	NS	MaS	NS	NS
APR	HiS	HiS	HiS	HiS	HiS	HiS	HiS	HiS	MoS	MoS	MaS	NS	MaS	NS	NS
MAY	HiS	HiS	HiS	HiS	HiS	HiS	HiS	HiS	HiS	MoS	MoS	MaS	MaS	NS	NS
JUN	HiS	HiS	HiS	HiS	HiS	HiS	HiS	HiS	HiS	MoS	MaS	NS	MaS	NS	NS
JUL	HiS	HiS	HiS	HiS	HiS	MoS	HiS	HiS	MoS	MoS	NS	NS	MaS	NS	NS
AUG	HiS	HiS	HiS	HiS	HiS	HiS	HiS	HiS	HiS	HiS	MoS	NS	MaS	NS	NS
SEP	HiS	HiS	HiS	HiS	HiS	HiS	HiS	HiS	HiS	HiS	HiS	MoS	MoS	MoS	MaS
OCT	HiS	HiS	HiS	HiS	HiS	HiS	HiS	HiS	HiS	HiS	HiS	HiS	HiS	MoS	MoS
NOV	HiS	HiS	HiS	HiS	HiS	HiS	HiS	HiS	HiS	HiS	HiS	HiS	HiS	HiS	HiS
DEC	HiS	HiS	HiS	HiS	HiS	HiS	HiS	HiS	HiS	HiS	HiS	MoS	HiS	MoS	MoS

Table 4.3 – Annual cycle of agroclimatic suitability for banana and plantain in the four basins of Puerto Rico and in St. Croix during the baseline climatology (1981–2010), and the two future climatologies: mid-century (2041–2070) and late-century (2071–2100). Highly suitable class is in green, moderately suitable in yellow, marginally suitable in orange, and not suitable in red.

Banana / Plantain	East PR			North PR			West PR			South PR			St. Croix USVI		
Month	1981-2010	2041-2070	2071-2100	1981-2010	2041-2070	2071-2100	1981-2010	2041-2070	2071-2100	1981-2010	2041-2070	2071-2100	1981-2010	2041-2070	2071-2100
JAN	HiS	HiS	HiS	HiS	HiS	HiS	HiS	MaS	MaS	MoS	MaS	NS	MoS	MoS	NS
FEB	HiS	HiS	HiS	HiS	HiS	MoS	MoS	MaS	NS	MaS	NS	NS	MaS	NS	NS
MAR	HiS	HiS	HiS	HiS	HiS	MoS	MaS	MaS	NS	NS	NS	NS	NS	NS	NS
APR	HiS	HiS	HiS	HiS	HiS	MoS	HiS	MoS	MoS	MoS	NS	NS	NS	NS	NS
MAY	HiS	HiS	HiS	HiS	HiS	HiS	HiS	HiS	HiS	MoS	MaS	MaS	NS	NS	NS
JUN	HiS	HiS	MoS	HiS	HiS	HiS	HiS	HiS	MoS	MoS	MaS	NS	NS	NS	NS
JUL	HiS	HiS	MoS	HiS	MoS	NS	HiS	HiS	MaS	MaS	NS	NS	NS	NS	NS
AUG	HiS	HiS	HiS	HiS	HiS	MoS	HiS	HiS	HiS	HiS	MaS	NS	NS	NS	NS
SEP	HiS	HiS	HiS	HiS	HiS	HiS	HiS	HiS	HiS	HiS	HiS	MoS	MoS	MaS	NS
OCT	HiS	HiS	HiS	HiS	HiS	HiS	HiS	HiS	HiS	HiS	HiS	HiS	MoS	MoS	MaS
NOV	HiS	HiS	HiS	HiS	HiS	HiS	HiS	HiS	HiS	HiS	HiS	HiS	HiS	HiS	HiS
DEC	HiS	HiS	HiS	HiS	HiS	HiS	HiS	HiS	HiS	HiS	MoS	MaS	MoS	MoS	MoS

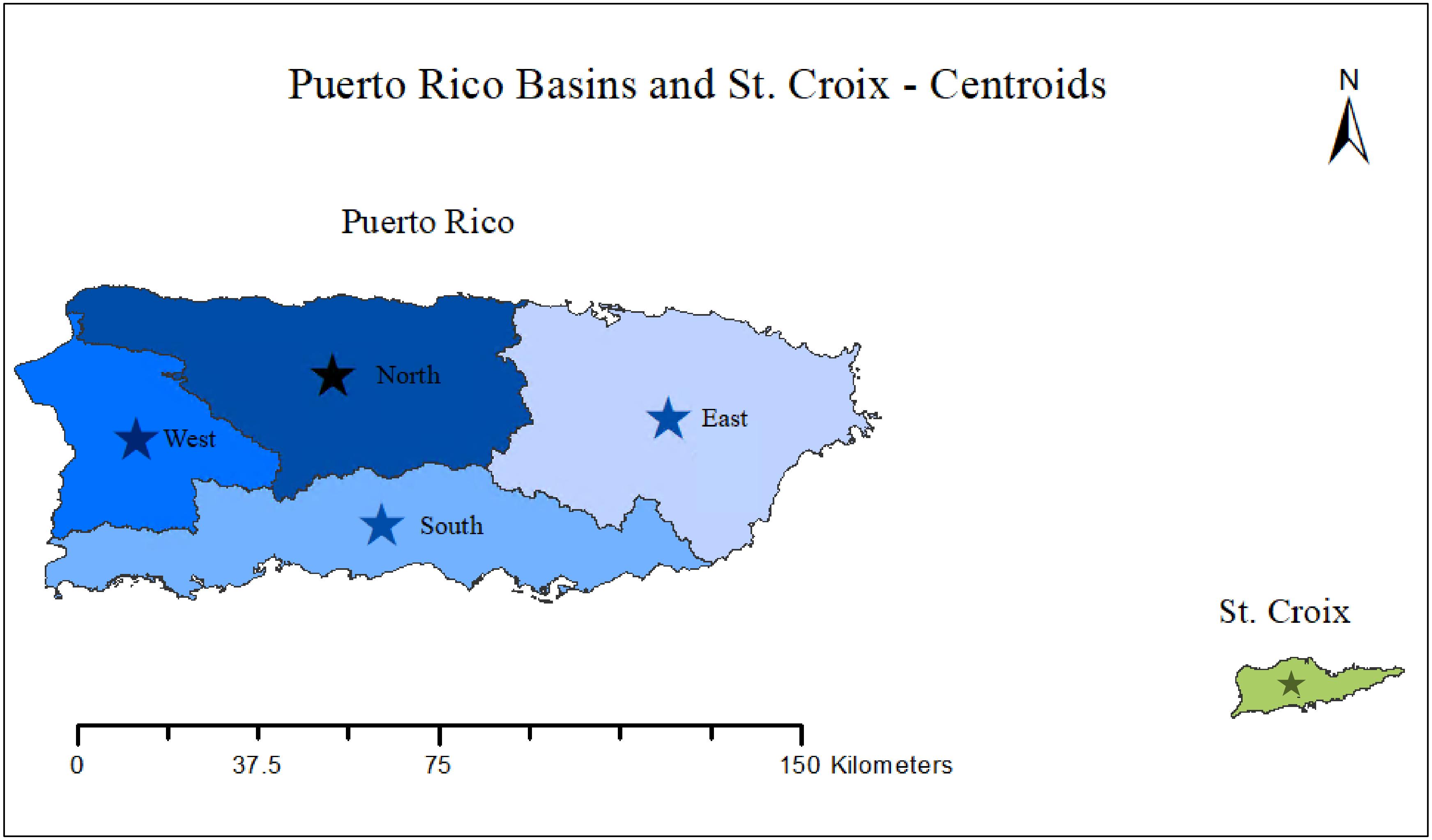

Figure 4.1 – Puerto Rico 8-digit Hydrologic Units used to divide the island in North, South, East West (source: US Geological Survey), and St. Croix island. The stars indicated the centroids of each basin/island used to remap the CMIP6 models data.

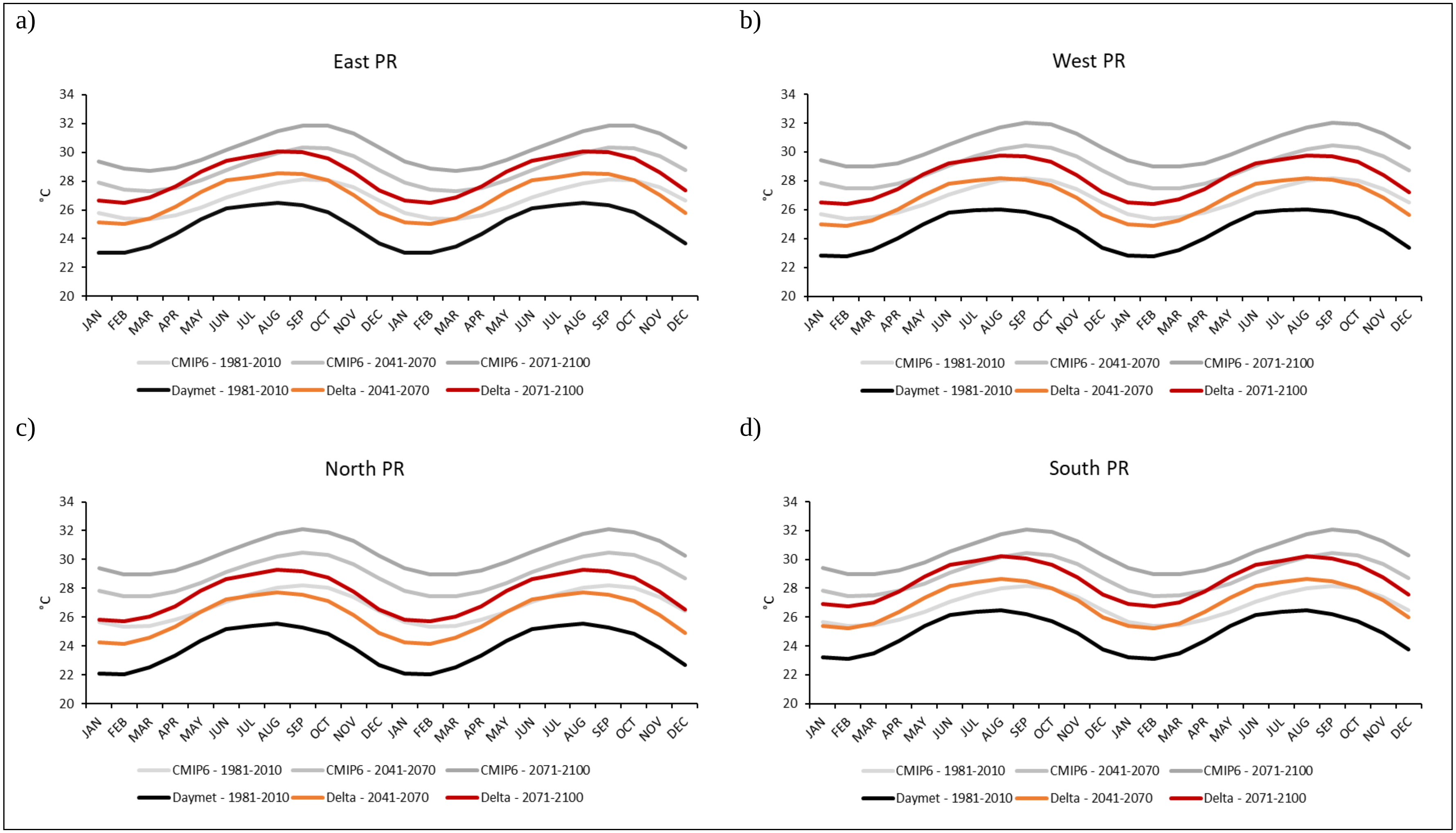

Figure 4.2 – The 24-month annual cycle of temperature (°C) for Puerto Rico basins: (a) East, (b) West, (c) North, and (d) South. Daymet baseline climatology (1981–2010) is in black, bias corrected Delta – 2041–2070 is in orange, and bias corrected Delta – 2071–2100 is in red. The CMIP6 outputs are in shades of gray.

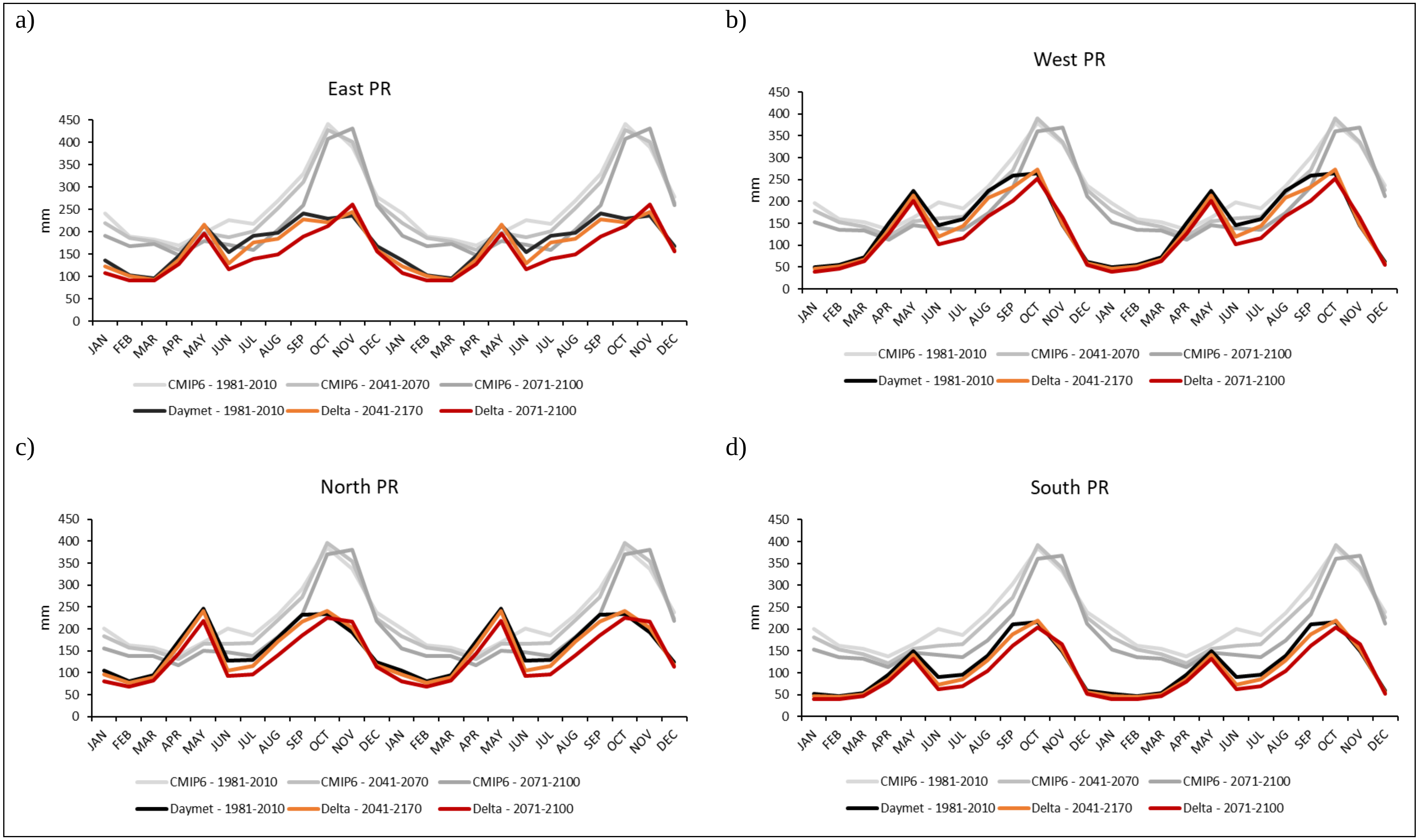

Figure 4.3 – The 24-month annual cycle of precipitation (mm) for Puerto Rico basins: (a) East, (b) West, (c) North, and (d) South. Daymet baseline climatology (1981–2010) is in black, bias corrected Delta – 2041–2070 is in orange, and bias corrected Delta – 2071–2100 is in red. The CMIP6 outputs are in shades of gray.

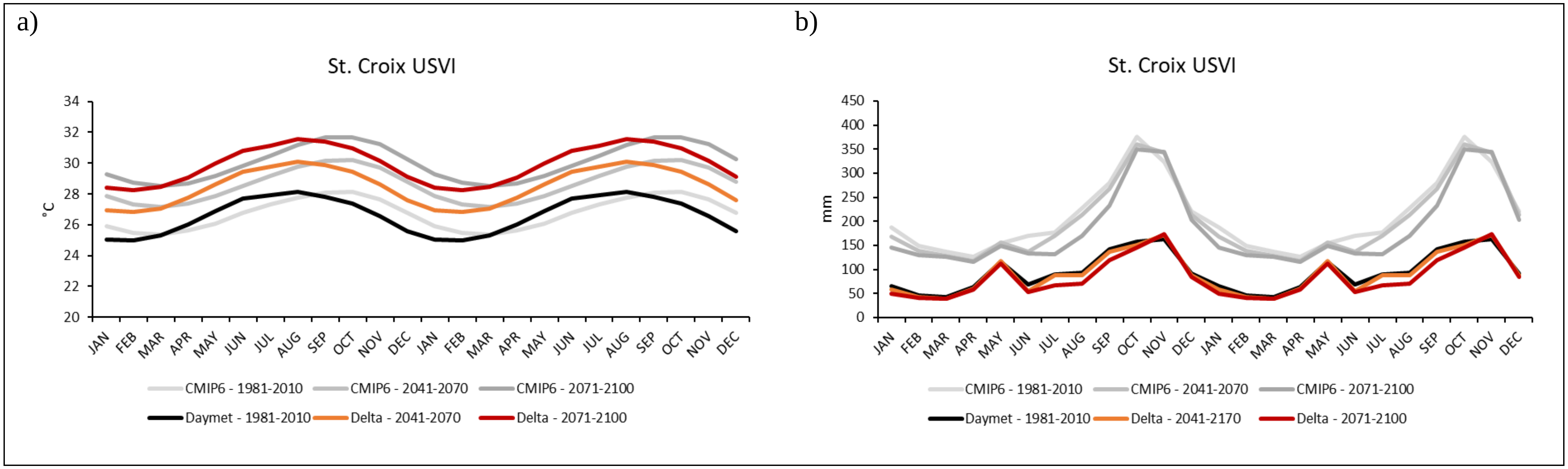

Figure 4.4 – The 24-month annual cycle of (a) temperature (°C) and (b) precipitation (mm) for the US Virgin Island of St. Croix. Daymet baseline climatology (1981–2010) is in black, bias corrected Delta – 2041–2070 is in orange, and bias corrected Delta – 2071–2100 is in red. The CMIP6 outputs are in shades of gray.

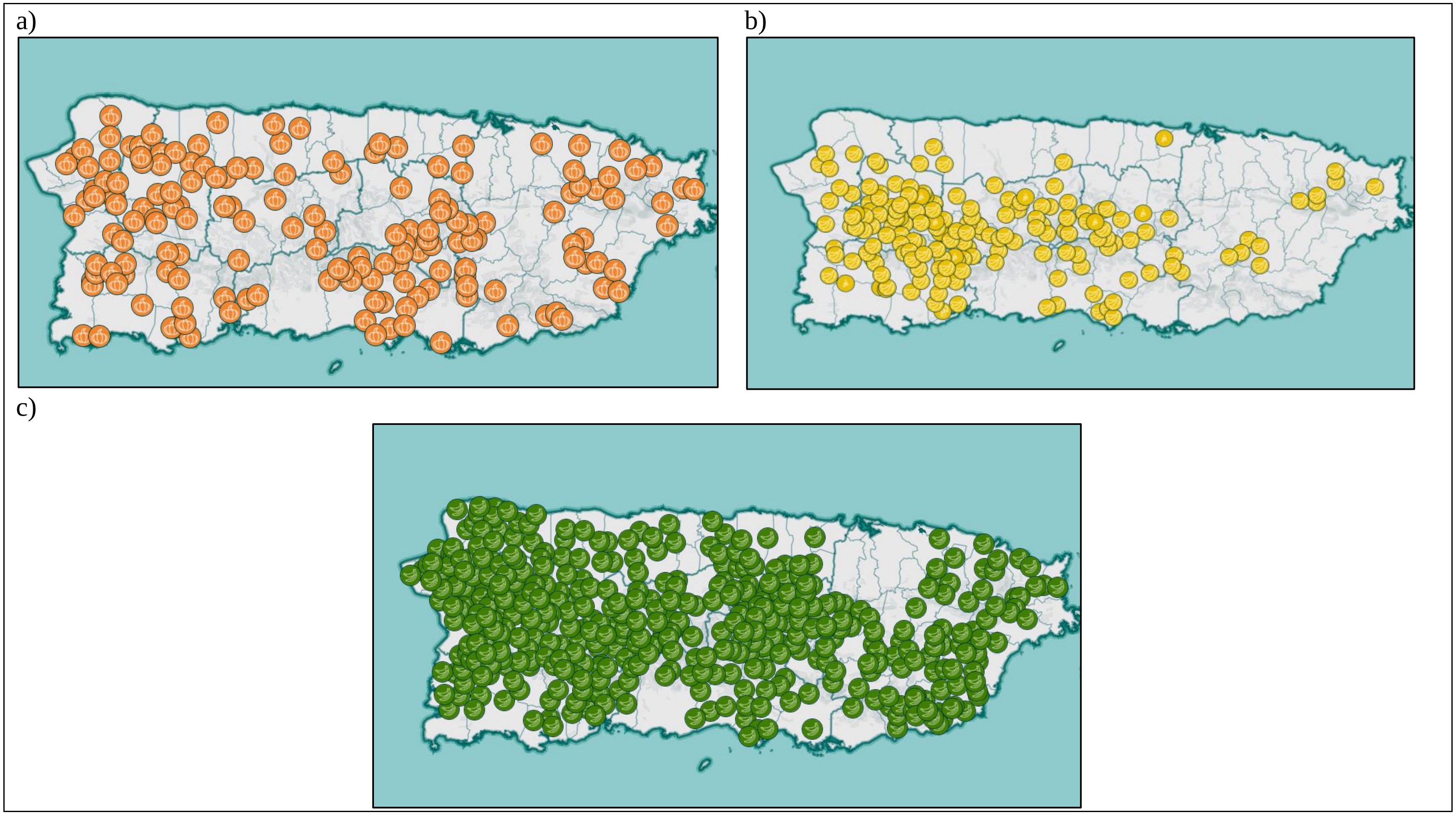

Figure 4.5 – Spatial distribution of (a) sweet pepper, (b) banana, and (c) plantain over Puerto Rico in 2016 (Source: USDA, https://caribbeanclimatehub.org/tools-apps/agricultural-statistics/).

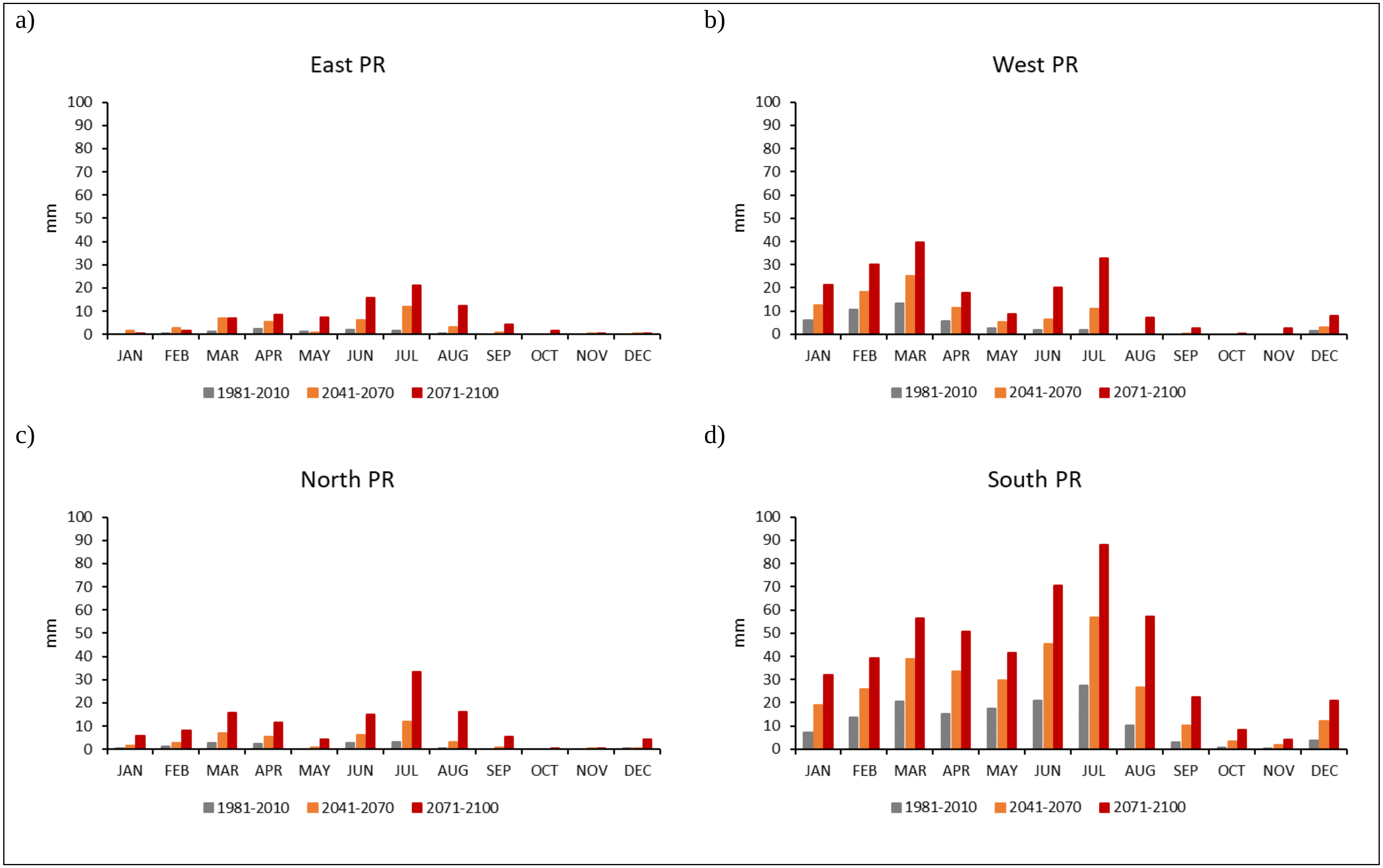

Figure 4.6 – Annual water stress (PET – AET) for Puerto Rico basins (a) East, (b) West, (c) North, (d) South, and (e) St. Croix. The gray bars represent the water stress for baseline climatology (1981–2010), the orange bars are for mid-century (2041–2070), and red bars are for late-century (2071–2100) climatologies.

e)

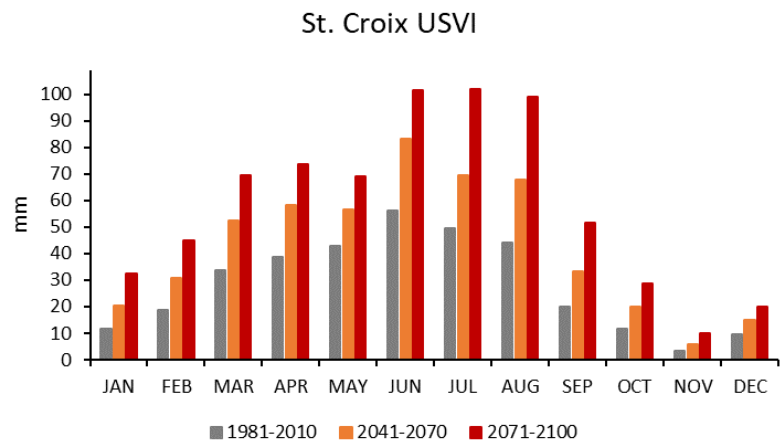

Figure 4.6 – Continued.

5 CONCLUSIONS

5.1 Summary

The insular Caribbean is a region where multiple hazard-related events occur, including but not limited to hurricanes, floods, earthquakes, volcanic eruption, and drought. While hurricane hazards are well explored in scientific literature, drought is considered one of the neglected hazards because of the lack of studies focusing on its causes and effects. Meanwhile, global climate models have predicted drought events to be more intense and frequent in the Caribbean due to a warming world, which accentuates the need to better understanding of this hazard.

Geomorphic characteristics (volcanic and karts landscapes), which make the region dependent on rainfall as freshwater resources due to the lack of reservoirs and/or aquifers on some islands, make the insular Caribbean more sensitive to drought. Because rainfall variability in the area is related to low-frequency atmospheric circulation (e.g., ENSO, NAO, AMM), understanding the extent of regional and temporal effects of the teleconnections in the insular Caribbean is essential. Moreover, analysis of the water budget and potential groundwater recharge during periods of drought as well as understanding the potential impacts of climate change on crop water needs are also important to improve drought planning. Therefore, this dissertation brings awareness about three important facets of drought in the insular Caribbean: the climatological influence from teleconnection patterns, the physical geography influence on water resources availability, and the sensitivity of crop water need to projected temperature and precipitation changes.

The spatial and temporal distribution of drought events in the insular Caribbean as well as the relationship of these events with low-frequency atmospheric circulation patterns such as EP and CP ENSO, AMM, and NAO were analyzed in Chapter 2. This work brought a new perspective over the region by dividing the Caribbean into western (Greater Antilles and Bahamas, here referred as Greater Antilles), and the eastern Caribbean (Lesser Antilles) to compare the role of those three teleconnection patterns on drought events over larger versus smaller islands, as well as to investigate how intense and widespread drought events compare on those regions. This chapter is the first time that CP and EP ENSO have been related to drought in the Caribbean. The work used the scPDSI drought atlas from Herrera and Ault (2017) at 4 km resolution to assess the distribution of drought events from 1950 to 2017. It also used correlation, regression, and EOF analysis to relate the EP and CP ENSO, NAO, and AMM indices with spatial and temporal distribution of drought. Both the analysis of the relationship between peak season teleconnections and seasonal drought in the Greater and Lesser Antilles, as well the combined effects of all appropriately lagged teleconnections on seasonal drought are intended to improve drought predictability on a seasonal timescale. While NAO is the teleconnection most commonly related to drought in some of the Caribbean islands, this work is among the first examining the effects of the two types of ENSO and the AMM on drought in the region. Furthermore, composites of SLP, 700 hPa winds, and PW complemented the analysis to assess the possible effects of other large-scale atmospheric events, such as the SAL intrusion, on Caribbean drought.

In Chapter 3, the objective was to analyze the physical geography role on water resources, with a focus on understanding how Puerto Rico physical characteristics can affect its water budget and potential groundwater recharge, measured as net infiltration. This study used the SWB2 model from the USGS to run the water budget for Puerto Rico for three periods of analysis: baseline climatology (1981–2010), recent decade (2010–2019), and drought events (1991, 1994, 1997, and 2015). Because a drying trend has been already registered in the Caribbean since 1950, and drought is expected to be more frequent and severe in the Caribbean (Cashman et al. 2010; Herrera et al. 2018; Karnauskas et al. 2018), understanding the water balance of Puerto Rico is important to understand where are the areas in the island with less net infiltration in order to help local governments to plan for water management. Additionally, this chapter presented opportunity to evaluate the performance of a recently released and open-access water budget model on a tropical Atlantic island.

Finally, Chapter 4 discussed the potential impacts of projected temperature and precipitation changes on a Greater Antilles (Puerto Rico) and a Lesser Antilles (St. Croix) agricultural suitability of sweet pepper, banana, and plantain. This chapter used observed Daymet (Version 3) daily weather data and CMIP6 five-models ensemble to compare water stress and agriculture suitability during the baseline climatology (1981–2010) and two future climatologies: mid-century (2041–2070), and late-century (2071–2100). By assessing the impacts of climate change on agriculture and comparing islands with different sizes, this work intended to bring the awareness on how smaller islands will suffer earlier with the changing climate and where in the larger islands are the areas more vulnerable to future water stress. The results can support local governments' decisions about where to focus regarding drought mitigation plan, specifically focused on agriculture and food security, as well as to help local farms to plan if they should favor drought-tolerant crops in the future.

5.2 Conclusions

The findings from this dissertation add to our current understanding on drought in the insular Caribbean by bringing a new perspective that includes the analysis of low-frequency atmospheric drivers related to drought, the role of physical geography on water resources, and the assessment of how projected changes in temperature and precipitation can affect future water stress and agriculture suitability. As drought events become more frequent and intense, understanding the mechanisms that can lead to drought, how the aspects of the environment can exacerbate or alleviate the effects of drought, and how water stress can impact agriculture are very important for the islands to prepare for those events.

This dissertation first manuscript indicated that although a drying trend in all seasonal-average scPDSI occurred from 1950 to 2017 for both the Greater Antilles and the Lesser Antilles, it is the latter where more intense, widespread, and frequent drought events occurred. The Lesser Antilles was the only region that had a clear pattern of wind and PW that suggests an early SAL intrusion occurring during March–May when the LA experienced drought during the ERS and MSD. Although further investigation is needed, this additional forcing could be one of the reasons why the most intense and widespread events have occurred there when compared to the Greater Antilles. Negative AMM was the teleconnection most strongly related with drought events in the insular Caribbean during April–November, followed by positive NAO affecting drought during the second half of the year, mainly in the Greater Antilles, while CP warm event indicated drought events in the Lesser Antilles from December–July. The relationship between the two types of ENSO and the Greater Antilles was not statistically significant.

The vulnerability of smaller islands of the Lesser Antilles when compared to the Greater Antilles was also evident in Chapter 4. When comparing the four basins of Puerto Rico and St.

Croix, it was evident that St. Croix is already suffering with limited water, while Puerto Rico still has areas free of water stress. St. Croix is expected to not be suitable for sweet pepper, banana, and plantain at least half of the year by 2041, while the drier basin of Puerto Rico (i.e., South basin) will follow the same path only after 2071. For other regions of Puerto Rico, such as East and North basins, the greater precipitation values and the smaller increase in projected temperature will help maintain crop suitability and lower water stress for almost the entire year during the 21st Century.

Nevertheless, when analyzing a high-resolution (300 m) water budget model for Puerto Rico in Chapter 3, we see that some regions of this island are also vulnerable to drought due to its physical geography. Southern Puerto Rico was confirmed to be the drier region, with the lowest net infiltration of the island, mainly due to its location on the rain shadow side of the Cordillera Central, which blocks the moisture source from the Atlantic Ocean. The reduced net infiltration registered in the south and north Puerto Rico during drought is critical because those areas include the North Coast and South Coast Aquifers, the most important aquifers for drinking water, irrigation, and public supply in Puerto Rico. Eastern Puerto Rico also presented a reduced rainfall and net infiltration in the recent decade (2010–2019) and during drought events (1991, 1994, 1997, and 2015). This is where the greatest amount of rainfall is registered in Puerto Rico due to the orographic effect resultant from the northeast trade winds and the Luquillo Mountains. However, an indication of potential SAL intrusion, also found in Chapter 2, can be affecting the decrease in rainfall and net infiltration in eastern Puerto Rico in the recent decade as well as acting together with positive NAO during drought events, such as 1994 and 2015, resulting in less water availability in the region.

Although a significant contribution has been made by this dissertation to understand drought events, water resources, and agriculture suitability in the insular Caribbean, additional investigation should follow. Future studies could investigate the main reasons why the Lesser Antilles experienced more widespread, frequent, and intense drought in the insular Caribbean, as well as why the individual relationship of the two ENSO types did not present significant correlation with drought in the Greater Antilles. Further investigation into the combined effects of EP ENSO, NAO, and AMM on Caribbean drought is warranted in order to better predict drought onset. Future work should also test the SWB2 model performance in Puerto Rico using different model parameters than used here, as well as adding other input data, such as fog interception or irrigation, that could help to improve the model estimation of net infiltration. The application of the SWB2 model in other Caribbean islands would also be valuable and allow for the comparison of SWB2 performance in different areas of the insular Caribbean. Finally, further investigation could assess the spatial distribution of the impacts of climate change on Puerto Rico and St. Croix's agriculture. This work points to the value in applying a similar approach to Chapter 4 to other nations in the insular Caribbean to better understand the regional impacts of future climate on crop water stress, and, hopefully, to encourage a regional action to better prepare and mitigate food insecurity.

REFERENCES

Allen, R. G., L. S. Pereira, D. Raes, and M. Smith, 1998: FAO Irrigation and drainage paper No. 56. *Rome: Food and Agriculture Organization of the United Nations*, **56,** e156.

Allen, T. L., S. Curtis, and D. W. Gamble, 2010: The midsummer dry spell's impact on vegetation in Jamaica. *Journal of Applied Meteorology and Climatology*, **49,** 1590-1595.

Álvarez-Berríos, N. L., S. Soto-Bayó, E. Holupchinski, S. J. Fain, and W. A. Gould, 2018: Correlating drought conservation practices and drought vulnerability in a tropical agricultural system. *Renewable Agriculture and Food Systems*, **33,** 279-291.

Ang, R., and C. Oeurng, 2018: Simulating streamflow in an ungauged catchment of Tonlesap Lake Basin in Cambodia using Soil and Water Assessment Tool (SWAT) model. *Water Science*, **32,** 89-101.

Angeles, M. E., J. E. Gonzalez, N. D. Ramírez-Beltrán, C. A. Tepley, and D. E. Comarazamy, 2010: Origins of the Caribbean rainfall bimodal behavior. *Journal of Geophysical Research: Atmospheres*, **115**.

Ashok, K., S. K. Behera, S. A. Rao, H. Weng, and T. Yamagata, 2007: El Niño Modoki and its possible teleconnection. *Journal of Geophysical Research: Oceans*, **112**.

Ault, T., 2016: Island water stress. *Nature Climate Change*, **6,** 1062-1063.

Ault, T. R., 2020: On the essentials of drought in a changing climate. *Science*, **368,** 256-260.

Barker, D., 2012: Caribbean agriculture in a period of global change: vulnerabilities and opportunities. *Caribbean Studies*, **40,** 41-61.

Bates, B., Z. Kundzewicz, and S. Wu, 2008: *Climate change and water.* Intergovernmental Panel on Climate Change Secretariat.

Batjes, N., 1987: CROPRISK: A computerized procedure to assess the agro-ecological suitability of land for rainfed annual crops. *Technical Soils Bulletin*.

Bernal, R. L., 2020: The importance of bananas in the Caribbean. *Corporate versus National Interest in US Trade Policy*, Springer, 41-61.

Björnsson, H., and S. Venegas, 1997: A manual for EOF and SVD analyses of climatic data. *CCGCR Report*, **97,** 112-134.

Brovkin, V., 2002: Climate-vegetation interaction. *Journal de Physique IV (Proceedings)*, **12,** 57-72.

Campbell, D., D. Barker, and D. McGregor, 2011: Dealing with drought: small farmers and environmental hazards in southern St. Elizabeth, Jamaica. *Applied Geography*, **31,** 146-158.

Cane, M. A., 1983: Oceanographic events during el nino. *Science*, **222,** 1189-1195.

Cant, R. V., 1996: Water supply and sewerage in a small island environment: the Bahamian experience. *Small islands: marine science and sustainable development*, **51,** 329.

Capotondi, A., and Coauthors, 2015: Understanding ENSO diversity. *Bulletin of the American Meteorological Society*, **96,** 921-938.

Casella, G., and R. L. Berger, 2021: *Statistical inference.* Cengage Learning.

Cashman, A., L. Nurse, and C. John, 2010: Climate change in the Caribbean: the water management implications. *The Journal of Environment & Development*, **19,** 42-67.

CEHI, 2002: Water and climate change in the Caribbean.

Charlery, J., L. Nurse, and K. Whitehall, 2006: Exploring the relationship between the North Atlantic oscillation and rainfall patterns in Barbados. *International Journal of Climatology: A Journal of the Royal Meteorological Society*, **26,** 819-827.

Connell, J., K. Lowitt, A. Saint Ville, and G. M. Hickey, 2020: Food security and sovereignty in small island developing states: contemporary crises and challenges. *Food Security in Small Island States,* J. Connell, and K. Lowitt, Eds., Springer Singapore, 1-23.

Cook, K. H., and E. K. Vizy, 2010: Hydrodynamics of the Caribbean Low-Level Jet and its relationship to precipitation. *Journal of Climate*, **23,** 1477-1494.

Curtis, S., and D. W. Gamble, 2008: Regional variations of the Caribbean mid-summer drought. *Theoretical and Applied Climatology*, **94,** 25-34.

Curtis, S., D. W. Gamble, and J. Popke, 2014: Sensitivity of crop water need to 2071–95 projected temperature and precipitation changes in Jamaica. *Earth Interactions,* **18,** 1-17.

Dai, A., K. E. Trenberth, and T. Qian, 2004: A global dataset of Palmer Drought Severity Index for 1870–2002: relationship with soil moisture and effects of surface warming. *Journal of Hydrometeorology*, **5,** 1117-1130.

Dawson, A., 2016: eofs: A Library for EOF Analysis of meteorological, oceanographic, and climate data. *Journal of Open Research Software*, **4**.

Dieter, C. A., and Coauthors, 2018: Estimated use of water in the United States in 2015141134233X.

Dunion, J. P., 2011: Rewriting the climatology of the Tropical North Atlantic and Caribbean Sea atmosphere. *Journal of Climate*, **24,** 893-908.

Durrant, S., L. Nurse, and A. Stoddard, 2007: Monitoring the effect of below average precipitation on water resources in Paget Farm, Bequia, Grenadines.

Fain, S. J., M. Quiñones, N. L. Álvarez-Berríos, I. K. Parés-Ramos, and W. A. Gould, 2018: Climate change and coffee: assessing vulnerability by modeling future climate suitability in the Caribbean island of Puerto Rico. *Climatic Change*, **146,** 175-186.

Falkland, T., 1999: Water resources issues of small island developing states. *Natural Resources Forum*, **23,** 245-260.

Farrell, D., L. Nurse, and L. Moseley, 2007: *Managing water resources in the face of climate change: A Caribbean perspective.* UWI.

Farrell, D., A. Trotman, and C. Cox, 2010: Drought early warning and risk reduction.

Fetcher, N., S. F. Oberbauer, and B. R. Strain, 1985: Vegetation effects on microclimate in lowland tropical forest in Costa Rica. *International Journal of Biometeorology*, **29,** 145-155.

Foltz, G. R., M. J. McPhaden, and R. Lumpkin, 2012: A strong Atlantic Meridional Mode event in 2009: the role of mixed layer dynamics. *Journal of Climate*, **25,** 363-380.

Gamble, D., 2014: The neglected climatic hazards of the Caribbean: overview and prospects in a warmer climate. *Geography Compass*, **8,** 221-234.

Gamble, D. W., 2004: Water resource development on small carbonate islands: solutions offered by the Hydrologic Landscape concept. *WorldMinds: Geographical Perspectives on 100 Problems: Commemorating the 100th Anniversary of the Association of American Geographers 1904–2004*, D. G. Janelle, B. Warf, and K. Hansen, Eds., Springer Netherlands, 503-507.

Gamble, D. W., 2017: Droughts and water shortages. *The International Encyclopedia of Geography*.

Gamble, D. W., and S. Curtis, 2008: Caribbean precipitation: review, model and prospect. *Progress in Physical Geography*, **32,** 265-276.

Gamble, D. W., D. B. Parnell, and S. Curtis, 2008: Spatial variability of the Caribbean mid-summer drought and relation to north Atlantic high circulation. *International Journal of Climatology*, **28,** 343-350.

Garcia-Martino, A. R., G. S. Warner, F. N. Scatena, and D. L. Civco, 1996: Rainfall, runoff and elevation relationships in the Luquillo Mountains of Puerto Rico. *Caribbean Journal of Science*, **32,** 413-424.

Geoghegan, T., and Y. Renard, 2002: Beyond community involvement: lessons from the insular Caribbean. *Parks*, **12,** 16-27.

George, S. E., and M. A. Saunders, 2001: North Atlantic Oscillation impact on tropical north Atlantic winter atmospheric variability. *Geophysical Research Letters*, **28,** 1015-1018.

Giannini, A., Y. Kushnir, and M. A. Cane, 2000: Interannual variability of Caribbean rainfall, ENSO, and the Atlantic Ocean. *Journal of Climate*, **13,** 297-311.

Giannini, A., Y. Kushnir, and M. Cane, 2001a: Seasonality in the impact of ENSO and the North Atlantic high on Caribbean rainfall. *Physics and Chemistry of the Earth, Part B: Hydrology, Oceans and Atmosphere*, **26,** 143-147.

Giannini, A., M. A. Cane, and Y. Kushnir, 2001b: Interdecadal changes in the ENSO teleconnection to the Caribbean region and the North Atlantic Oscillation. *Journal of Climate*, **14,** 2867-2879.

Giannini, A., J. C. Chiang, M. A. Cane, Y. Kushnir, and R. Seager, 2001c: The ENSO teleconnection to the tropical Atlantic Ocean: contributions of the remote and local SSTs to rainfall variability in the tropical Americas. *Journal of Climate*, **14,** 4530-4544.

Gould, W. A., F. H. Wadsworth, M. Quiñones, S. J. Fain, and N. L. Álvarez-Berríos, 2017: Land use, conservation, forestry, and agriculture in Puerto Rico. *Forests*, **8,** 242.

Granger, O. E., 1985: Caribbean climates. *Progress in Physical Geography,* **9,** 16-43.

——, 1996: Geography of small tropical islands: implications for sustainable development in a changing world. *Coastal and Estuarine Studies***,** 157-204.

Hargreaves, G. H., and Z. A. Samani, 1985: Reference crop evapotranspiration from temperature. *Applied engineering in agriculture*, **1,** 96-99.

Harlow, J., and B. Hagedorn, 2018: SWB modeling of groundwater recharge on Catalina Island, California, during a Period of Severe Drought. *Water*, **11,** 58.

Harmsen, E., J. Colon Trinidad, C. Lis Arcelay, and D. Cadiz Rodriguez, 2003: Evaluation of percolation and nitrogen leaching from a sweet pepper crop grown on an oxisol soil in Northwest Puerto Rico.

Harmsen, E. W., 2019: Puerto Rico South Coast Aquifer recharge analysis. *Press conference presentation*.

Hatzaki, M., H. Flocas, D. Asimakopoulos, and P. Maheras, 2007: The eastern Mediterranean teleconnection pattern: identification and definition. *International Journal of Climatology*, **27,** 727-737.

Hawkins, E., T. M. Osborne, C. K. Ho, and A. J. Challinor, 2013: Calibration and bias correction of climate projections for crop modelling: an idealised case study over Europe. *Agricultural and Forest Meteorology*, **170,** 19-31.

Hayhoe, K., 2013: Quantifying key drivers of climate variability and change for Puerto Rico and the Caribbean. *Raleigh, North Carolina: Caribbean Landscape Conservation Cooperative*.

Healy, R. W., 2010: *Estimating groundwater recharge.* Cambridge University Press.

Heileman, S., 2007: Thematic report for the insular Caribbean sub-region. *The CLME Synthesis Workshop*, Citeseer, 53.

Hendry, M. D., 1996: The geological legacy of small islands at the Caribbean-Atlantic boundary. *Coastal and Estuarine Studies***,** 205-224.

Herrera, D., and T. Ault, 2017: Insights from a new high-resolution drought atlas for the Caribbean spanning 1950–2016. *Journal of Climate*, **30,** 7801-7825.

Herrera, D. A., T. R. Ault, J. T. Fasullo, S. J. Coats, C. M. Carrillo, B. I. Cook, and A. P. Williams, 2018: Exacerbation of the 2013–2016 Pan-Caribbean drought by anthropogenic warming. *Geophysical Research Letters*, **45,** 10,619-610,626.

Holding, S., D. M. Allen, S. Foster, A. Hsieh, I. Larocque, J. Klassen, and S. C. Van Pelt, 2016: Groundwater vulnerability on small islands. *Nature Climate Change*, **6,** 1100-1103.

Holdridge, L. R., 1967: Life zone ecology. *Life zone ecology*.

Hosannah, N., J. E. González, C. Lunger, and D. Niyogi, 2019: Impacts of local convective processes on rain on the caribbean island of Puerto Rico. *Journal of Geophysical Research: Atmospheres*, **124,** 6009-6026.

Huang, B., and Coauthors, 2017: Extended reconstructed sea surface temperature, version 5 (ERSSTv5): upgrades, validations, and intercomparisons. *Journal of Climate*, **30,** 8179-8205.

Huang, J., K. Higuchi, and A. Shabbar, 1998: The relationship between the North Atlantic Oscillation and El Niño-Southern Oscillation. *Geophysical Research Letters*, **25,** 2707-2710.

Huffman, R. L., D. D. Fangmeier, W. J. Elliot, S. R. Workman, and G. Schwab, 2011: *Soil and water conservation engineering.* American Society of Agricultural and Biological Engineers St. Joseph.

Hurrell, J. W., 1995: Decadal trends in the North Atlantic Oscillation: regional temperatures and precipitation. *Science*, **269,** 676-679.

Jury, M., B. A. Malmgren, and A. Winter, 2007: Subregional precipitation climate of the Caribbean and relationships with ENSO and NAO. *Journal of Geophysical Research: Atmospheres*, **112**.

Jury, M. R., 2020: Resolution-dependent perspectives on Caribbean hydro-climate change. *Hydrology*, **7,** 93.

Kao, H.-Y., and J.-Y. Yu, 2009: Contrasting eastern-Pacific and central-Pacific types of ENSO. *Journal of Climate*, **22,** 615-632.

Karnauskas, K. B., J. P. Donnelly, and K. J. Anchukaitis, 2016: Future freshwater stress for island populations. *Nature Climate Change*, **6,** 720-725.

Karnauskas, K. B., C.-F. Schleussner, J. P. Donnelly, and K. J. Anchukaitis, 2018: Freshwater stress on small island developing states: population projections and aridity changes at 1.5 and 2 °C. *Regional Environmental Change*, **18,** 2273-2282.

Kent, K., 1973: A method for estimating volume and rate of runoff in small watersheds.

Khudoley, K. M., and A. A. Meyerhoff, 1971: Paleogeography and geological history of Greater Antilles. *Paleogeography and Geological History of Greater Antilles*, K. M. Khudoley, and A. A. Meyerhoff, Eds., Geological Society of America.

Kisekka, I., K. Migliaccio, M. D. Dukes, J. H. Crane, and B. Schaffer, 2010: Evapotranspiration-based irrigation for agriculture: crop coefficients of some commercial crops in Florida. *EDIS*, **2010**.

Kossin, J. P., 2008: Is the North Atlantic hurricane season getting longer? *Geophysical Research Letters*, **35**.

Kuciauskas, A. P., P. Xian, E. J. Hyer, M. I. Oyola, and J. R. Campbell, 2016: Providing the Caribbean community with VIIRS-derived weather satellite and dust model output in preparation for African dust impacts. IN31A-1750.

Kuciauskas, A. P., P. Xian, E. J. Hyer, M. I. Oyola, and J. R. Campbell, 2018: Supporting weather forecasters in predicting and monitoring Saharan Air Layer dust events as they impact the Greater Caribbean. *Bulletin of the American Meteorological Society*, **99,** 259-268.

Kumar, N., S. K. Singh, P. K. Srivastava, and B. Narsimlu, 2017: SWAT Model calibration and uncertainty analysis for streamflow prediction of the Tons River Basin, India, using Sequential Uncertainty Fitting (SUFI-2) algorithm. *Modeling Earth Systems and Environment*, **3,** 30.

Lamb, P. J., and R. A. Peppler, 1987: North Atlantic Oscillation: concept and an application. *Bulletin of the American Meteorological Society*, **68,** 1218-1225.

Lawrence, D., and K. Vandecar, 2015: Effects of tropical deforestation on climate and agriculture. *Nature Climate Change*, **5,** 27-36.

Lim, K. J., B. A. Engel, Z. Tang, J. Choi, K. S. Kim, S. Muthukrishnan, and D. Tripathy, 2005: Automated web GIS based hydrograph analysis tool, WHAT 1. *JAWRA Journal of the American Water Resources Association*, **41,** 1407-1416.

Lincoln Lenderking, H., S.-A. Robinson, and G. Carlson, 2021: Climate change and food security in Caribbean small island developing states: challenges and strategies. *International Journal of Sustainable Development & World Ecology*, **28,** 238-245.

Lugo, A. E., and Coauthors, 2001: Puerto Rican karst-a vital resource.

Magaña, V., J. A. Amador, and S. Medina, 1999: The midsummer drought over Mexico and Central America. *Journal of Climate*, **12,** 1577-1588.

Maihemuti, B., R. Ghasemizadeh, X. Yu, I. Padilla, and A. N. Alshawabkeh, 2015: Simulation of regional karst aquifer system and assessment of groundwater resources in Manati-Vega Baja, Puerto Rico. *Journal of Water Resource and Protection*, **07,** 909-922.

Malmgren, B. A., A. Winter, and D. Chen, 1998: El Nino–southern oscillation and North Atlantic oscillation control of climate in Puerto Rico. *Journal of Climate*, **11,** 2713-2717.

Marshall, J., and Coauthors, 2001: North Atlantic climate variability: phenomena, impacts and mechanisms. *International journal of climatology*, **21,** 1863-1898.

Martinez, C., L. Goddard, Y. Kushnir, and M. Ting, 2019: Seasonal climatology and dynamical mechanisms of rainfall in the Caribbean. *Climate Dynamics*.

McCabe, G. J., and S. L. Markstrom, 2007: A monthly water-balance model driven by a graphical user interface. Report 2007-1088.

McGregor, D., D. Barker, and D. Campbell, 2009: Environmental change and Caribbean food security: recent hazard impacts and domestic food production in Jamaica. *Global change and Caribbean vulnerability: Environment, economy and society at risk*, 273-297.

Mecikalski, J. R., and E. W. Harmsen, 2019: The use of visible geostationary operational meteorological satellite imagery in mapping the water balance over Puerto Rico for water resource management. IntechOpen.

Mendez-Tejeda, R., R. Richards, and A. Emiliano, 2016: Analysis of groundwater in Puerto Rico, **4,** 68-76.

Miller, J. A., R. Whitehead, D. S. Oki, S. B. Gingerich, and P. G. Olcott, 1997: Ground water atlas of the United States: Segment 13, Alaska, Hawaii, Puerto Rico, and the US Virgin Islands0607881267.

Miller, P. W., and C. A. Ramseyer, 2020: Did the Climate Forecast System anticipate the 2015 Caribbean drought? *Journal of Hydrometeorology*, **21,** 1245-1258.

Miller, P. W., T. L. Mote, and C. A. Ramseyer, 2019: An empirical study of the relationship between seasonal precipitation and thermodynamic environment in Puerto Rico. *Weather and Forecasting*, **34,** 277-288.

Miller, P. W., M. Williams, and T. Mote, 2021: Modeled atmospheric optical and thermodynamic responses to an exceptional trans-Atlantic dust outbreak. *Journal of Geophysical Research: Atmospheres*, **126,** e2020JD032909.

Mimura, N., and Coauthors, 2007: Small islands. *Climate change*, **16,** 687-716.

Mo, K. C., 2010: Interdecadal modulation of the impact of ENSO on precipitation and temperature over the United States. *Journal of climate*, **23,** 3639-3656.

Moriasi, D. N., J. G. Arnold, M. W. Van Liew, R. L. Bingner, R. D. Harmel, and T. L. Veith, 2007: Model evaluation guidelines for systematic quantification of accuracy in watershed simulations. *Transactions of the ASABE*, **50,** 885-900.

Mote, T. L., C. A. Ramseyer, and P. W. Miller, 2017: The Saharan Air Layer as an early rainfall season suppressant in the Eastern Caribbean: The 2015 Puerto Rico drought. *Journal of Geophysical Research: Atmospheres*, **122**.

Navarro-Racines, C., J. Tarapues, P. Thornton, A. Jarvis, and J. Ramirez-Villegas, 2020: High-resolution and bias-corrected CMIP5 projections for climate change impact assessments. *Scientific Data*, **7**.

Neelin, J. D., M. Münnich, H. Su, J. E. Meyerson, and C. E. Holloway, 2006: Tropical drying trends in global warming models and observations. *Proceedings of the National Academy of Sciences*, **103,** 6110-6115.

Nurse, L. A., and Coauthors, 2014: Small islands.

O'Neill, B. C., and Coauthors, 2016: The scenario model intercomparison project (ScenarioMIP) for CMIP6. *Geoscientific Model Development*, **9,** 3461-3482.

OCHA, U. N. O. f. t. C. o. H. A., 2015: Annual Report 2015.

Padilla, I., C. Irizarry, and K. Steele, 2011: Historical contamination of groundwater resources in the north coast karst aquifers of Puerto Rico. *Rev Dimens*, **3,** 7-12.

Palada, M. C. M., Jeanmarie M., and O'Keefe, Daniela 2003: Growth and yield response of Puerto Rican sweet pepper to levels of drip irrigation in the Virgin Islands *Caribbean Food Crops Society, Thirty Ninth Annual Meeting*.

Pandey, R. P., A. Pandey, R. V. Galkate, H.-R. Byun, and B. C. Mal, 2010: Integrating hydro-meteorological and physiographic factors for assessment of vulnerability to drought. *Water Resources Management*, **24,** 4199-4217.

Patricola, C. M., R. Saravanan, and P. Chang, 2014: The impact of the El Niño–Southern Oscillation and Atlantic Meridional Mode on seasonal Atlantic tropical cyclone activity. *Journal of Climate*, **27,** 5311-5328.

Patricola, C. M., P. Chang, and R. Saravanan, 2016: Degree of simulated suppression of Atlantic tropical cyclones modulated by flavour of El Niño. *Nature Geoscience*, **9,** 155-160.

Peterson, T. C., and Coauthors, 2002: Recent changes in climate extremes in the Caribbean region. *Journal of Geophysical Research: Atmospheres*, **107,** ACL 16-11-ACL 16-19.

Prospero, J. M., and O. L. Mayol-Bracero, 2013: Understanding the transport and impact of african dust on the Caribbean Basin. *Bulletin of the American Meteorological Society*, **94,** 1329-1337.

Pulwarty, R. S., L. A. Nurse, and U. O. Trotz, 2010: Caribbean islands in a changing climate. *Environment: Science and Policy for Sustainable Development*, **52,** 16-27.

Ramseyer, C. A., and T. L. Mote, 2016: Atmospheric controls on Puerto Rico precipitation using artificial neural networks. *Climate Dynamics*, **47,** 2515-2526.

——, 2018: Analysing regional climate forcing on historical precipitation variability in Northeast Puerto Rico. *International Journal of Climatology*, **38,** e224-e236.

Rhiney, K., 2015: Geographies of Caribbean vulnerability in a changing climate: Issues and trends. *Geography Compass*, **9,** 97-114.

Rhiney, K., A. Eitzinger, A. D. Farrell, and S. D. Prager, 2018: Assessing the implications of a 1.5 °C temperature limit for the Jamaican agriculture sector. *Regional Environmental Change*, **18,** 2313-2327.

Robinson, S.-A., and C. Wren, 2020: Geographies of vulnerability: a research note on human system adaptations to climate change in the Caribbean. *Geografisk Tidsskrift-Danish Journal of Geography***,** 1-8.

Rodriguez-Vera, G., R. Romero-Centeno, C. L. Castro, and V. M. Castro, 2019: Coupled interannual variability of wind and sea surface temperature in the Caribbean Sea and the Gulf of Mexico. *Journal of Climate*, **32,** 4263-4280.

Ropelewski, C. F., and M. S. Halpert, 1987: Global and regional scale precipitation patterns associated with the El Niño/Southern Oscillation. *Monthly weather review*, **115,** 1606-1626.

Rugg, A., G. R. Foltz, and R. C. Perez, 2016: Role of mixed layer dynamics in tropical North Atlantic interannual sea surface temperature variability. *Journal of Climate*, **29,** 8083-8101.

Scheffer, M., M. Holmgren, V. Brovkin, and M. Claussen, 2005: Synergy between small-and large-scale feedbacks of vegetation on the water cycle. *Global Change Biology*, **11,** 1003-1012.

Smerdon, J. E., B. I. Cook, E. R. Cook, and R. Seager, 2015: Bridging past and future climate across paleoclimatic reconstructions, observations, and models: a hydroclimate case study. *Journal of Climate*, **28,** 3212-3231.

Smirnov, D., and D. J. Vimont, 2011: Variability of the Atlantic Meridional Mode during the Atlantic hurricane season. *Journal of Climate*, **24,** 1409-1424.

Sobel, A. H., C. D. Burleyson, and S. E. Yuter, 2011: Rain on small tropical islands. *Journal of Geophysical Research*, **116**.

Stephenson, N., 1998: Actual evapotranspiration and deficit: biologically meaningful correlates of vegetation distribution across spatial scales. *Journal of Biogeography*, **25,** 855-870.

Taylor, M. A., D. B. Enfield, and A. A. Chen, 2002: Influence of the tropical Atlantic versus the tropical Pacific on Caribbean rainfall. *Journal of Geophysical Research: Oceans*, **107,** 10-11-10-14.

Taylor, M. A., F. S. Whyte, T. S. Stephenson, and J. D. Campbell, 2013: Why dry? Investigating the future evolution of the Caribbean Low Level Jet to explain projected Caribbean drying. *International Journal of Climatology*, **33,** 784-792.

Thornthwaite, C. W., 1948: An approach toward a rational classification of climate. *Geographical Review*, **38,** 55.

Thornthwaite, C. W., and J. R. Mather, 1957: Instructions and tables for computing potential evapotranspiration and the water balance.

Thornton, P. E., S. W. Running, and M. A. White, 1997: Generating surfaces of daily meteorological variables over large regions of complex terrain. *Journal of Hydrology*, **190,** 214-251.

Thornton, P. E., M. M. Thornton, B. W. Mayer, Y. Wei, R. Devarakonda, R. S. Vose, and R. B. Cook, 2016: Daymet: daily surface weather data on a 1-km grid for North America, Version 3. ORNL Distributed Active Archive Center.

Tomlinson, J., and K. Rhiney, 2018: Experiential learning as a tool for farmer engagement and empowerment in a changing regional climate. *Caribbean Quarterly*, **64,** 114-135.

Torres-Gonzalez, S., and J. M. Rodriguez, 2016: Hydrologic conditions in the South Coast aquifer, Puerto Rico, 2010–15. Report 2015-1215.

Torres-Valcárcel, Á., J. Harbor, C. González-Avilés, and A. Torres-Valcárcel, 2014: Impacts of urban development on precipitation in the tropical maritime climate of Puerto Rico. *Climate*, **2,** 47-77.

Torres-Valcárcel, A. R., 2018: Teleconnections between ENSO and rainfall and drought in Puerto Rico. *International Journal of Climatology*, **38,** e1190-e1204.

Trenberth, K. E., 1997: The definition of el nino. *Bulletin of the American Meteorological Society*, **78,** 2771-2778.

Trotman, A., R. M. Gordon, S. D. Hutchinson, R. Singh, and D. McRae-Smith, 2009: Policy responses to GEC impacts on food availability and affordability in the Caribbean community. *Environmental Science & Policy*, **12,** 529-541.

UNDESA, 2012: Climate change adaptation in Grenada: water resources, coastal ecosystems and renewable energy.

USACE, J. B., Alan Fong, Laura Roebuck, Nancy M. Ferris, Sheri Zettle, 2004: Water resources assessment of Dominica, Antigua, Barbuda, St. Kitts and Nevis.

USDA, U. S. D. o. A., 2020a: 2017 Census of agriculture - Puerto Rico (2018), 230 pp.

——, 2020b: 2017 Census of agriculture - Virgin Islands of the United States (2018) 55 pp.

Van der Schrier, G., J. Barichivich, K. R. Briffa, and P. D. Jones, 2013: A scPDSI-based global data set of dry and wet spells for 1901–2009, **118,** 4025-4048.

Vimont, D. J., and J. P. Kossin, 2007: The Atlantic Meridional Mode and hurricane activity. *Geophysical Research Letters*, **34**.

Wang, A., F. Dominguez, and A. Schmidt, 2019: Extreme precipitation spatial analog: in search of an alternative approach for future extreme precipitation in urban hydrological studies. *Water*, **11,** 1032.

Wells, N., S. Goddard, and M. J. Hayes, 2004: A self-calibrating Palmer Drought Severity Index. *Journal of Climate*, **17,** 2335-2351.

Westenbroek, S. M., J. A. Engott, V. A. Kelson, and R. J. Hunt, 2018: SWB Version 2.0—A soil-water-balance code for estimating net infiltration and other water-budget components. Report 6-A59.

Westenbroek, S. M., V. A. Kelson, W. R. Dripps, R. J. Hunt, and K. R. Bradbury, 2010: SWB-A modified Thornthwaite-Mather soil-water-balance code for estimating groundwater recharge. Report 6-A31.

Wilhite, D. A., 2000: Drought as a natural hazard: concepts and definitions.

Williams, A. P., R. Seager, J. T. Abatzoglou, B. I. Cook, J. E. Smerdon, and E. R. Cook, 2015: Contribution of anthropogenic warming to California drought during 2012–2014. *Geophysical Research Letters*, **42,** 6819-6828.

Wolock, D., and G. McCabe, 1999: Effects of potential climatic change on annual runoff in the conterminous United States. *Journal of the American Water Resources Association*, **35,** 341-341,350.

APPENDICES

Appendix A. Root depth (cm) of each hydrologic soil type (1 to 9) used as input in the Soil Water Balance Model 2 (SWB2). Hydrologic soil group numbers correspond to soil types as follows: B (1), C (2), A (3), C/D (4), D (5), B/D (6), W (7), ROut (8), and A/D (9).

LULC	RZ_1	RZ_2	RZ_3	RZ_4	RZ_5	RZ_6	RZ_7	RZ_8	RZ_9
High Intensity Developed	3.81	3.81	3.81	3.81	3.81	3.81	0.51	0.25	3.81
Medium Intensity Developed	3.81	3.81	3.81	3.81	3.81	3.81	0.51	0.25	3.81
Low Intensity Developed	3.81	3.81	3.81	3.81	3.81	3.81	0.51	0.25	3.81
Developed, Open Space	63.4	63.4	63.4	63.4	63.4	63.4	0.51	0.25	63.4
Cultivated Crops	6.87	6.47	6.34	4.02	4.02	4.02	0.51	0.25	63.4
Pasture/Hay	6.87	6.47	6.34	4.02	4.02	4.02	0.51	0.25	63.4
Grassland/Herbaceous	6.87	6.47	6.34	4.02	4.02	4.02	0.51	0.25	63.4
Mixed Forest	3.17	3.17	3.97	2.54	2.54	2.54	0.51	0.25	3.97
Shrub/Scrub	6.34	6.34	6.34	4.23	4.23	4.23	0.51	0.25	6.34
Palustrine Forested Wetland	3.17	3.17	3.97	2.54	2.54	2.54	0.51	0.25	3.97
Palustrine Scrub/Shrub Wetland	6.34	6.34	6.34	4.23	4.23	4.23	0.51	0.25	6.34
Palustrine Emergent Wetland	8.57	8.57	8.57	8.57	8.57	8.57	0.51	0.25	8.57
Estuarine Forested Wetland	3.17	3.17	3.97	2.54	2.54	2.54	0.51	0.25	3.97
Estuarine Scrub/Shrub Wetland	6.34	6.34	6.34	4.23	4.23	4.23	0.51	0.25	6.34
Estuarine Emergent Wetland	8.57	8.57	8.57	8.57	8.57	8.57	0.51	0.25	8.57
Unconsolidated Shore	0.51	0.51	0.51	0.51	0.51	0.51	0.51	0.25	0.51
Bare Land	3.81	3.81	3.81	3.81	3.81	3.81	0.51	0.25	3.81
Open Water	0.51	0.51	0.51	0.51	0.51	0.51	0.51	0.25	0.51
Palustrine Aquatic Bed	0.51	0.51	0.51	0.51	0.51	0.51	0.51	0.25	0.51
Estuarine Aquatic Bed	0.51	0.51	0.51	0.51	0.51	0.51	0.51	0.25	0.51

Source: Westenbroek et al. (2018).

Appendix B. Puerto Rico control file including the parameters used as input in the Soil Water Balance Model 2 (SWB2).

```
# Puerto Rico

#Grid definition:
#          nx    ny              xll         yll     resolution
GRID   603   330   3104681.862  -67609.2    300.0

#Projection:United States Contiguous Albers Equal Area Conic (U.S. Geological Survey
version)
BASE_PROJECTION_DEFINITION +proj=aea +lat_1=29.5 +lat_2=45.5 +lat_0=23
+lon_0=-96 +x_0=0 +y_0=0 +ellps=GRS80 +datum=NAD83 +units=m +no_defs

#Define methods
-----------------

INTERCEPTION_METHOD                         BUCKET
EVAPOTRANSPIRATION_METHOD                   HARGREAVES-SAMANI
RUNOFF_METHOD                               CURVE_NUMBER
SOIL_MOISTURE_METHOD                        THORNTHWAITE-MATHER
PRECIPITATION_METHOD                        GRIDDED
ROOTING_DEPTH_METHOD                        STATIC
SOIL_STORAGE_MAX_METHOD                     CALCULATED
AVAILABLE_WATER_CONTENT_METHOD   GRIDDED


(1) define location, projection, and conversions for weather data
-------------------------------------------------------------

PRECIPITATION NETCDF daymet_v3_prcp_%y_puertorico.nc4
PRECIPITATION_GRID_PROJECTION_DEFINITION +proj=lcc +lat_1=25.0 +lat_2=60.0
+lat_0=42.5 +lon_0=-100.0 +x_0=0.0 +y_0=0.0 +ellps=GRS80 +datum=NAD83 +units=m
+no_defs
PRECIPITATION_NETCDF_Z_VAR                          prcp
PRECIPITATION_SCALE_FACTOR                          0.03937008
PRECIPITATION_MISSING_VALUES_CODE          -9999.0
PRECIPITATION_MISSING_VALUES_OPERATOR      <=
PRECIPITATION_MISSING_VALUES_ACTION        zero

TMAX NETCDF daymet_v3_tmax_%y_puertorico.nc4
TMAX_GRID_PROJECTION_DEFINITION +proj=lcc +lat_1=25.0 +lat_2=60.0
+lat_0=42.5 +lon_0=-100.0 +x_0=0.0 +y_0=0.0 +ellps=GRS80 +datum=NAD83 +units=m
+no_defs
TMAX_SCALE_FACTOR                       1.8
```

```
TMAX_ADD_OFFSET                32.0
TMAX_MISSING_VALUES_CODE      -9999.0
TMAX_MISSING_VALUES_OPERATOR      <=
TMAX_MISSING_VALUES_ACTION      mean

TMIN NETCDF daymet_v3_tmin_%y_puertorico.nc4
TMIN_GRID_PROJECTION_DEFINITION +proj=lcc +lat_1=25.0 +lat_2=60.0 +lat_0=42.5
+lon_0=-100.0 +x_0=0.0 +y_0=0.0 +ellps=GRS80 +datum=NAD83 +units=m +no_defs
TMIN_SCALE_FACTOR                 1.8
TMIN_ADD_OFFSET                  32.0
TMIN_MISSING_VALUES_CODE        -9999.0
TMIN_MISSING_VALUES_OPERATOR      <=
TMIN_MISSING_VALUES_ACTION      mean

(2) Continuous Frozen-Ground Index initial value and parameters - based on Maui Example
-----------------------------------------------------------------

INITIAL_CONTINUOUS_FROZEN_GROUND_INDEX CONSTANT 0.0

UPPER_LIMIT_CFGI     9999.
LOWER_LIMIT_CFGI    9999.

(3) Initial conditions for soil moisture, snow - based on Maui Example
-------------------------------------------------

INITIAL_PERCENT_SOIL_MOISTURE    CONSTANT 75.0
INITIAL_SNOW_COVER_STORAGE       CONSTANT 0.0

(4) specify location and projection for input GIS grids
--------------------------------------------------------

FLOW_DIRECTION ARC_GRID D8/flowdir_pr.asc
FLOW_DIRECTION_PROJECTION_DEFINITION  +proj=utm +zone=19+north
+ellps=GRS80 +datum=NAD83 +units=m +no_defs

HYDROLOGIC_SOILS_GROUP ARC_GRID Soiltype/soilspr_swb_ssurgo.asc
HYDROLOGIC_SOILS_GROUP_PROJECTION_DEFINITION +proj=aea +lat_1=29.5
+lat_2=45.5 +lat_0=23 +lon_0=-96 +x_0=0 +y_0=0 +ellps=GRS80 +datum=NAD83
+units=m +no_defs

LAND_USE ARC_GRID LandCover/landcoverpr.asc
LANDUSE_PROJECTION_DEFINITION +proj=aea +lat_1=29.5 +lat_2=45.5 +lat_0=23
+lon_0=-96 +x_0=0 +y_0=0 +ellps=GRS80 +datum=NAD83 +units=m +no_defs
```

```
AVAILABLE_WATER_CONTENT ARC_GRID AWC/awcpr_swb_ssurgo.asc
AVAILABLE_WATER_CONTENT_PROJECTION_DEFINITION +proj=aea +lat_1=29.5
+lat_2=45.5 +lat_0=23 +lon_0=-96 +x_0=0 +y_0=0 +ellps=GRS80 +datum=NAD83
+units=m +no_defs
AVAILABLE_WATER_CONTENT_SCALE_FACTOR  12.


(5) specify location and names for all lookup tables
--------------------------------------------------

LAND_USE_LOOKUP_TABLE st_input_2001/Lookup_Table_PR_2001_CN.txt
LAND_USE_LOOKUP_TABLE st_input_2001/Lookup_Table_PR_2010_CN.txt


(6) Output control
________________________________
#start and end date may be any valid dates in SWB version 2.0
#remember to allow for adequate model spin up;

#baseline climatology
START_DATE 01/01/1980
END_DATE 12/31/2010

#recent decade
START_DATE 01/01/2010
END_DATE 12/31/2019
```